Improving the Accuracy of Occupational Hygiene Models Used to Estimate Worker Exposure to Solvent Vapours

Spéro Abattan
Stéphane Hallé
Daniel Drolet
Ali Bahloul
Patrick Eddy Ryan
Wejden Chouchene
Carlos Castro Ruiz
Jérôme Lavoué
Maximilien Debia

STUDIES AND
RESEARCH PROJECTS

R-1077-en

CHEMICAL
AND BIOLOGICAL
HAZARD PREVENTION RESEARCH

OUR RESEARCH
is working for you !

The Institut de recherche Robert-Sauvé en santé et en sécurité du travail (IRSST), established in Québec since 1980, is a scientific research organization well-known for the quality of its work and the expertise of its personnel.

Mission
To contribute, through research, to the prevention of industrial accidents and occupational diseases and to the rehabilitation of affected workers;

To disseminate knowledge and serve as a scientific reference centre and expert;

To provide the laboratory services and expertise required to support the public occupational health and safety network.

Funded by the Commission des normes, de l'équité, de la santé et de la sécurité du travail, the IRSST has a board of directors made up of an equal number of employer and worker representatives.

To find out more
Visit our Web site for complete up-to-date information about the IRSST. All our publications can be downloaded at no charge.
www.irsst.qc.ca

To obtain the latest information on the research carried out or funded by the IRSST, subscribe to our publications:

- *Prévention au travail,* the free magazine published jointly by the IRSST and the CNESST (preventionautravail.com)
- InfoIRSST, the Institute's electronic newsletter

Improving the Accuracy of Occupational Hygiene Models Used to Estimate Worker Exposure to Solvent Vapours

Spéro Abattan[1], Stéphane Hallé[2], Daniel Drolet[1], Ali Bahloul[3], Patrick Eddy Ryan[1], Wejden Chouchene[2], Carlos Castro Ruiz[1], Jérôme Lavoué[1], Maximilien Debia[1]

[1] Department of Environmental Health and Occupational Health, School of Public Health, Université de Montréal

[2] École de technologie supérieure

[3] Institut de recherche Robert-Sauvé en santé et en sécurité du travail (IRSST)

STUDIES AND RESEARCH PROJECTS

R-1077-en

ACKNOWLEDGMENTS

ABSTRACT

Every year, Quebec workers suffer the health effects of exposure to chemicals, and particularly solvents. The modelling of occupational exposure plays a major role in risk prevention. The goal of this research project was to study various aspects of modelling for the purpose of estimating occupational exposure to solvent vapours and improving prediction accuracy. The study was carried out in two stages. It involved both small-scale (Stage I) and human-scale (Stage II) testing that focused on determining emission rates for pure solvents and mixtures, as well as on investigating the behaviour of solvent vapours released into the air and subject to different experimental ventilation conditions.

In Stage I, exponentially decreasing emission rates (α) were determined experimentally in a controlled environment (temperature, humidity, air speed) for five pure solvents under different conditions. Multiple linear regression analyses were conducted to assess the influence of the various tested parameters on α values. Emission rates were also calculated for pure solvents and mixtures, while vapour concentrations in a 0.085 m³ box were estimated using the well-mixed room model with exponentially decreasing emissions. All in all, 18 scenarios were carried out with different solvents: 4 pure solvents, 12 aqueous mixtures (10%, 5% and 1% solvent in water) and 2 organic solvent mixtures. The concentration estimates assumed both ideality (use of non-corrected emission rates) and non-ideality (use of emission rates corrected by activity coefficients). These estimated figures were compared with concentrations measured using a gas phase chromatography system coupled with a thermal conductivity detector (TCD). The concentrations were compared graphically with the values predicted by the model, and ratios of the measured to estimated maximum concentrations were calculated.

In Stage II, 19 different experimental situations, created in a human-scale room with a volume of 53.4 m³, were tested three times. The room was ventilated by means of two ventilation strategies (floor/ceiling) and at different airflow rates (low rate [L] at 0.8 air changes per hour [ACH] [12 L/s], high rate [H] at 2.3 ACH [32 L/s] and very high rate (VH) at 4.5 ACH [64 L/s]). Four scenarios were tested: (1) evaporation on a table, (2) spill on the floor, (3) application of solvent using a rag followed by manual cleaning and (4) spraying of solvent followed by manual cleaning. The evaporation and spill tests were conducted using a watch glass containing 20 mL of acetone placed on an analytical balance. The cleaning tests were conducted by an operator who simulated cleaning an aluminum part with a rag. The solvent vapour concentrations were measured using direct-reading instruments placed in the near field (NF, 30 cm from source) and far field (FF, rest of the room). For the near field, two photoionization detectors (PIDs) were used to measure the concentrations. For the far field, two Varian Micro GC chromatographs connected to TCDs were used. For each test, concentrations in the near and far fields were modelled using the two-zone model, and these concentrations were compared with the measured values. The near field radius values were optimized so that the measured and estimated concentrations corresponded. Statistical analyses were conducted to determine whether significant differences existed between the near and far concentrations. Variance and multiple linear regression analyses were also performed to assess the influence of different variables in the models. Computational fluid dynamics (CFD) modelling of air movements and gas contaminant dispersion was carried out for some scenarios. Solvent evaporation was modelled in the code as a boundary condition at the surface of the watch glass whereby a predetermined mass of solvent was injected into the ambient air. Estimated values were compared with measured values.

For Stage I, the variations observed in coefficient α values were primarily due to the variables vapour pressure, surface area/volume ratio and air speed above the spill. Estimates of concentrations in the box that considered non-ideality in the case of mixtures, i.e., corrected estimates, were higher than the non-corrected estimates and closer to the measured values. In addition, the times required to reach the concentration peaks of the corrected estimates provided a means of estimating emission kinetics with sufficient accuracy.

For Stage II, the analysis of variance showed that all of the variables had an effect on the near field concentrations, whereas only airflow rate and air intake position had an effect on the far field. The increase in ventilation rates caused a significant drop in concentrations in both fields. The radii obtained through optimization of the measured and estimated concentrations for the evaporation and spill scenarios were very homogeneous, with a mean radius of 0.72 m (geometric standard deviation, GSD, of 1.3) and the corresponding mean estimated coefficient β (interzonal airflow rate) was 3.9 m³/min (0.92–16.9). Using this radius for near field geometry allows sufficiently accurate estimation of solvent vapour concentrations at a distance of 30 cm from the source. In contrast, for the rag application and spray scenarios, the optimized radii were larger and varied more broadly, with respective mean radii of 1.1 m (GSD of 1.6) and 1.2 m (GSD of 1.9). The CFD modelling provided a means of studying the concentration gradient around the source for the evaporation and spill scenarios. The concentration gradient diminished rapidly, with concentrations dropping from 1,757 mg/m³ to 83 mg/m³ for a cube-shaped near field of 14 cm a side and 64 cm a side, respectively. The CFD modelling also highlighted contaminant displacements due to vapour density relative to the air, without the need to involve advection. This transport mechanism is especially significant when the air delivery rate in the room is low.

This study has demonstrated the importance of the different variables used to estimate emission rates for small spills, the importance of considering non-ideality in cases of the use of non-ideal mixtures and the importance of various concentration determinants in near and far fields. These data improve our general understanding of solvent vapour dispersion and the models used in occupational health and safety to estimate worker exposure to such emissions.

CONTENTS

LIST OF TABLES

LIST OF FIGURES

LIST OF ACRONYMS AND ABBREVIATIONS

ACH   air changes per hour

CFD   computational fluid dynamics

DRI   direct-reading instrument

FDS   fire dynamics simulator

FF   far field

FSA   field surface area

G   generation or emission rate

GC   gas chromatography

GSD   geometric standard deviation

NF   near field

OHS   occupational health and safety

PID   photoionization detector

P_{vap} vapour pressure

Q   general ventilation rate

S   mean interzonal airflow speed

TLV   threshold limit value

UNIFAC   UNIQUAC functional activity coefficient

VFF   volume of far field

VNF   volume of near field

α   constant or first-order emission rate

β   interzonal airflow rate

γi   activity coefficient

1. INTRODUCTION

In Quebec, it is estimated that 9% of all workers (i.e., approximately 321,000 people), equating to 11% of men and 6% of women, are exposed to solvent vapours in their main job. Twenty percent of manual workers say they are exposed often or all the time to solvent vapours (Vézina et al., 2011). Every year, Quebec workers suffer the harmful health consequences of exposure to chemicals, and particularly solvents. These consequences include nervous system effects, eye and mucous membrane irritation, carcinogenic effects, effects on reproduction and fetal development, effects on the liver and kidneys, cardiovascular effects, scleroderma, hematotoxicity, acquired intolerance to solvents, irritant and allergic contact dermatitis and hives (Gérin, 2002a). In France, the occupational injury compensation system associates a number of diseases with exposure to solvents, including hypoplasia, acquired myelodysplastic syndromes, leukemia, myeloproliferative disorders, apyretic gastrointestinal disorders, acute and chronic irritant or eczema-like dermatitis, acute ventricular or supraventricular hyperexcitability cardiac disorders, acute cytolytic hepatitis, tubular nephropathies and polyneuropathies (INRS, 2013).

A number of cases of fire and explosion linked to the use of flammable solvents that have caused worker injuries and deaths have been recorded. According to the Institut national de recherche et de sécurité pour la prévention des accidents du travail et des maladies professionnelles (INRS), more than one explosion a day occurs in France (INRS, 2003). While not all of these explosions are due to solvent vapours, many are. In Quebec, the accident that occurred in November 2014 at the Neptune Technologies plant is an example of an explosion associated with the use and storage of solvents. The solvent in question in that explosion was acetone.

A significant number of studies have been conducted in Quebec in recent years on the topic of solvent substitution (Bégin, Debia and Gérin, 2008; Gérin, 2002b). They have led to the development of the Solub website. It presents a solvent substitution method and allows users to consult substitution fact sheets for 12 user sectors or processes. The fact sheets provide information on occupational health and safety (OHS) issues, hazardous products (exposure levels and effects), possible solutions, preventive steps to take and recommendations. Despite all this research, occupational exposure to solvents is still a major source of concern for OHS specialists and public health authorities.

Given the increasing need to control and anticipate all sorts of risks, modelling has become an indispensable tool in many fields, including finance, public safety, transportation, medicine and pharmacology. In occupational hygiene, the modelling of workplace exposure plays a key role in the prevention of work-related hazards. Developing a virtual model to perform calculations and forecast contaminant behaviour is a flexible, inexpensive alternative method of estimating concentrations. According to the INRS, the speed of implementation, the optimization of analysis protocols, the capability of working retrospectively and prospectively, and the limitation of judgmental bias and uncertainty are all advantages of exposure modelling techniques (Bertrand and Vincent, 2010b).

The use of exposure models is also being boosted by changes in various regulations that require stricter monitoring of chemical exposure levels and that seek to reduce the uncertainties associated with exposure assessments. In Europe, under the REACH regulation (Registration, Evaluation and Authorization of Chemicals), when products are evaluated for their chemical

safety, an exposure evaluation, including the production of exposure scenarios and an estimate of exposure, must be performed (European Parliament and Council of the European Union, 30 December 2006). In Australia, the modelling of occupational exposure is recognized as a method that can be used under certain circumstances to estimate exposure as part of an overall occupational exposure assessment process (Australia, 2012). In Quebec, in a report that the IRSST published on strategies for diagnosing worker exposure to chemicals, Drolet and colleagues (Drolet et al., 2010) stated that exposure estimating models are tools that are bound to see further development and their use should be encouraged.

Models are, by definition, representations of reality. Underlying the models are a variety of hypotheses, ranging from the extremely simple to the highly complex, based on computational fluid dynamics equations. Modellers seek a balance between simplicity and model accuracy (Keil, Simmons and Anthony, 2009; Morency and Hallé, 2012).

This project involved conducting a range of experiments for the purpose of improving the accuracy of the occupational hygiene models used to estimate workplace exposure to solvent vapours.

2. STATE OF KNOWLEDGE

Physical models (referred to also as physico-chemical models) are exposure models that predict exposure by means of mathematical equations simulating the emission and dispersion of contaminants in the air (Bertrand and Vincent, 2010a; Bruzzi, 2007; Flynn, 2004; Nicas, 2003). It is assumed in these models that the contaminant is generated in a volume of air defined by the geometry of the room, dispersed in the environment of the room over a certain length of time, and then eliminated by general ventilation (Drolet et al., 2010; Keil, 1998; Keil et al., 2009). The development of physico-chemical models is based on a combination of the characteristics of the emission of the contaminants (emission models) and those of their dispersion in the work environment (dispersion models) (Reinke and Brosseau, 1997).

A number of mathematical models have been developed to simulate occupational exposure. Most current knowledge on the subject can be found in the American Industrial Hygiene Association (AIHA) manual titled *Mathematical Models for Estimating Occupational Exposure to Chemicals* (Keil et al., 2009).

IH Mod software, the scientific content of which is based on the AIHA manual (Keil et al., 2009), is one of the main chemical hazard modelling tools used in industrial hygiene. It sets out 11 models for estimating exposure according to different work situations that include different contaminant generation and dispersion models. Since the development of IH Mod, a number of studies aimed at adjusting and validating the models have been published (Arnold, Shao and Ramachandran, 2017b; Cherrie et al., 2011; Fransman et al., 2011; Nicas, 2016; Tielemans et al., 2011; van Tongeren et al., 2011; Williams and Mani, 2015; Zhang, Banerjee, Yang, Lungu and Ramachandran, 2009). Among the dispersion models, the well-mixed room model and the two-zone model are described in this report, while among the emission models, the constant generation model and the exponentially decreasing emissions model are presented for pure solvents and for mixtures.

In addition to the mathematical models, computational fluid dynamics (CFD) can offer an alternative solution to measurement methods. CFD can generate contaminant dispersal simulations with great accuracy when simulation conditions are well defined. CFD could also be used as a validation reference tool for simple mathematical models like those in IH Mod (Keil et al., 2009).

2.1   Dispersion models

2.1.1 *Well-mixed room model*

The well-mixed room model is a simple model that can be used to estimate a uniform concentration of chemical agents in a workplace. It has been used by a number of authors to estimate contaminant concentrations in workplaces (Arnold, Shao and Ramachandran, 2017a; Arnold et al., 2017b; Demou, Hellweg, Wilson, Hammond and McKone, 2009; Earnest and Corsi, 2013; Gaffney et al., 2008; Keil and Murphy, 2006; Keil and Nicas, 2003; Keil, 2000; Persoons, Maitre and Bicout, 2011). With this model, everyone who is working in a room is exposed to the same concentrations. Contaminant dispersion is determined by general room ventilation. According to Nicas, the model provides a sufficiently accurate estimation of exposure far from the

emission source (d ≥ 3 m), but generally underestimates exposure near the source (Nicas, 2009). A diagram of the model is shown in Figure 1.
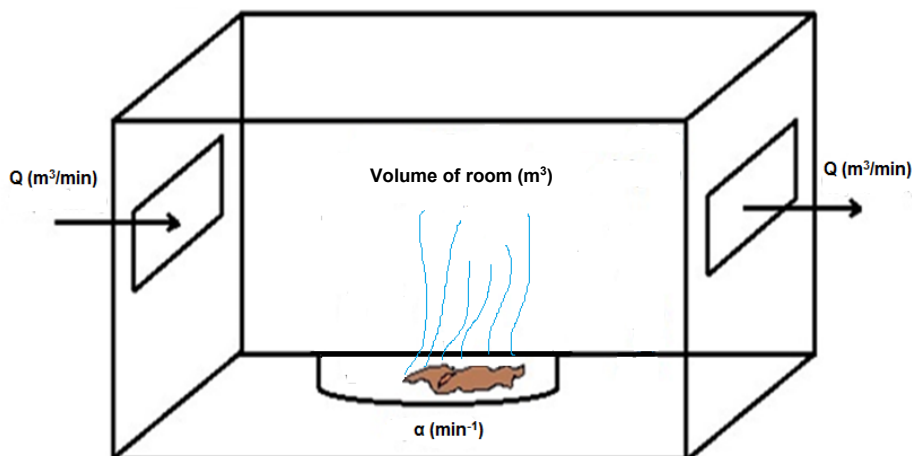
Figure 1. **Diagram of well-mixed room model (adapted from Reinke and Keil, 2009).**

Arnold et al. used the well-mixed room model to evaluate occupational exposure in four different scenarios: solvent recovery, sand casting in an iron foundry, manicure in a nail salon, and cleaning the blades and cover of a mixer in a clean room. The solvents evaluated were, respectively, methylene chloride, phenol and, in the last two cases, acetone. The model underestimated the exposure concentrations in three scenarios by factors of 1.3, 1.45 and 37, and overestimated exposure in one of the four scenarios by a factor of 19 (Arnold et al., 2017b).

Persoons et al. examined the prediction accuracy of the well-mixed room model as part of an assessment of occupational exposure to formaldehyde and toluene in a university hospital pathology lab. Out of 22 evaluations (10 for formaldehyde, 12 for toluene), none of the time profiles generated by the model was comparable to those obtained from concentration measurements taken in real time near the emission sources. In all cases, the model underestimated the exposure, especially with respect to concentration peaks (Persoons et al., 2011).

In a study by Demou et al., the well-mixed room model was used to assess worker exposure to a complex volatile chemical (compound containing hexane, acetone, toluene, methanol, 2-butanone (MEK), xylene, isopropanol) used in the vehicle repair industry. Three exposure scenarios were assessed according to different ventilation airflow rates and generation rates. The model underestimated the actual concentrations measured in the workers' breathing zone by a factor of 1.3 to 6.4 for the scenarios evaluated (Demou et al., 2009).

Keil and Murphy assessed occupational exposure to methylene chloride in a university chemistry lab. They compared the concentrations predicted by the model with the measured concentrations for two exposure scenarios: 20 workers performing extraction and distillation tasks were involved in the first scenario, while 4 others carrying out the same tasks took part in the second scenario. The researchers found that the well-mixed room model underestimated the personal exposure of

the workers for all the scenarios by a factor of two (the measured concentrations were 70% to two times higher than the predicted concentrations) (Keil and Murphy, 2006).

2.1.2 Two-zone model

In contrast to the single-zone model that assumes homogeneous concentrations throughout the workplace room, the two-zone model takes into account the spatial variability of exposure by dividing the room into two zones: a near field (NF) and a far field (FF) (Nicas, 1996). The theory underlying this model is that a person working in the near field is exposed to higher concentrations than someone working in the far field. The advantage of the two-zone model is that it corrects for the underestimation of the exposure predicted by the one-zone model near the emission source (Keil et al., 2009).

The two-zone model is the main one relied on by risk assessors (Jayjock, Armstrong and Taylor, 2011). It is used in a variety of work situations such as the cleaning of equipment parts (Nicas, Plisko and Spencer, 2006), the application of cleaning products (Earnest and Corsi, 2013) and during solvent spills (Jayjock, Logan et al., 2011).

In addition to the contaminant generation or emission rate (G), the two-zone model uses four parameters to estimate the dispersion of contaminants in the near and far fields: the far field volume (VFF for Volume Far Field), the near field volume (VNF for Volume Near Field), the interzonal airflow rate (β) and the general ventilation rate of the room (Q) (Nicas, Plisko and Spencer, 2006).

A diagram of the model is shown in Figure 2.
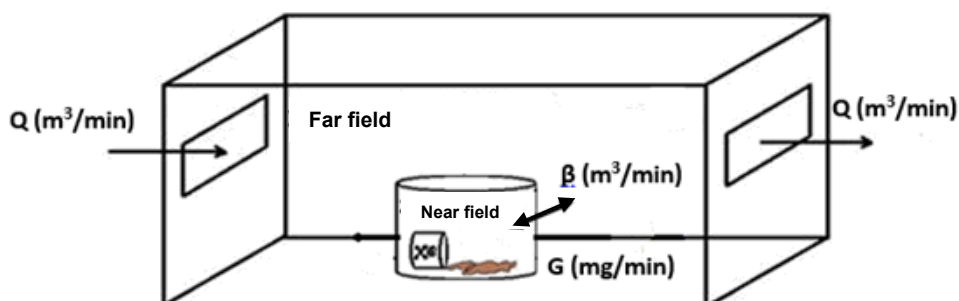
Figure 2.   Diagram of the two-zone model (adapted from Jayjock, Logan et al., 2011).

Volume of far field (VFF)

The VFF is calculated by subtracting the volume of the near field (VNF) from the total volume of the room. The VFFs reported in the literature range from 11.79 m^3 for solvent evaporation scenarios in an experimental chamber (Arnold et al., 2017a) to volumes of 6,500 m^3 for exposure evaluations performed in vehicle repair garages (Williams and Mani, 2015).

Volume of near field (VNF)

The near field corresponds to a virtual field that encompasses a worker's breathing zone and the source of the contaminant emissions. The volume of the near field is defined by researchers based on their expertise and the exposure scenarios being studied.

The geometric shapes used are the hemisphere (Arnold et al., 2017b; Demou et al., 2009; Nicas, 2009; Persoons et al., 2011; Persoons, Maitre and Bicout, 2012; Robbins, Krause, Atallah and Plisko, 2012; Williams and Mani, 2015), the rectangular box (Arnold et al., 2017a; Nicas and Neuhaus, 2008; Nicas et al., 2006a; Plisko and Spencer, 2008), the cube (Hofstetter, Spencer, Hiteshew, Coutu and Nealley, 2013; Nicas, 2016; von Grote, Hurlimann, Scheringer and Hungerbuhler, 2003, 2006) and the cylinder (Earnest and Corsi, 2013; Jayjock, Logan et al., 2011). The volumes reported for the near field range from 0.1 m^3 (Arnold et al., 2017b) to 100 m^3 (von Grote et al., 2003, 2006).

In studies of mechanics moving around spraying aerosols on car carburetors, of spraying paint on a surface, of spilling a litre of solvent, of washing clothes in large washing machines, and of degreasing metal parts in large machines, the reported volumes were, respectively, 7.4 m^3 (Williams and Mani, 2015), 8 m^3 (Hofstetter et al., 2013), 25 m^3 (Jayjock, Logan et al., 2011) and 100 m^3 (von Grote et al., 2003, 2006). The exposure scenarios corresponding to these volumes required broad and/or moving emission sources and the performance of tasks over a large area (involving workers moving around).

In studies of solvent evaporation from a 30 or 50 mL syringe, of cleaning small equipment parts on a work bench, of pouring out small amounts of solvent into a watch glass, and of doing manicures in a nail salon, the volumes reported were, respectively, 0.1 m^3 (Arnold et al., 2017a), 0.5 m^3 (Nicas, 2016), 0.26 m^3 (Keil and Nicas, 2003) and 1 m^3 (Arnold et al., 2017b). The exposure scenarios corresponding to these volumes required restricted and/or fixed emission sources and the performance of localized tasks.

The volume of the near field therefore depends on the size (restricted or broad) and character (fixed or mobile) of the emission source, as well as on the nature (focalized or spread out) of the task being performed. The broader the source and/or the more it moves around, and the larger the area the task is performed in, the greater the volume of the near field.

Interzonal airflow rate (β)

The interzonal airflow rate (β) is the rate at which contaminants are carried between the near field and the far field. This rate depends on the airflow speed at the near field-far field boundary. Nicas (1996) proposed a method for calculating the parameter β as a function of the free near field surface area and the mean interzonal airflow speed (S), according to the following equation:

$$\beta = \tfrac{1}{2}\,FSA \times S \qquad\qquad\qquad (1)$$

where S is in m/min, FSA in m² and β in m³/min.

This calculation method has subsequently been used widely in studies that have been reported on in scientific publications. Researchers measured air speeds in real situations (Arnold et al., 2017b; Earnest and Corsi, 2013; Jayjock, Logan et al., 2011; Keil and Nicas, 2003; Persoons et

al., 2011) or estimated the speeds based on an expert's judgment or on data from the literature (Demou et al., 2009; Gaffney et al., 2008; Nicas, 2016; Nicas et al., 2006a; Plisko and Spencer, 2008; Robbins et al., 2012; Williams and Mani, 2015). The near field surfaces were determined based on the description of the near field volumes and the corresponding surface area calculations. The airflow speeds at the intersection of the near and far fields reported in the literature ranged between 0.9 and 61 m/min, although most publications reported speeds greater than 3.6 m/min.

Last, the reported β values ranged from 0.1 to 191 m³/min, with 80% of the values included between 1 and 30 m³/min. It should be noted that the airflow rate of 191 m³/min represents an especially well-ventilated workplace that the authors describe as being a "semi-outdoor" work environment (Spencer and Plisko, 2007).

Room general ventilation airflow rate (Q)

The general ventilation airflow rate is the rate of airflow allowing the dilution and extraction of contaminants in a room. Rates are estimated on the basis of studies of tracer gas concentration decay (Arnold, Ramachandran and Jayjock, 2009; Arnold et al., 2017a; Hofstetter et al., 2013; Nicas and Neuhaus, 2008; Persoons et al., 2011; Robbins et al., 2012), expert judgment (Earnest and Corsi, 2013; Nicas et al., 2006a; Persoons et al., 2012; von Grote et al., 2003, 2006) or measurement of the air speeds at air intakes and outlets (Arnold et al., 2017b; Keil and Nicas, 2003; Keil, 1998).

The general ventilation rates (Q) reported in the literature ranged from 0.04 (Arnold et al., 2017a) to 3,250 m³/min (Williams and Mani, 2015). In terms of number of air changes per hour (ACH), the rates ranged from 0.3 (Arnold et al., 2017a) to 63 ACH (Nicas and Neuhaus, 2008). The 63 ACH value was measured in a very open garage-like workplace where the doors and windows were open (Nicas and Neuhaus, 2008).

2.1.3 Computational fluid dynamics

Numerical simulation using CFD is well suited to the simulation of occupational exposure. A number of researchers have assessed this method of estimating gas and vapour concentrations (Chauhan, Chauhan, Joshi, Agarwal and Sapra, 2015; Hyun and Kleinstreuer, 2001). Although CFD methods offer flexibility for setting parameters, they require conditions with precisely defined limits, which means a certain degree of condition idealization (Bennett, Feigley, Khan and Hosni, 2000).

The dispersion of a tracer gas (sulfur hexafluoride, SF_6) in a room ventilated by means of four different strategies was studied by He, Yang and Srebric. Experimental measurements and numerical modelling were carried out. The dispersion of SF_6 caused by the airflow and according to the location of the source was studied using a model validated in the same study. The authors claim that a close relationship exists between contaminant dispersion and the global airflow pattern. They also state that the position of the exhaust diffuser can affect the exposure level in the room (He, Yang and Srebric, 2005).

A study of the performance of displacement ventilation systems in a 63 m³ environmental chamber, equipped with swirl diffusers and perforated panels, was conducted by Lau and Chen.

Numerical simulations using a CFD program were compared with experimental measurements taken in the chamber. The researchers used CFD to establish a link between several parameters and indoor air quality. The numerical results showed that the air change rates, ventilation airflow speed and temperature, as well as the number of diffusers used, all had a significant impact on indoor air quality (Lau and Chen, 2007).

Highly toxic chemicals are used in the semiconductor manufacturing industry. Occupational exposure to hydrochloric acid (HCl) fumes and the effectiveness of engineering control measures were studied by Li and Zhou. A CFD program was used to estimate the air speed field and the dispersion of HCl fumes after a leak during a chemical pickling process. A quantitative analysis of the effectiveness of the control measures was presented. Due to the geometric complexity of the modelled room, however, the authors had to make a number of simplifying assumptions (Li and Zhou, 2015).

CFD estimations of occupational exposure are not restricted to indoor spaces. In a recently published paper, Bayatian et al. used CFD to estimate the dispersion of benzene fumes on a 4,800 m^2 oil refinery site. By means of simulations conducted with a commercial software package, they determined the daily exposure dose and associated it with an estimation of the risk of cancer over a lifetime (Bayatian et al., 2018).

2.2   Emission models

To be able to estimate solvent vapour concentrations in the air, the transfer rate from the liquid phase to the gas phase must be known. The parameter required for *a priori* estimation of the evaporation of a pure solvent is its vapour pressure (P_{vap}). A substance with a high vapour pressure is considered to be a volatile substance. The lower the vapour pressure, the harder it is for a compound to evaporate; in that case it is non-volatile or has low volatility. In Europe, a volatile organic compound is defined as a compound having a vapour pressure greater than 0.01 kPa at a temperature of 20°C (European Parliament and of the Council, 21 April 2004).

Two main types of emissions are described when exposure estimation models are used: exponentially decreasing emissions and constant emissions.

2.2.1 Exponentially decreasing emissions

Exponentially decreasing emission models have been described and used to estimate solvent vapour concentrations in the workplace (Jayjock, Logan et al., 2011). These are situations involving the "degassing" of contaminants adsorbed by surfaces (Nicas, 2016; Reinke, Jayjock and Nicas, 2009) or small solvent spill situations (Keil and Nicas, 2003). In these situations, the emission rate is not considered to be constant. It tends to be higher at the start of the emission and then declines progressively over time as a result of the cumulative effect of the cooling of the spilled liquid and the progressive reduction in the surface area initially covered by the liquid. The cooling decreases the vapour pressure of the solvent, which in turn causes a decline in its capacity to vaporize (Keil and Nicas, 2003; Reinke et al., 2009).

The contaminant emission rate can be calculated using the following equation (Keil and Nicas, 2003; Reinke et al., 2009):

$$G_t = \alpha M_0 \, e^{(-\alpha t)} \tag{2}$$

where G_t is the emission rate in mg/min, α the constant or first-order emission rate in min^{-1} and M_0 the initial mass of contaminant present in the liquid (mg).

On the basis of experimental data, Keil and Nicas (2003) have proposed an equation for determining the parameter α as a function of vapour pressure and the ratio of spill surface area to spill volume (Keil and Nicas, 2003). This relationship is expressed in equation 3:

$$\alpha = 0.000524 \times Pvap + 0.0108 \times S/Vol \qquad (3)$$

where P_{vap} = saturation vapour pressure of the solvent in mmHg at 20^{0}C; S = initial surface area of spill of liquid (cm^2), Vol = volume of spilled liquid in cm^3.

2.2.2 Constant emissions

Constant emission models estimate a fixed generation rate for the length of the emission. The generation rate represents the amount of contaminant generated per unit of time (mg/min). These emission rates can be estimated simply on the basis of the relationship of the total amount of contaminant emitted over a set period of time or on the basis of the time it takes for the solvent to evaporate entirely.

To estimate the generation rate, a variety of predictive equations have been proposed. On the basis of experimental data, the INRS has formulated an equation for estimating an emission rate in the case of a liquid spread out on a surface or contained in an open container and subject to a flow of air.

$$G = 22.01 \times S \times V \times MM^{0.4} \times \frac{Pvap}{Patm} \qquad (4)$$

where G is the rate of emission (g/s), S the surface area of evaporation in m², V the air speed at surface level (m/s), MM the molecular mass (kg/mol), P_{vap} the vapour pressure of the liquid in Pa and P_{atm} the atmospheric pressure in Pa.

This equation will never underestimate evaporation speeds, and the authors associate an uncertainty of 33% with the estimates (Triolet and Sallé, 2009). They add that the equation only applies in cases where the level of the liquid is close to the edges of the container and when no "vapour lock" forms above the liquid. A vapour lock would significantly slow the speed of evaporation.

Popendorf proposes an equation for determining the emission rates of a spill of organic solvent (Popendorf, 2006a):

$$G = 0.0706 \times MM \times A \times V^{0.625} \times Pvap \qquad (5)$$

where G is the rate of emission (mg/min), A the evaporation surface area in ft², V the air speed at the surface level (ft/min), MM the molecular mass (g/mol) and P_{vap} the vapour pressure of the liquid in mmHg.

To conclude, many factors can influence a substance's volatility. On the basis of equations 4 and 5 above, it would appear that the temperature of the liquid and the corresponding vapour pressure, the air speed at surface level and the size of the emission source are the key parameters.

2.2.3 Emission of solvent mixtures

The use of mixtures is certainly not an exception in the area of industrial solvents. The emission rate of each constituent of a mixture must therefore be evaluated in order to estimate workplace concentrations. The emission rate in a solvent mixture exposure situation can be estimated in various ways.

Raoult's law (ideal conditions), modified Raoult's law (non-ideal conditions) and Henry's law (aqueous mixtures or mixtures with infinite dilution) are different approaches that can be used to calculate partial pressures in the case of mixtures (Popendorf, 2006b). These partial pressures can be used to estimate the different generation rates of the various components in the place of the vapour pressures of pure substances.

If the conditions are ideal, that is, if the solvents in the mixture are similar (low intermolecular interactions), Raoult's law applies:

$$P_{vapour,i} = X_i \, P_{vapour} \qquad\qquad (6)$$

$P_{vapour,i}$ = vapour pressure of component *i* in the mixture
X_i = mole fraction of component *i* in the mixture
P_{vapour} = vapour pressure of component *i* in pure state

Non-ideality refers to the physico-chemical phenomenon whereby some solvents, when mixed together, usually become more volatile than provided for under Raoult's law owing to the effect of their activity coefficient. These mixtures are said to be "non-ideal." The use of activity coefficients (γi) is reflected in changes in evaporation kinetics and therefore changes in workers' exposure profile (Debia, Bégin and Gérin, 2009; Popendorf, 2006b). Popendorf reports that deviations from ideality can be significant, reaching 10^6 when poorly water-soluble solvents, like n-hexane, are diluted in water (Popendorf, 2006b). That means that the partial pressure of the n-hexane, and therefore its theoretical capacity to evaporate, is 10^6 times greater than when it is in a pure state or slightly diluted.

In the case of non-ideality, Raoult's law therefore must be adjusted using the activity coefficients (γi) of the components of the mixture and applying modified Raoult's law:

$$P_{vapour,i} = \gamma_i \, X_i \, P_{vapour} \qquad\qquad (7)$$

where $P_{vapour,i}$ = vapour pressure of component *i* in the mixture
       γ_i = activity coefficient of component *i* in the mixture
       X_i = mole fraction of component *i* in the mixture
       P_{vapour} = vapour pressure of component *i* in pure state

To calculate the activity coefficient, the UNIFAC method, which counts the functional groups present on the molecules in the mixture, can be used (Popendorf, 2006b). The goal of the method is to be able to predict the equilibrium of the phases in the system, even if no experimental data are available. The UNIFAC model is based on two components in the calculation of γ, i.e., a combinatorial component, γ_c, which takes into account differences between the size and the form

of each molecule in the mixture, and a residual component, γ_R, which accounts for the interaction energy.

Henry's law assumes that the partial pressure of substance i in the mixture depends on a unique coefficient called the Henry constant (Hi) and the mole fraction. This law applies to infinitely dilute aqueous solutions, in other words, when the activity coefficient described earlier becomes a constant (Popendorf, 2006b). Henry's law can be written as follows:

$$P_{vapour,i} = H_i \times X_i. \tag{8}$$

where $P_{vapour,i}$ = vapour pressure of component *i* in the mixture
        H_i = Henry's constant
        X_i = mole fraction of component *i* in the mixture

2.3   Validation of models

A number of researchers have compared experimental data and estimated data for the purpose of validating the use of models to measure occupational exposure. The calculation of a ratio of predicted to measured concentrations is reported in several studies (Arnold et al., 2017b; Hofstetter et al., 2013; Nicas, 2016; Plisko and Spencer, 2008; Spencer and Plisko, 2007). In these studies, the predictions/measurements ratios range from 0.03 to 8.26.

The ASTM D5157-97 method compares predictions with measurements based on five criteria: (i) the correlation coefficient (r), (ii) the slope of the regression line (b), (iii) the *y* intercept of the regression line (a), (iv) the normalized mean square error, and (v) the normalized bias. A model's performance is deemed to be sufficiently accurate when the following five conditions are all met simultaneously: (i) correlation coefficient r ≥ 0.9; (ii) slope of the regression line 0.75 ≤ b ≤ 1.25; (iii) *y* intercept a ≤ (0.25 x mean of the predicted concentrations); (iv) normalized mean square error ≤ 0.25; (v) normalized bias ≤ 0.25 (Arnold et al., 2017a; ASTM, 1997).

Arnold et al. used this method to evaluate the predictive performance of the two-zone model for 324 pairs of predicted and measured concentrations (n = 81 pairs for the near field, n = 243 pairs for the far field) resulting from tests conducted with three solvents. The performance was deemed sufficiently accurate (validation of the five criteria simultaneously) in 11% (acetone), 19% (2-butanone) and 33% (toluene) of the evaluations done for the near field, and in 69% (toluene), 91% (2-butanone) and 96% (acetone) of the evaluations carried out for the far field. Keil and Nicas (2003) also used this method and reported that the performance was sufficiently accurate (validation of the five criteria simultaneously) only for the evaluations done for the far field.

Furthermore, Arnold et al. validated the use of the models using the AIHA exposure control categories (Arnold et al., 2009; Arnold et al., 2017a). These categories are: (i) category 1 for highly controlled exposures (95th percentile ≤ 0.10 x occupational exposure limit (OEL)); (ii) category 2 for well-controlled exposures (0.10 x OEL ≤ 95th percentile ≤ 0.50 x OEL); (iii) category 3 for controlled exposures (0.50 x OEL ≤ 95th percentile ≤ OEL); (iv) category 4 for poorly controlled exposures (OEL ≤ 95th percentile). Validation consists in verifying whether the predicted and measured concentrations are ranked in the same categories.

In the study by Arnold et al.*,* 27 evaluations were performed. For the near field, the model accurately predicted the categories in over 74% of situations. For the far field, the model correctly predicted them in 96% of cases (Arnold et al., 2017a).

In another study by Arnold et al., eight short (15-minute) evaluations were done, i.e., four for the near field and four for the far field. The model correctly predicted the categories in 75% of the evaluations done for either of the two fields (Arnold et al., 2017b).

2.4   Limitations of models

The attraction of the physico-chemical models is that they are flexible, and results are readily available. They also offer insight into the relationships that exist between contaminant emissions, airflows in the room and the resulting exposure concentrations (Bertrand and Vincent, 2010a; Persoons et al., 2011). On the other hand, their main drawback is their simplification and the potential lack of understanding associated with the estimation of some input parameters (Keil, 2000).

The physico-chemical models frequently used in industrial hygiene (one- or two-zone models) do not include certain parameters that can influence exposure concentrations, such as the position of the ventilation system in relation to the emission source, the geometry of the emission source, the position and movements of the worker, and body temperature (Earnest and Corsi, 2013; Persoons et al., 2011; Plisko and Spencer, 2008; Spencer and Plisko, 2007).

In addition, some input parameters used in the models are difficult to estimate. This is true, for instance, for determining the interzonal airflow rate β, which is described as being the most critical parameter for a two-zone model (Earnest and Corsi, 2013; Keil and Murphy, 2006; Keil, 2000; Persoons et al., 2011). Estimating the contaminant generation rate is also regarded as a key factor in the accuracy of physico-chemical models (Persoons et al., 2011, 2012). These emission rates can be especially complex to estimate, particularly in exponentially decreasing emission situations or for solvent mixtures (Popendorf, 2006b). Persoons et al. note that the performance of the various models is limited by the lack of available data on emission sources and that there is still insufficient experimental data (Persoons et al., 2012).

3. RESEARCH OBJECTIVES

3.1   General objective

The purpose of this project was to improve the accuracy of the occupational hygiene models used to estimate workplace exposure to solvent vapours.

3.2   Specific objectives

The project's specific objectives were to:

- Propose a method for estimating the generation rate in the event of small spills

- Validate the concept of non-ideality and integrate it into the calculation of the generation rate for solvent mixtures

- Evaluate the ventilation parameters of the two-zone model in various work situations

4. METHOD

The method was structured around two stages: small-scale laboratory testing and human-scale laboratory testing. The purpose of the first stage was to propose an improved method for estimating the generation rate in the case of small spills and to incorporate the concept of non-ideal mixtures into the calculation of the emission rate for solvent mixtures. The purpose of the second stage was to assess the ventilation parameters of the two-zone model in various work situations

4.1   Stage I – Small-scale laboratory testing

4.1.1 Experimental determination of emission rates α

4.1.1.1 Equipment

Five solvents covering a wide range of vapour pressures were used under a variety of experimental conditions. These solvents were acetone, hexane, 2-butanone (MEK), 2-propanol (IPA) and toluene.

A scientific analytical balance (Sartorius CPA423S) connected to a computer was used for the gravimetric measuring of the loss of mass due to solvent evaporation. A VelociCalc Plus TSI meter was used to measure environmental parameters such as ambient temperature, relative humidity and airflow speed around the emission source.

4.1.1.2 Experimentation

The experimentation consisted in conducting solvent evaporation tests in a controlled environment (temperature, humidity, air speed). It was done in two stages. In the first stage, the tests were performed on a lab bench, while in the second, they were carried out under a lab fume hood to assess the effect of airflow speed on emission rates.

To determine the emission rates, small spill scenarios were simulated with different volumes of solvents (1 mL, 3 mL, 6 mL, 10 mL, 20 mL) and in different types of spill equipment (12.4 cm diameter watch glasses and 10 cm diameter Petri dishes).

The spill equipment was set out beforehand on the analytical balance so that the mass of solvent remaining could be recorded automatically every 15 seconds. The tests were conducted until all the solvent had evaporated. For each test, the diameter of the spill field was measured to calculate the spill surface area. The tests were done three times to verify the reproducibility of the results. The masses recorded were imported directly into an Excel file, where emission rates were determined in accordance with the method used by Keil and Nicas (2003). This method consists in calculating the slope of the mass decay curve established as a function of time (t) and as a function of the natural logarithm of the ratio of the remaining mass over the initial mass.

The laboratory tests were performed at relatively constant temperature and pressure (22 to 24°C), with relative humidity of between 20% and 40%.

4.1.2 Incorporation of concept of non-ideal mixtures into calculation of generation rate for solvent mixtures

The solvents used in this stage of the testing were toluene, butan-2-one (MEK), propan-2-ol (IPA), methanol and acetone. They were chosen because they cover a broad range of vapour pressures and because they are found in commercial mixtures identified in the literature, including aqueous cleaners. Emission rates were first determined for the pure solvents following the method indicated in section 4.1.1. Then various mixture scenarios were drawn up. Aqueous mixtures, comprising solvent percentages in mole fraction of 1%, 5% and 10%, were selected for the five solvents.

The activity coefficients of each mixture component were determined using UNIFAC Activity Coefficient calculating software in which data are entered that include the names of the components of the mixtures being studied, their mole fraction and temperature. The design of the software is based on the principle of the UNIFAC model (UNIQUAC Functional Activity Coefficient) (Choy and Reible, 1996). The mole fractions of components i in the mixture were then calculated by the following equation:

$$\alpha_m = \alpha_{exp} \times X_i \tag{9}$$

where α_m is the coefficient α of substance i in the mixture, α_{exp} is the coefficient α of the pure substance, and X_i is the mole fraction of substance i in the mixture.

To account for the fact that the mixture may be non-ideal, coefficients γ_i were introduced into equation 9, as follows:

$$\alpha_{m,corr} = \alpha_{exp} \times X_i \times \gamma_i \tag{10}$$

4.1.3 Measurement of concentrations in small-scale tests

A gas phase chromatography system, connected to a thermal conductivity detector(TCD), i.e., the GC Variant CP2003-P with a gas vector (helium), an injector and a column having a dimethylpolysiloxane stationary phase (CP-Sil-5), was used to measure the solvent concentrations in a box built for the project. Analytical methods were developed for each solvent and for each mixture in order to optimize the detection parameters.

Spill tests were conducted at the centre of a 42 cm x 44 cm x 46 cm box. Air was sampled 20 cm above the spill area by means of a Tygon® pipe connected to a pump (0.04 L/min) (Figure 3). A second pump, with a throughput of 2.5 L/min, was used to extract air to ventilate the box, i.e., the equivalent of two air changes per hour (Figure 4).
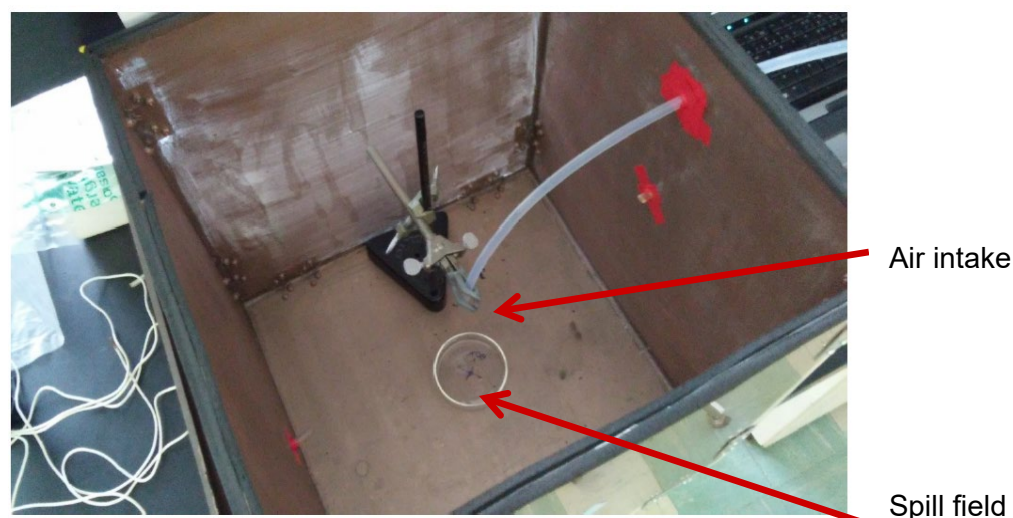
Figure 3.   Set-up inside box.
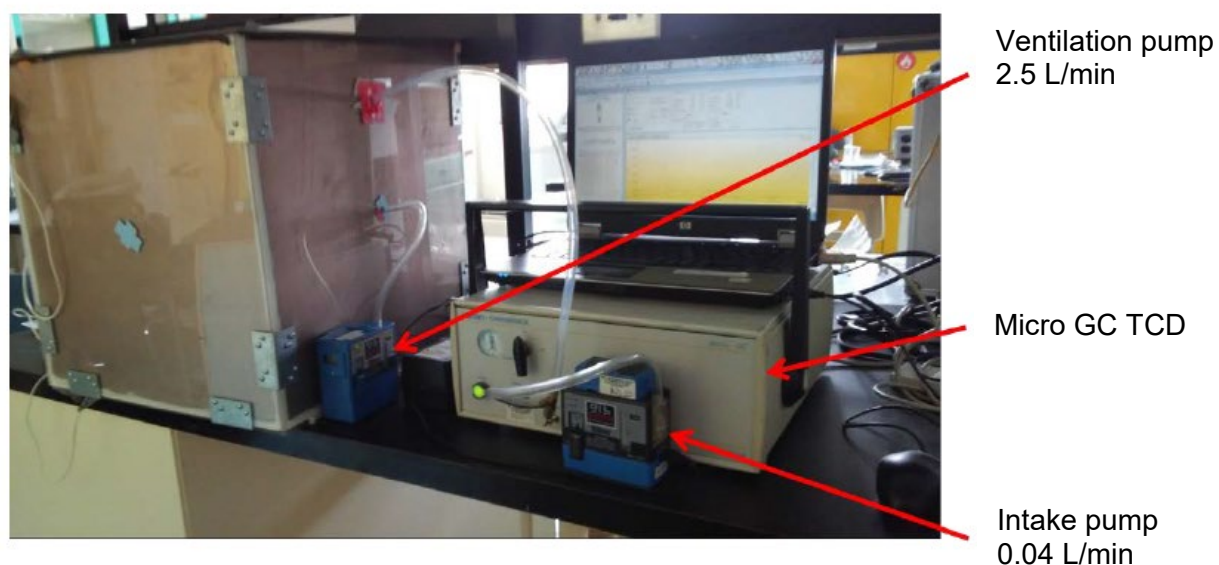
Figure 4.   Set-up with GC, intake pump and ventilation pump.

A total of 18 scenarios were conducted: 4 for pure solvents, 12 for aqueous mixtures (10%, 5% and 1%) and 2 for organic solvent mixtures.

4.1.4 Modelling of concentrations

To predict the concentrations, IH Mod software and the well-mixed room model with exponentially decreasing emissions were used, assuming both ideality (use of non-corrected emission rates) and non-ideality (use of emission rates corrected by activity coefficients). The model input parameters were the volume of the box (0.085 m³), the ventilation rate Q (0.15 m³/h), the initial mass M_0 of the solvent and the coefficient α (measured or estimated using mole fractions and activity coefficients).

4.1.5 Data analysis for small-scale tests

The measured concentrations were compared graphically with the values predicted by the model. The parameters of the concentration profile at peak concentration (C_{max}) and at the time required to reach it (T_{max}) were recorded for each test and for each concentration. Ratios of the measured maximum concentrations to those estimated were then calculated.

Multiple linear regression analyses were conducted to assess the influence of various explicative variables on α values. The significance level of the tests was set at 5% and the analyses were carried out using the SPSS software package.

4.2   Stage II – Laboratory testing in a human-scale room

At this stage of the project, the task was to assess certain determinants likely to influence solvent vapour concentrations under different experimental conditions on a human scale. The measured concentrations were compared with concentrations modelled using the two-zone model.

4.2.1 Description of environment and instrumentation

The assessment was conducted in a human-scale room having a volume of 53.4 m^3 (Figure 5). Two strategies were used to ventilate the room. The first involved blowing air through the floor by means of a 20.3-cm diameter swirl diffuser. The floor ventilation system was able to provide a maximum airflow rate equivalent to 2.8 air changes per hour (ACH). The second ventilation strategy was based on blowing air through the ceiling. This system could blow air at a maximum airflow rate of 5.2 m^3/min, i.e., 6 ACHs. In both cases, the airflow rate was controlled by a variable-frequency drive connected to the fans. The return-air grille, measuring 0.6 m x 0.12 m, was located in the ceiling of the room.

Different tests were simulated by varying:

- the scenario, according to four configurations: (1) evaporation on a table, (2) spill on the floor, (3) application of solvent using a rag followed by manual cleaning and (4) spraying of solvent followed by manual cleaning;

- the ventilation rate, according to three scenarios: low rate (L): 0.8 ACH (12 L/s); high rate (H): 2.3 ACH (32 L/s); and very high rate (VH): 4.5 ACH (64 L/s);

- the position of the air vent (floor as opposed to ceiling).

As each test was repeated three times, a total of 57 simulations were performed, with 19 different combinations (the only combination that could not be performed was "spray – high rate ventilation – air intake through the floor").
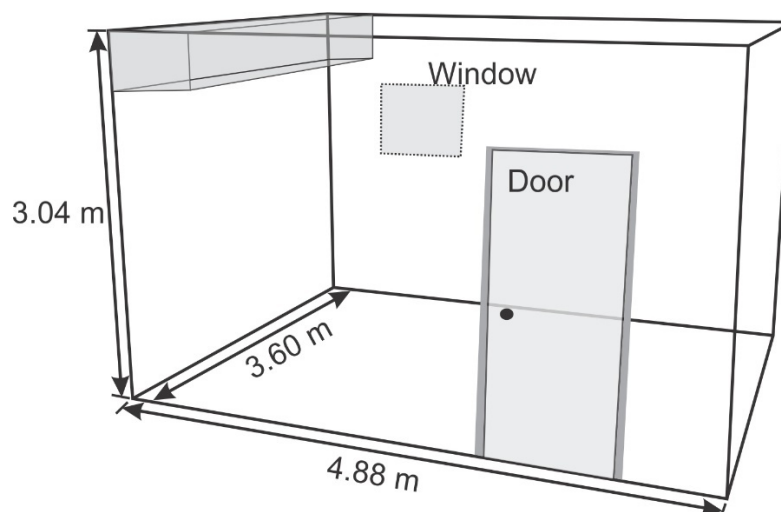
Figure 5.   Diagram of model room.

The evaporation and spill tests were conducted using a watch glass containing 20 mL of acetone placed on an analytical balance. The gravimetric measurement of the loss of mass of 20 mL of acetone was used to determine the exponentially decreasing emission rates of the contaminants in the air of the room, following the method of Keil and Nicas (2003) (see Method, section 4.1.1) and the constant emission rate by determining the time required for the evaporation of 75% of the initial mass of the solvent. The cleaning tests were performed with the help of an operator who simulated cleaning an aluminum part with a rag. Approximately 2 mL of acetone were added (manually or by spraying), every 10 minutes, for a total of 20 mL per test. The emission rates of the tests with manual application and spraying could not be calculated gravimetrically, but estimates were made based on the quantity of solvent and the duration of the tests for G and based on the evaporation test results for α.

The air intake ventilation rates were measured using an air capture hood (TSI). The air speeds at the virtual interzonal boundary were measured using an air velocity meter (VelociCalc 9545, TSI) at a distance of approximately 50 cm from the source in two opposing directions. The tests were done at relatively constant temperature and pressure (24°C, 769 mmHg), with mean relative humidity of 40%.

Solvent vapour concentrations were measured using direct-reading instruments (DRI) placed in the near field (NF, 30 cm from source) and far field (FF, rest of the room).

For the near field, two photoionization detectors (PIDs) (MiniRae, Rae Systems, Sunnyvale, CA) were used to measure the concentrations (Figure 6).
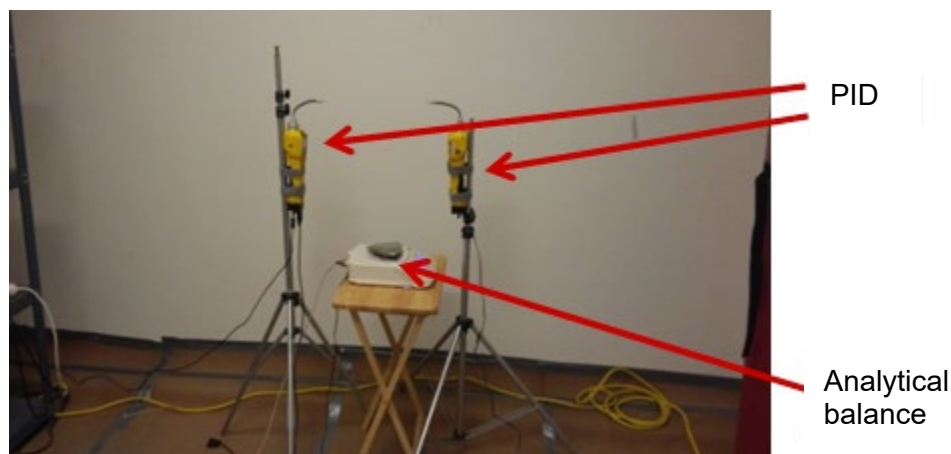
Figure 6.   Measurement of exposure concentrations in the near field.

For the far field, two Varian micro gas chromatographs (CP 2003 and CP 490), connected to thermal conductivity detectors (TCD), were used to measure concentrations at different distances from the emission source. The first measurement point was 1.2 m from the source, near a wall of the room (Figure 7), while the second point was 3 m from the source, near the air outlet (Figure 8). Before the study, calibrations and comparative measurements were performed with the direct-reading instruments to ensure the different instruments were responding homogeneously.
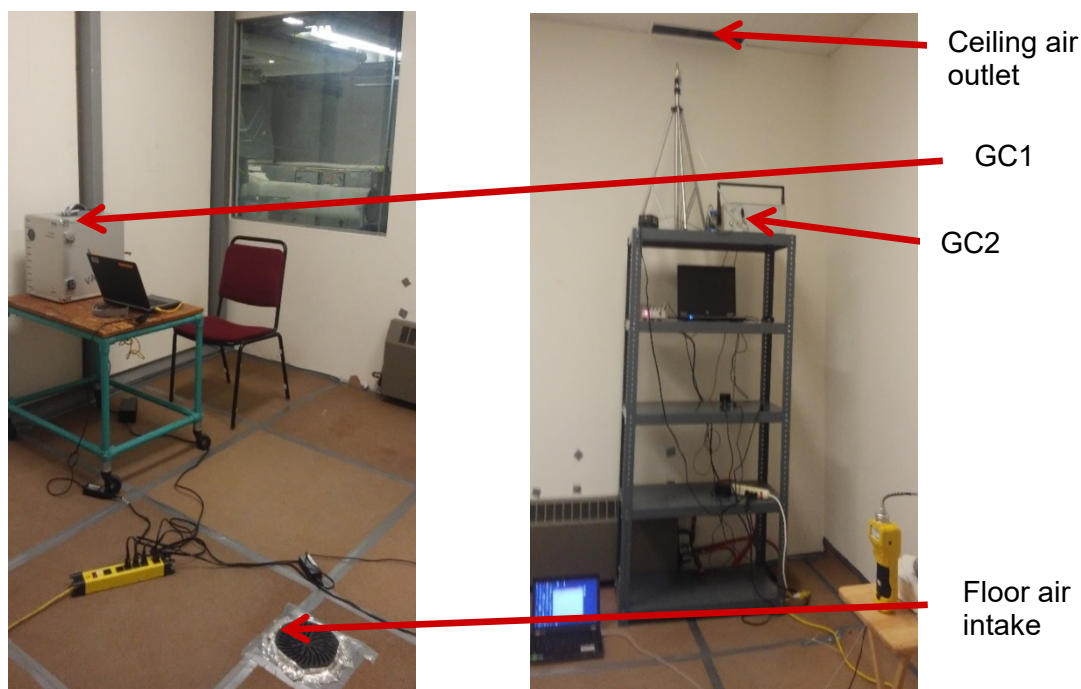
Figure 8.   First measurement point for far field.

Figure 7.   Second measurement point for far field.

Comparisons were done at concentrations of 200 ppm and 1,000 ppm. The concentrations reported by the GC method at these two levels gave concentration measurements higher by 7% and 16%, respectively, in relation to the concentrations indicated by the photoionization methods.

4.2.2 Modelling of concentrations using the two-zone model with exponentially decreasing emissions or constant emissions

For each test, modelling of concentrations in the near and far fields was done using IH Mod software. The input parameters of the models were the initial masses M_0 of acetone, i.e., 20 mL or 15.8 g, the emission rates α (min^{-1}) or the emission rates G (mg/min) calculated by gravimetry or estimated, the volume of the room (53.4 m^3), the geometry and volume of the NF, the air speed at the interzonal boundary determined experimentally (S), and the rate of general ventilation (Q) determined by the measurement of the airflow rate at the air intake. The geometry of the near field chosen for this study was a half sphere.

4.2.3 CFD modelling of concentrations

The modelling of air movements and the dispersion of gas contaminants were done using Fire Dynamics Simulator software (FDS, release 6.6). Developed by the National Institute of Standards and Technology (McGrattan et al., 2017b), FDS is based on the large eddy simulation method. The conservation equations solved in FDS include the modified Navier-Stokes equations for low-speed, thermally induced flows, combined with a passive scalar transport equation for gas contaminants. The transport equation is as follows (McGrattan et al., 2017a):

$$\underbrace{\frac{\partial}{\partial t}\left(\rho Z\right)}_{transient\ term} + \underbrace{\nabla \cdot \left(\rho Z \vec{U}\right)}_{convection} = \underbrace{\nabla \cdot \left(\rho D \nabla Z\right)}_{diffusion} + \underbrace{\dot{m}'''}_{\substack{addition \\ of\ mass}} \tag{11}$$

where Z represents the mass fraction of the gas contaminant in the air expressed in kg/kg of air, $\vec{U}$ is the airflow velocity, and the mass density of the air is represented by ρ. The contaminant's diffusion coefficient (D) is the sum of the Brownian diffusion coefficient and the eddy diffusion coefficient divided by the turbulent Schmidt number, which was set at 0.7 for all the simulations. The right-hand term $\dot{m}'''$ is a source term representing the addition of mass in the computational domain following the evaporation of droplets. However, this term is not considered in the numerical simulations, as solvent evaporation occurs through a boundary condition.

The room, modelled in FDS, is shown schematically in Figure 9. The boundary conditions defined in the digital code include the adherence condition (airflow speed of zero) on all the solid walls of the rooms. Note that all the simulations were performed under isothermal conditions. In other words, the walls, the floor and the ceiling were considered to be adiabatic, and the air blowing temperature was assumed to be identical to the temperature of the air in the room. The rationale for this approximation is that the temperature difference between the blowing air and the air in the room was less than 2°C for all the experimental tests.
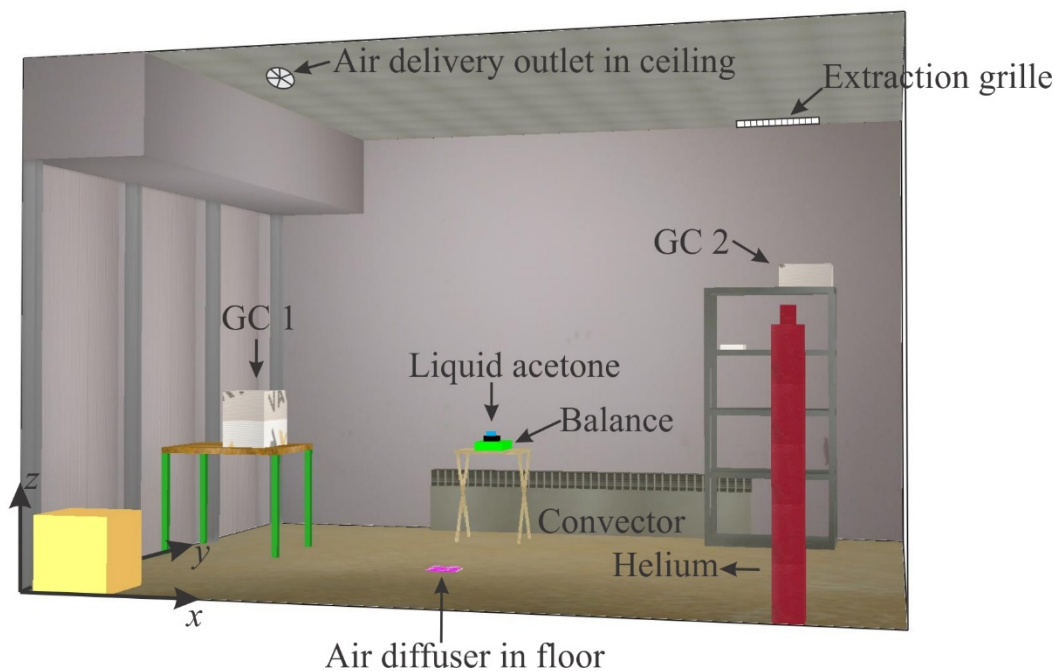
Figure 9.   **Model room.**

Solvent evaporation was modelled in the code as a boundary condition at the surface of the watch glass whereby a predetermined mass of solvent expressed in kg/(m$^2 \times$s) was injected into the ambient air. This mass flow of evaporation was determined experimentally for each tested scenario based on the variation in the mass of the solvent as a function of time. Since the rate of emission decreases over time, the initial mass flow is multiplied by a dimensionless coefficient that varies over time ($0 \leq f(t) \leq 1.0$) to account for the decline.

Numerical simulations were carried out on a workstation having two Xeon E5-2643 processors (Intel, CA, USA). The calculation time required to model the dispersion of acetone over one hour ranged from 40 to 60 hours, depending on the air delivery rate in question. It is therefore essential to choose an "optimal" mesh density so that results of an acceptable level of precision can be obtained within a reasonable length of time. However, the mesh density of the air delivery grilles and the watch glass had to be refined in order to represent them in the space as accurately as possible. The characteristics of the mesh chosen for the simulations are given in Table 1.

Figure 10 shows the mesh used in the vertical plane (*y-z*) for ventilation through the floor. It can be seen in the figure that the mesh density is greater in the lower part of the room, as that is where the concentration and speed gradients are the highest.

Table 1.   Characteristics of mesh chosen for simulations.

	Volume of an element in m³ (minimum/maximum)	Number of nodes in computational domain
Room studied	8.0×10^{-6} / 6.4×10^{-5}	1,384,094

Figure 10.   Spatial discretization in the _y-z_ plane (ventilation through the floor).

4.2.4 Data analysis

For all the experiments conducted in the human-scale room, mean concentrations were calculated over a period of time corresponding to the evaporation of 98% of the solvent mass based on experimental PID and GC data, as well as on estimates provided by the two-zone model. For the rag application and spray scenarios, calculation times corresponded to the time of the last application plus 10 minutes. These concentrations were also referred to as C_{98} concentrations.

The radius of the near field (half sphere) was adapted to obtain estimated concentrations (C_{98}) as close as possible to the mean of the two concentrations measured in the near field for each test. Using experimental air speeds, this stage also served to determine the corresponding value of coefficient β, according to equation 1. An Excel worksheet was developed on the basis of the two-zone model to allow users to perform this radius optimization.

Statistical analyses were conducted to determine whether significant differences existed between the near and far concentrations. Variance and multiple linear regression analyses were also performed to assess different variables in the models. The significance level of the tests was set at 5% and the analyses were carried out using the SPSS software package.

5. RESULTS

5.1   Stage I – Small-scale laboratory testing

5.1.1 Experimental determination of emission rates α

The calculated α coefficients (mean of three tests) for the five solvents and for the five volumes tested are given in Table 2. The highest coefficients were measured for n-hexane, and the lowest for toluene. The coefficients ranged between 0.0032 min^{-1} and 0.1553 min^{-1}. Figure 11 shows the same concentrations as a function of spill volumes. The α coefficients decrease when the volumes increase, according to an exponential decline.

Table 2.   Coefficient α (min^{-1}) values measured with watch glass.

		Volume				
	P_{vap} (mmHg)	1 mL	3 mL	6 mL	10 mL	20 mL
Acetone	185	0.1423	0.0681	0.0394	0.0256	0.0177
n-Hexane	124	0.1553	0.0746	0.0458	0.0327	0.0258
MEK	78	0.0656	0.0331	0.0203	0.0152	0.0099
2-Propanol	33	0.0303	0.0160	0.0094	0.0065	0.0041
Toluene	21	0.0267	0.0131	0.0080	0.0059	0.0032

The relationships between α coefficient values and vapour concentrations for 3 mL and 20 mL are shown in Figure 12. The two correlations are significant, with coefficients of determination of more than 60%. The two relationships are different, however, as the slope of the curve for the 3 mL spills is four times steeper.

Figure 13 illustrates the α coefficients calculated with and without ventilation for spill volumes of 1 mL. The speeds in the absence of ventilation ranged from 0.01 to 0.03 m/s, while those with ventilation varied from 0.2 to 0.25 m/s. The α coefficients were 65 to 100% higher with ventilation. Figure 14 gives the α coefficients calculated with different air speeds (0.05 to 2 m/s) for acetone spill volumes of 10 mL and 20 mL. Higher air speeds produced a significant increase in the α coefficients, which rose from 0.02 min^{-1} (0.05 m/s) to 0.13 min^{-1} (2 m/s) for the 20 mL spills.

Figure 15 gives the α coefficients for acetone, calculated on the basis of spill volumes and the lab apparatus used, either the watch glass or the Petri dish. A good correspondence between the coefficients, regardless of the apparatus, can be seen. The only α coefficients that differ are those for a 1 mL spill.
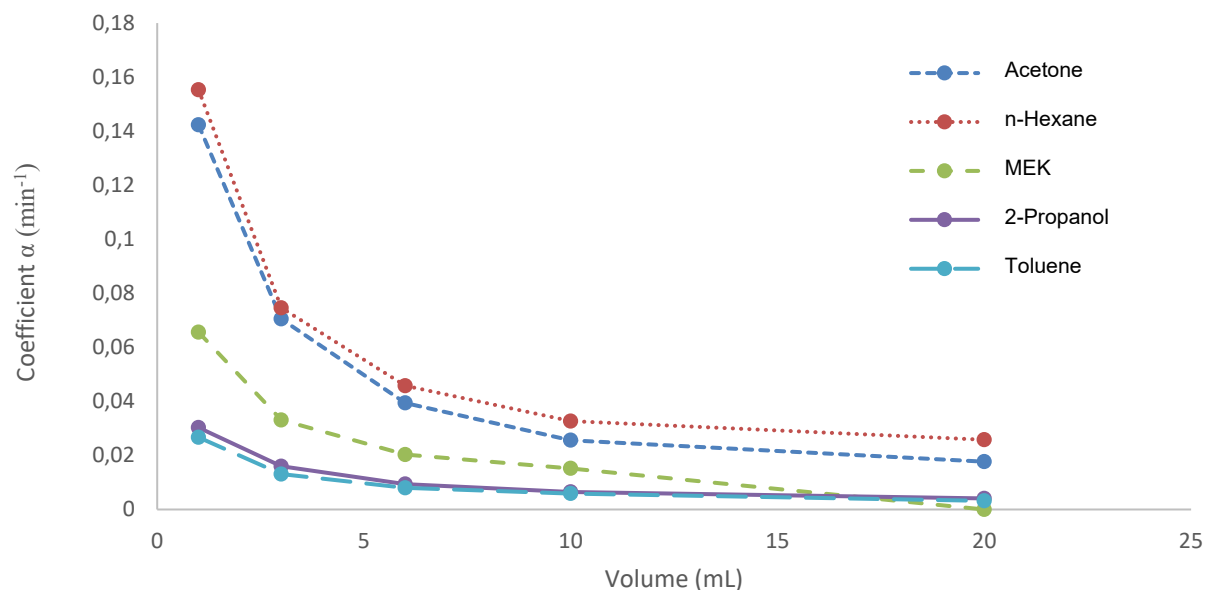
Figure 11.   Coefficient *α* values as a function of evaporation volumes.
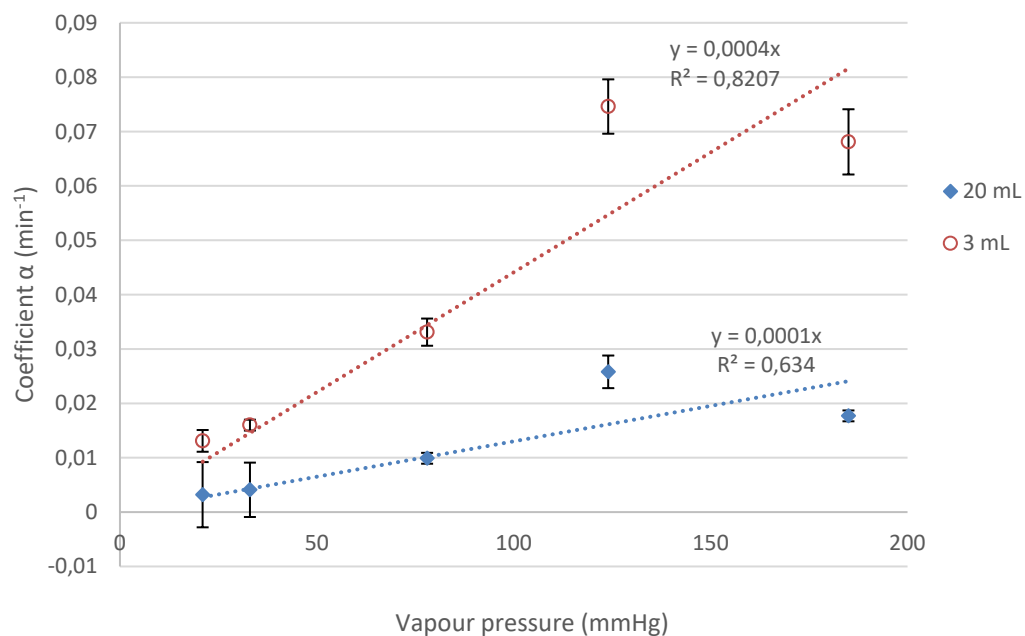
Figure 12.   Mean of coefficient *α* values and standard deviations as a function of solvent vapour pressure for 3 mL and 20 mL volumes.
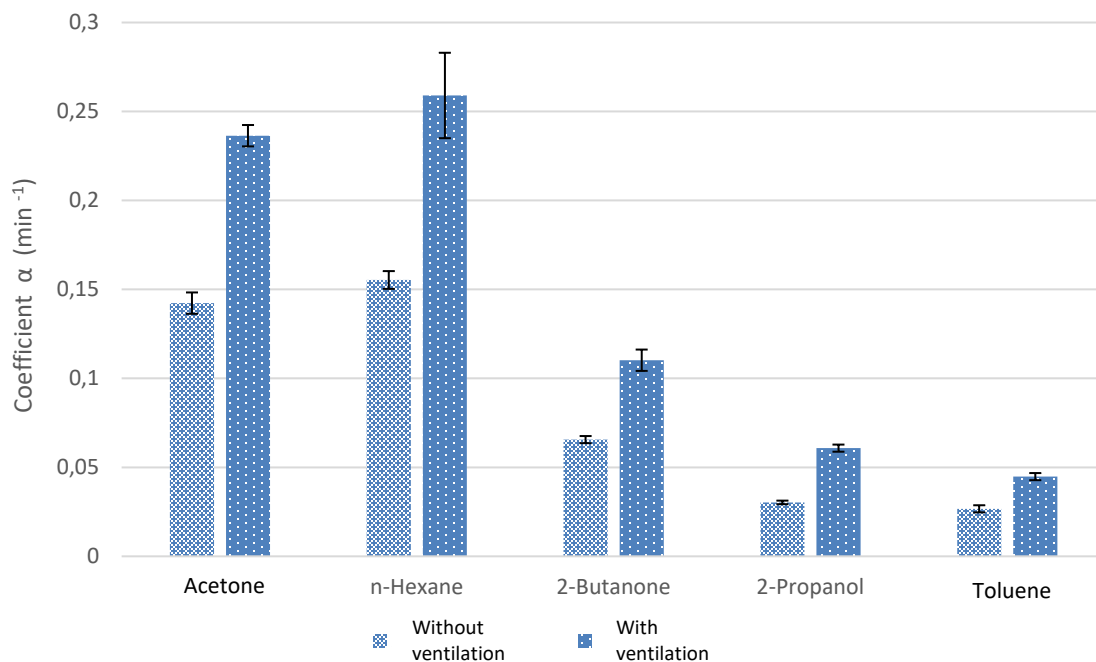
Figure 13.   Mean of coefficient *α* values and standard deviations as a function of ventilation for 1 mL volumes.
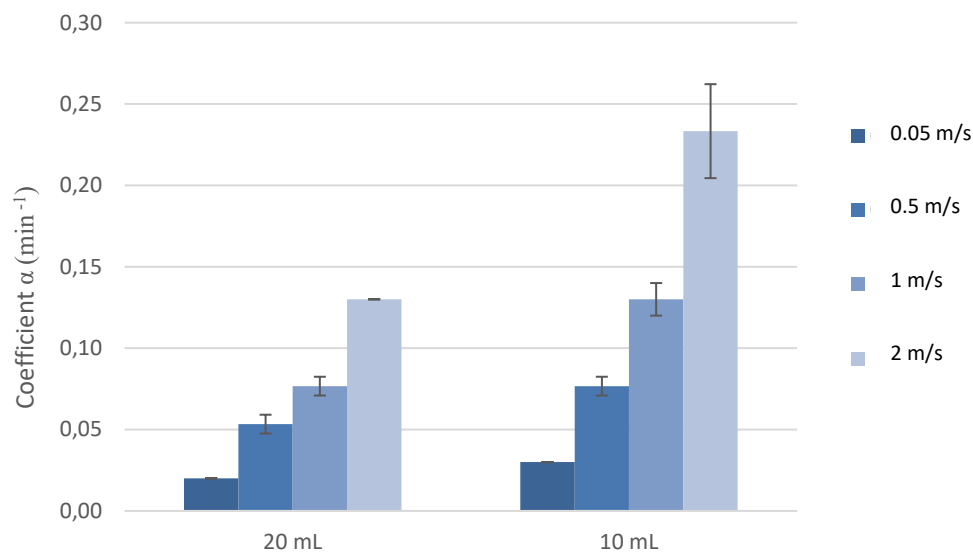
Figure 14.   Mean of coefficient *α* values and standard deviations for acetone as a function of air speeds above the evaporation field.
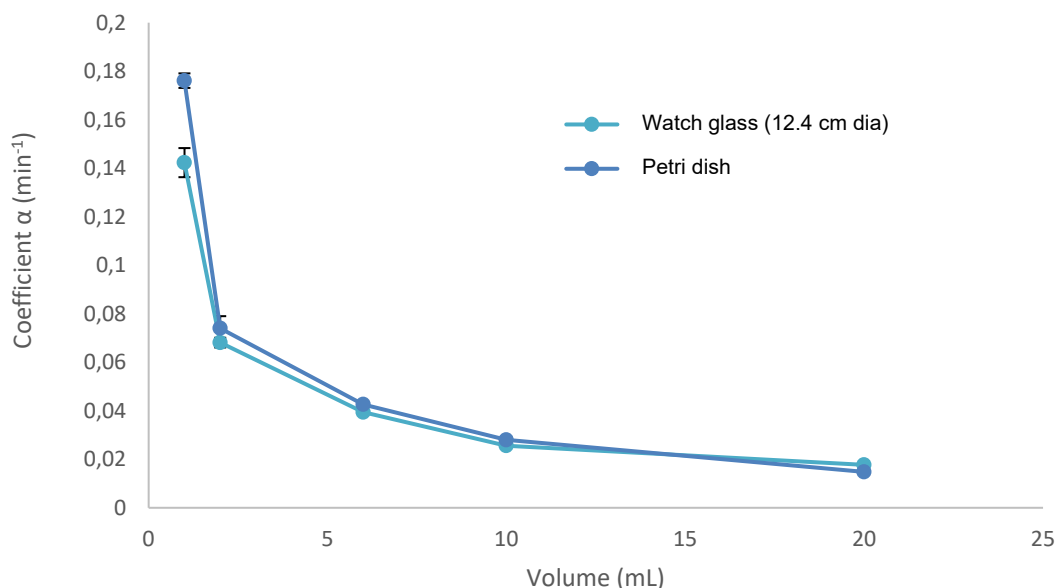
Figure 15. **Mean of coefficient *α* values and standard deviations for acetone as a function of volume and lab apparatus.**

Step-by-step regression analyses were performed based on the data in Table 2 with the variables vapour pressure and surface area/volume ratio. The variable surface area/volume ratio was used by Keil and Nicas to predict the α parameters.

Equation 12 sets out the parameters of the regression model equation as a function of the variable vapour pressure (P_{vap}). The coefficient of determination of this model indicates that 68% of the variability in the α coefficient values can be explained by vapour pressure.

$$1000 \times \alpha = 0.387 \times Pvap \tag{12}$$

where P_{vap} is in mmHg.

Equation 13 sets out the parameters of the regression model equation as a function of the variables vapour pressure (P_{vap}) and surface area/volume ratio (*Surf/Vol*). The multiple coefficient of determination indicates that 75% of the variability in the α coefficient values can be explained by the variables and that the addition of this variable significantly enhances the model.

$$1000 \times \alpha = 0.188 \times Pvap + 3.861 \times \left(\frac{Surf}{Vol}\right) \tag{13}$$

where α is in min⁻¹, P_{vap} in mmHg, *Surf* in cm², and *Vol* in mL.

5.1.2 Experimental measurements of solvent vapour concentrations and comparison with predictions from the single-zone model

Pure solvents

Figures 16, 17, 18 and 19 show the profiles of the concentrations measured in the small-scale tests as well as the profiles of the concentrations estimated by modelling using the single-zone model with exponentially decreasing emissions. In the four tests, a strong relationship can be seen between the two concentration profiles over time. An underestimate of the concentration peaks in the cases of methanol and MEK (figures 17 and 19) is to be noted, however.

The maximum concentrations reached during the tests ranged from 1400 to 2600 ppm. The four solvent vapour concentration peaks measured (corresponding T_{max} indicated in parentheses) were, respectively, 2527 ppm (34 min), 2122 ppm (13 min), 1554 ppm (20 min) and 1622 ppm (21 min) for the solvents toluene, methanol, acetone and MEK. The corresponding peaks estimated by the single-zone model were, respectively, 2383 ppm (28 min), 1430 ppm (12 min), 1550 ppm (12 min) and 1153 ppm (16 min).
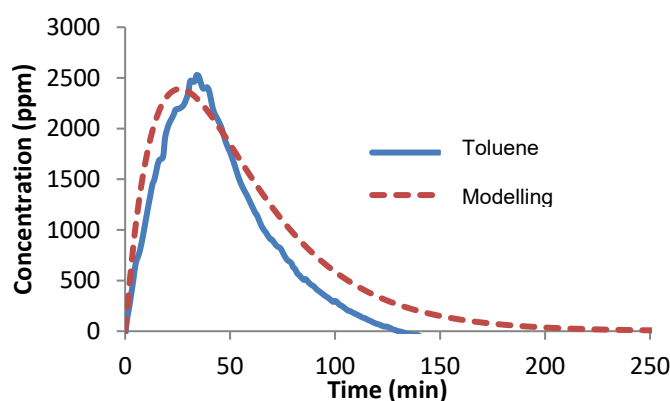
Figure 16.   Experimental and modelled concentration profiles of evaporation of 0.5 mL of toluene.
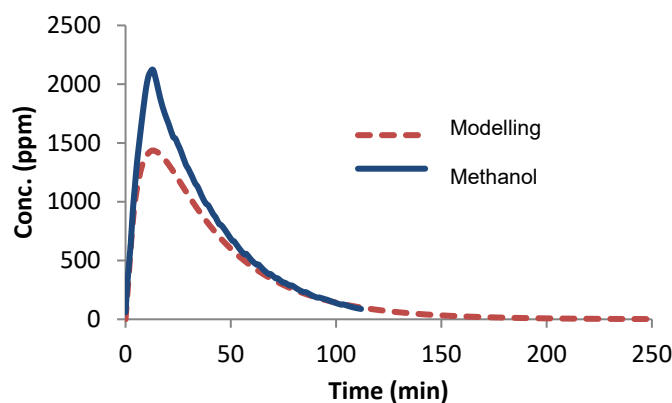
Figure 17.   Experimental and modelled concentration profiles of evaporation of 0.3 mL of methanol.
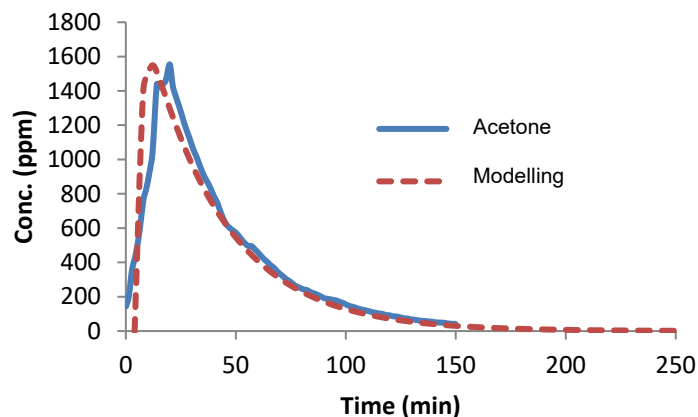
Figure 18.   **Experimental and modelled concentration profiles of evaporation of 0.5 mL of acetone.**
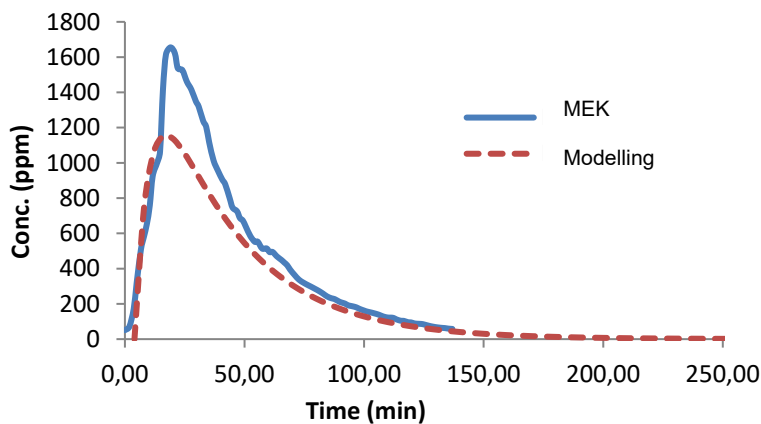
Figure 19.   **Experimental and modelled concentration profiles of evaporation of 0.5 mL of MEK.**

Aqueous mixtures

MEK

Figure 20 shows the profiles of the measured MEK concentrations as well as the profiles of the concentrations estimated by modelling using the single-zone model with exponentially decreasing emissions, indicating an emission rate corrected by the activity coefficient and a non-corrected emission rate. Activity coefficients of 8.5, 10 and 20 were used respectively for the modelling of the 10%, 5% and 1% mixtures.

The concentrations modelled with correction by activity coefficients were closer to the experimental measurements than the non-corrected concentrations were. The maximum concentrations measured (T_{max}) were 1209 ppm (20 min), 1076 ppm (18 min) and 676 ppm (47 min). The concentrations estimated by modelling that took correction into account were 1012 ppm (11 min), 879 ppm (20 min) and 587 ppm (32 min), respectively, for the 10%, 5% and 1% mixtures. The concentrations estimated by modelling that did not take correction into account

were 415 ppm (44 min), 264 ppm (56 min) and 73 ppm (105 min), respectively, for the 10%, 5% and 1% mixtures.
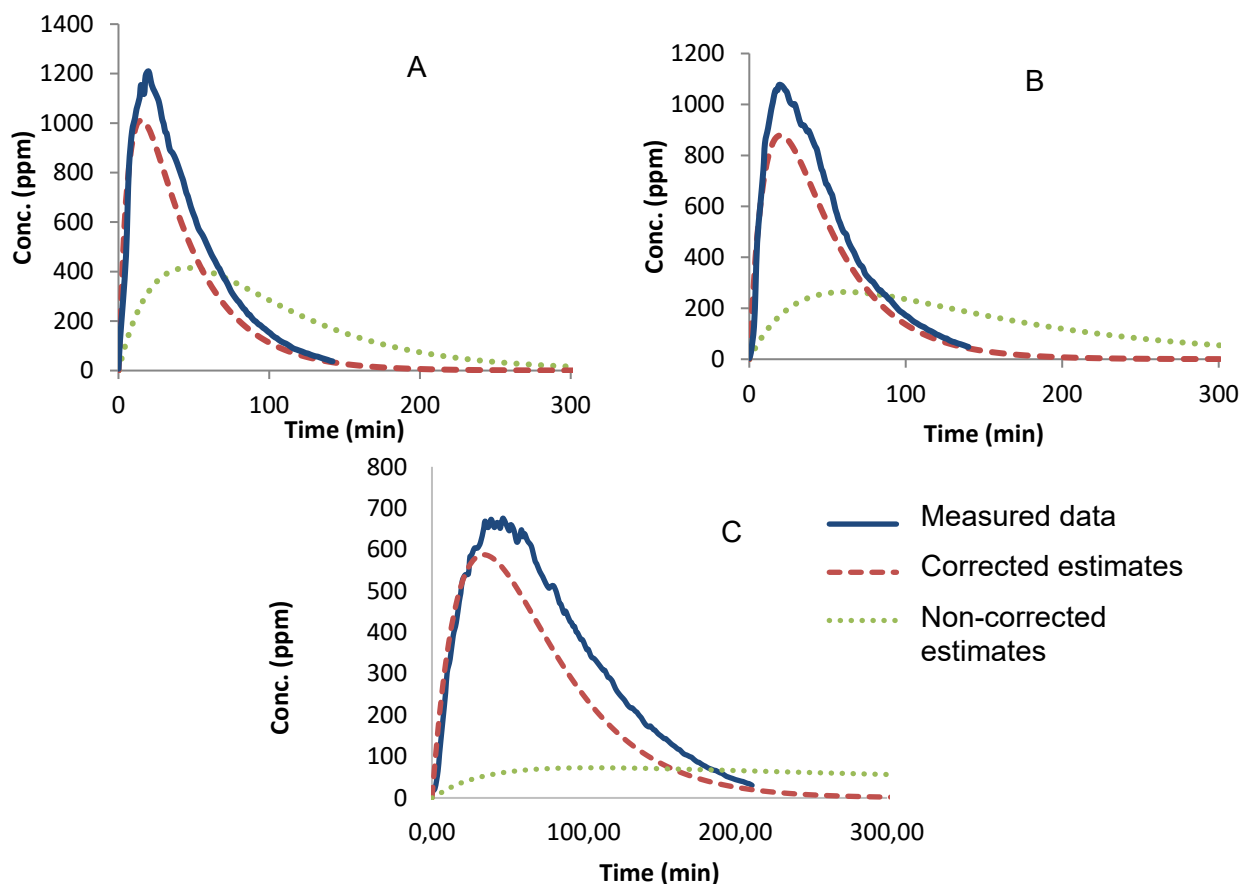
Figure 20.   **Experimental and modelled concentration profiles of evaporation of 10% (A), 5% (B) and 1% (C) MEK aqueous mixtures.**

Isopropanol (IPA)

Figure 21 shows the profiles of the measured IPA concentrations as well as the profiles of the concentrations estimated by modelling using the single-zone model with exponentially decreasing emissions, indicating an emission rate corrected by the activity coefficient and a non-corrected emission rate. Activity coefficients of 7.2, 9.4 and 20 were used respectively for the modelling of the 10%, 5% and 1% mixtures.

The concentrations modelled with correction by activity coefficients were closer to the experimental measurements than the non-corrected concentrations were. The maximum concentrations measured (T_{max}) were 832 ppm (44 min), 602 ppm (61 min) and 311 ppm (67 min). The concentrations estimated by modelling that took correction into account were 697 ppm (24 min), 543 ppm (52 min) and 274 ppm (66 min), respectively, for the 10%, 5% and 1% mixtures. The concentrations estimated by modelling that did not take correction into account were 194 ppm (80 min), 105 ppm (96 min) and 26 ppm (160 min), respectively, for the 10%, 5% and 1% mixtures.
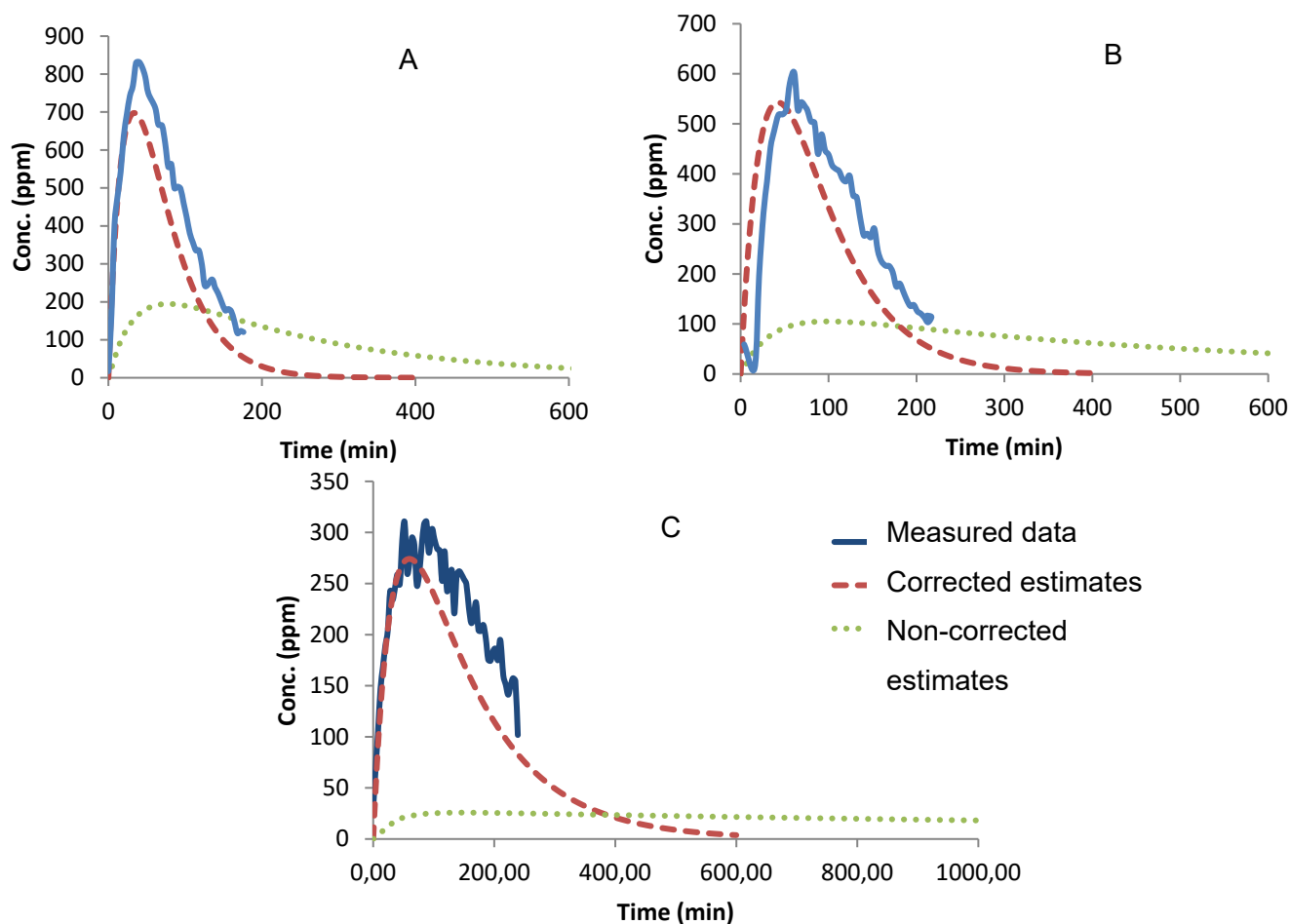
Figure 21.   **Experimental and modelled concentration profiles of evaporation of 10% (A), 5% (B) and 1% (C) IPA aqueous mixtures.**

Methanol

Figure 22 shows the profiles of the measured methanol concentrations as well as the profiles of the concentrations estimated by modelling using the single-zone model with exponentially decreasing emissions, indicating an emission rate corrected by the activity coefficient and a non-corrected emission rate. Activity coefficients of 1.7, 1.9 and 2.2 were used respectively for the modelling of the 10%, 5% and 1% mixtures.

The concentrations modelled with correction by activity coefficients were closer to the experimental measurements than the non-corrected concentrations were. The maximum concentrations measured (T_{max}) were 811 ppm (34 min), 618 ppm (44 min) and 250 ppm (52 min). The concentrations estimated by modelling that took correction into account were 806 ppm (32 min), 615 ppm (44 min) and 234 ppm (65 min), respectively, for the 10%, 5% and 1% mixtures. The concentrations estimated by modelling that did not take correction into account were 612 ppm (40 min), 413 ppm (56 min) and 125 ppm (88 min), respectively, for the 10%, 5% and 1% mixtures.
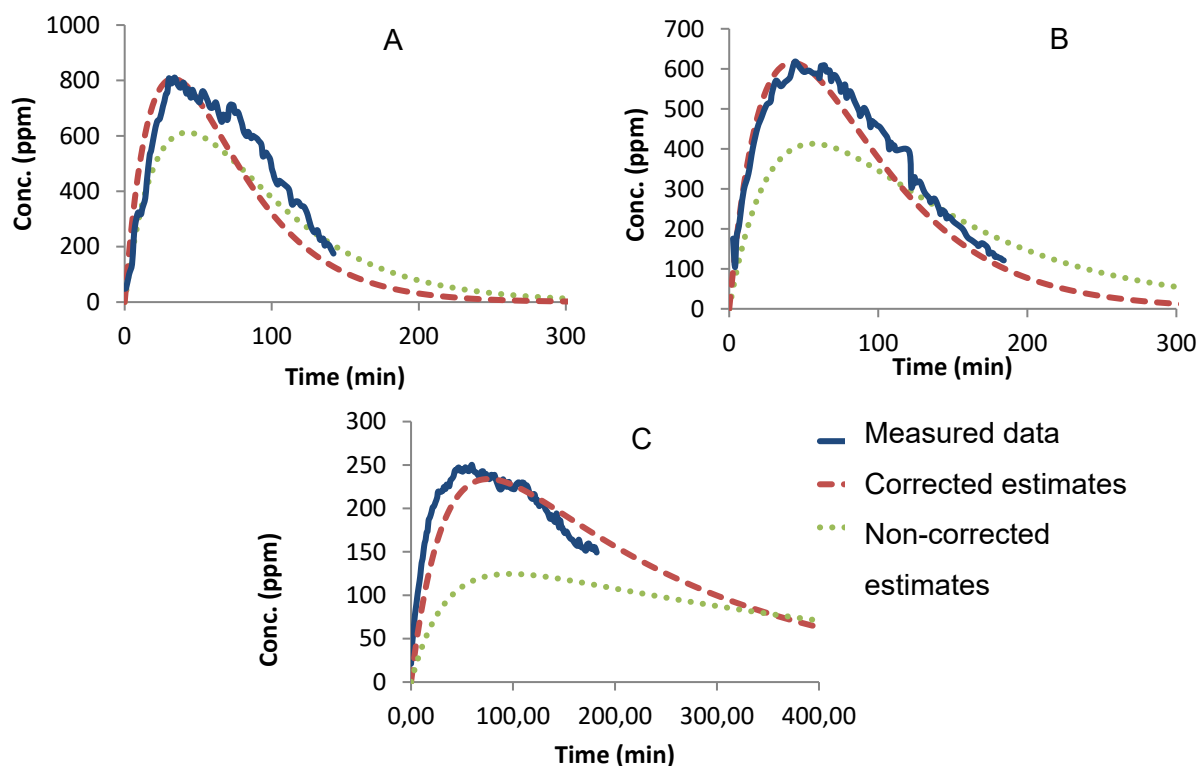
Figure 22.   Experimental and modelled concentration profiles of evaporation of 10% (A), 5% (B) and 1% (C) methanol aqueous mixtures.

Acetone

Figure 23 shows the profiles of the measured acetone concentrations as well as the profiles of the concentrations estimated by modelling using the single-zone model with exponentially decreasing emissions, indicating an emission rate corrected by the activity coefficient and a non-corrected emission rate. Activity coefficients of 5, 7.2 and 10.3 were used respectively for the modelling of the 10%, 5% and 1% mixtures.

The concentrations modelled with correction by activity coefficients were closer to the experimental measurements than the non-corrected concentrations were. The maximum concentrations measured (T_{max}) were 1126 ppm (20 min), 1011 ppm (24 min) and 760 ppm (40 min). The concentrations estimated by modelling that took correction into account were 1355 ppm (4 min), 1311 ppm (8 min) and 891 ppm (20 min), respectively, for the 10%, 5% and 1% mixtures. The concentrations estimated by modelling that did not take correction into account were 846 ppm (28 min), 619 ppm (33 min) and 219 ppm (72 min), respectively, for the 10%, 5% and 1% mixtures.
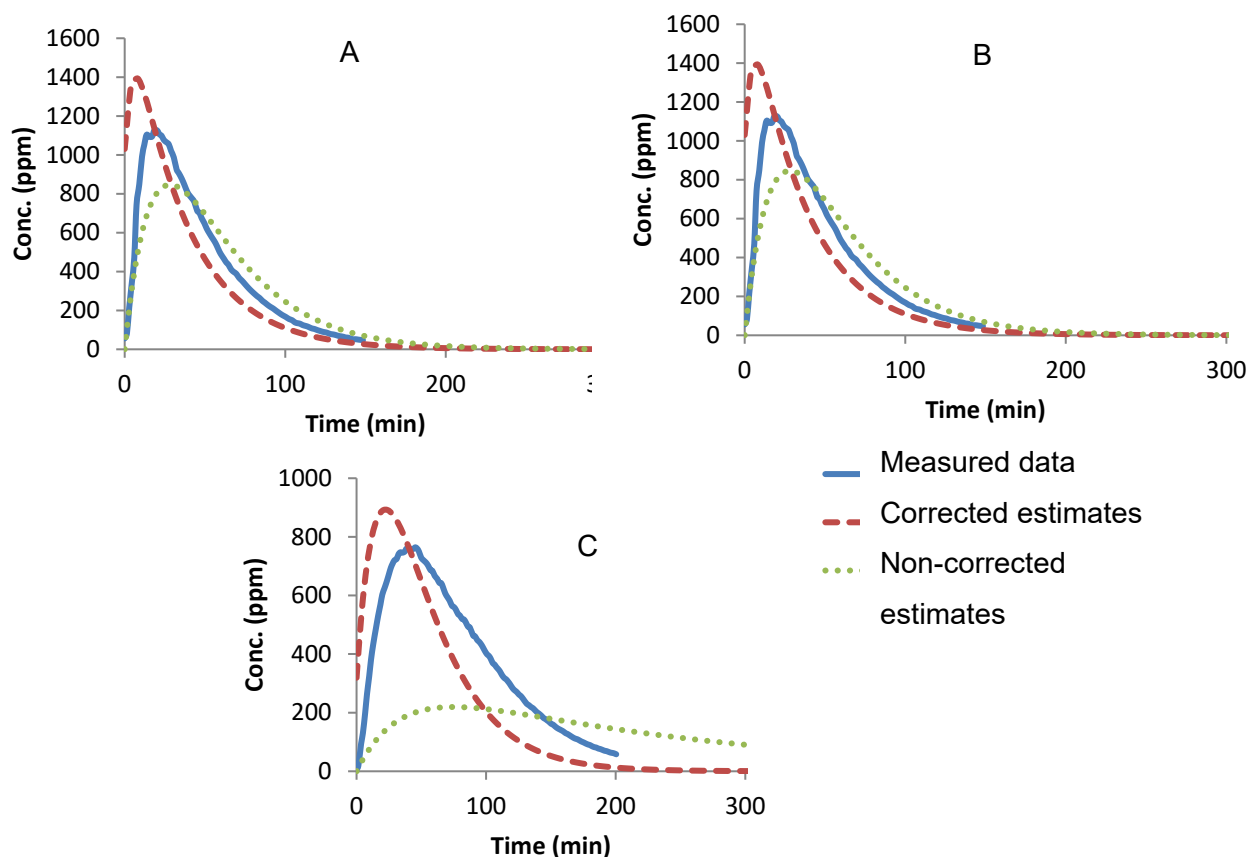
Figure 23.   Experimental and modelled concentration profiles of evaporation of 10% (A), 5% (B) and 1% (C) acetone aqueous mixtures.

Binary mixture of MEK and toluene

Figure 24 shows the concentrations of each of the two solvents, MEK and toluene, evaluated simultaneously. This was an ideal mixture, so the two corresponding activity coefficients were 1.

The maximum concentrations reached during the tests ranged from 500 to 1200 ppm. The solvent vapour concentration peaks measured for MEK and toluene (T_{max}) were 1122 ppm (19 min) and 581 ppm (40 min). The corresponding peaks estimated by the single-zone model were 879 ppm (20 min) and 459 ppm (36 min).
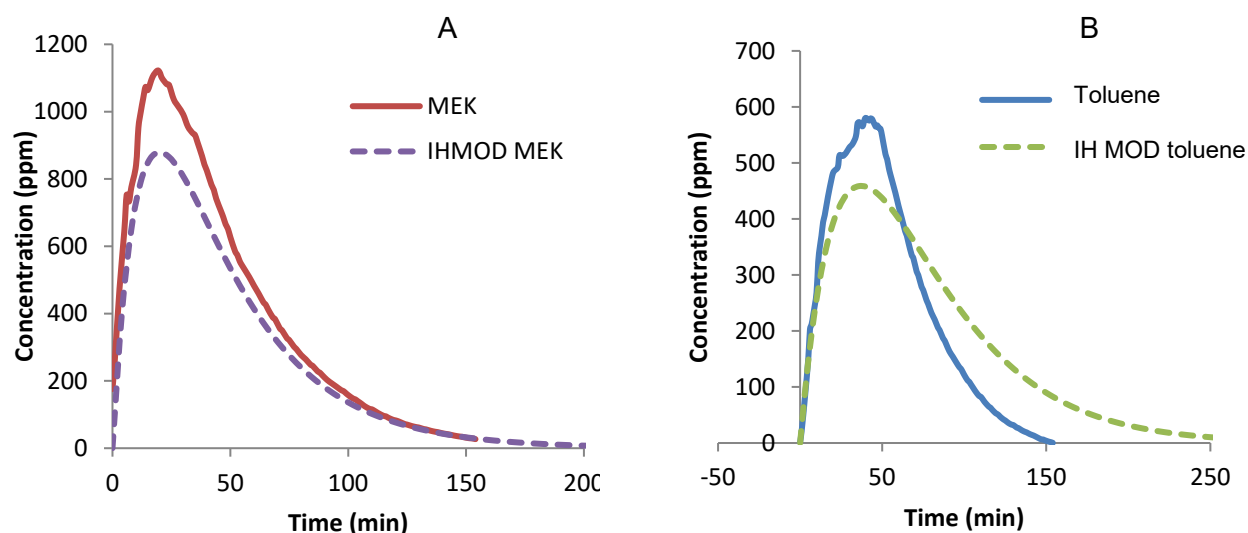
Figure 24.   Experimental and modelled concentration profiles of evaporation of mixture of MEK (A) and toluene (B).

Ternary mixture of toluene, acetone and IPA

Figure 25 shows the profiles of the measured solvent concentrations as well as the profiles of the concentrations estimated by modelling using the single-zone model with exponentially decreasing emissions, indicating an emission rate corrected by the activity coefficient and a non-corrected emission rate. Activity coefficients of 1.78, 1.46 and 1.1 were used respectively to correct the partial pressure and to do the modelling of the solvents IPA, toluene and acetone.

The mole fractions of the ternary mixture were 22% IPA, 32% toluene and 46% acetone.

The concentrations modelled with correction by activity coefficients were closer to the experimental measurements than the non-corrected concentrations were. The maximum concentrations measured (T_{max}) were respectively 902 ppm (63 min), 1425 ppm (62 min) and 1918 ppm (27 min) for IPA, toluene and acetone. The concentrations estimated by modelling that took correction into account were respectively 548 ppm (36 min), 645 ppm (56 min) and 1764 ppm (16 min). The concentrations estimated by modelling that did not take correction into account were respectively 466 ppm (36 min), 442 ppm (56 min) and 1425 ppm (28 min). It should be noted that the profile of toluene is special and does not follow a classic exponentially decreasing curve.
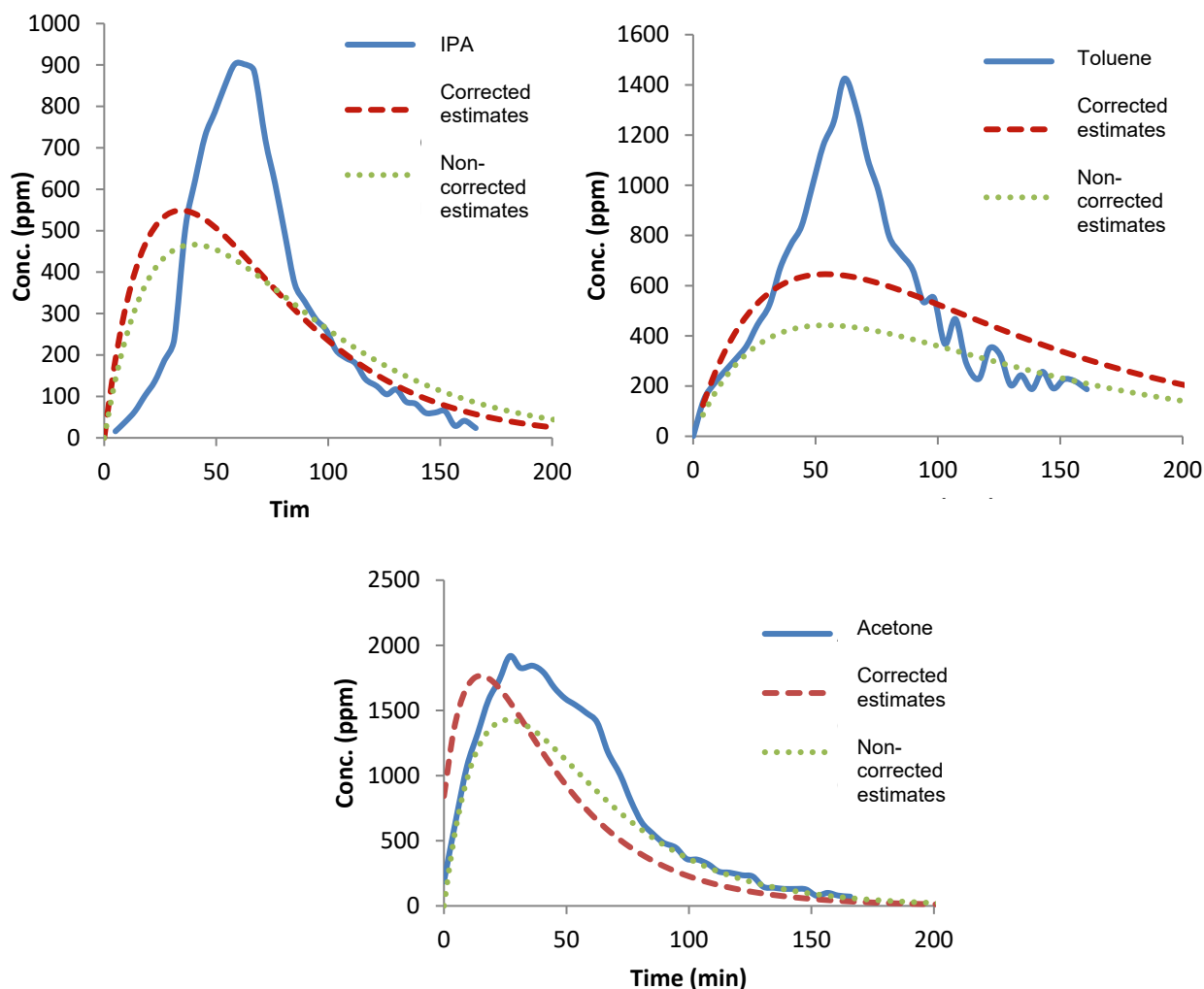
**Figure 25.   Experimental and modelled concentration profiles of evaporation of mixture
of IPA, toluene and acetone.**

Summary of results

The results of the small-scale evaporation tests and the percent agreement between the experimental concentrations and the modelled concentrations are summarized in Table 3. Times T_{max} are also given for each test, with the time difference between the time of the peak concentration measured and that estimated by the model. For the pure solvents, the four modellings show good agreement, with estimates that do not differ by a factor of more than 2 (between 50% and 200%) and a maximum time difference of 8 minutes between the maximum concentration measured and the simulation for acetone. For the aqueous mixtures, all of the corrected simulations (taking into account the activity coefficients) estimated the concentrations accurately enough (within a factor of 2) whereas the non-corrected simulations estimated the concentrations accurately enough in only 5 cases out of 15. The times T_{max} differed by a maximum of 20 minutes when the estimates were corrected, whereas time differences of over 30 minutes were seen in 5 of the 15 tests conducted without estimate correction, rising as high as 93 minutes for the test with a 1% IPA aqueous mixture.

Table 3.   Summary of small-scale evaporation tests.

Solvent	Experimental		Non-corrected modelling			Corrected modelling		
	C_{max}	T_{max}	C_{max}	T_{max}	Agreement	C_{max}	T_{max}	Agreement
	ppm	min	ppm	min	% (min)	ppm	min	% (min)
Toluene	2527	34	2383	28	94 (-6)	-	-	-
Methanol	2122	13	1430	12	67 (-1)	-	-	-
Acetone	1554	20	1550	12	100 (-8)	-	-	-
MEK	1622	21	1153	16	71 (-5)	-	-	-
MEK (H2O 10%)	1209	20	415	44	34 (+24)	1012	11	84 (-9)
MEK (H2O 5%)	1076	18	264	56	25 (+28)	879	20	82 (+2)
MEK (H2O 1%)	676	47	73	105	16 (+58)	587	32	87 (-15)
IPA (H2O 10%)	832	44	194	80	23 (+36)	697	24	84 (-20)
IPA (H2O 5%)	602	61	105	96	17 (+35)	543	52	90 (-9)
IPA (H2O 1%)	311	67	26	160	8 (+93)	274	66	88 (-1)
Methanol (H2O 10%)	811	34	612	40	75 (+6)	806	32	99 (-2)
Methanol (H2O 5%)	618	44	413	56	67 (+12)	615	44	99 (0)
Methanol (H2O 1%)	250	52	125	88	50 (+36)	234	65	94 (+12)
Acetone (H2O 10%)	1126	20	845	28	75 (+8)	1355	4	120 (-16)
Acetone (H2O 5%)	1011	24	619	33	61 (+9)	1311	8	130 (-16)
Acetone (H2O 1%)	760	40	219	72	29 (+32)	891	20	117 (-20)
MEK (toluene)	1122	19	879	20	78 (+1)	-	-	-
Toluene (MEK)	581	40	459	36	79 (-4)	-	-	-
IPA (toluene, acetone)	902	63	466	36	52 (-27))	548	36	61 (-27)
Toluene (IPA, acetone)	1425	62	442	56	31 (-6)	645	56	45 (-6)
Acetone (IPA, toluene)	1918	27	1425	28	74 (+1)	1764	16	92 (-11)

C_{max}: Maximum concentration of solvent (peak concentration)

T_{max}: Time required to reach peak concentration

5.2   Stage II – Human-scale testing in various work situations

5.2.1 Experimental results

Figures 26, 27, 28 and 29 show examples of profiles of acetone vapour concentrations measured during the various human-scale tests.

Figure 26 illustrates, more specifically, the concentrations measured during the evaporation tests of acetone on a table with ventilation through the top of the room at a low airflow rate (A), high rate (B) and very high rate (C). The far field concentrations decline when the room ventilation rate increases, with concentrations reaching 200 mg/m³ at the low rate (A), 140 mg/m³ at the high rate (B) and 70 mg/m³ at the very high rate (C). For the near field concentrations, a sharp variation in concentrations can also be noted as a function of changes in the ventilation rate. Concentrations swing between 150 and 250 mg/m³ at the low rate (A), between 100 and 200 mg/m³ at the high rate (B) and between 80 and 140 mg/m³ at the very high rate (C). The swings in the near field stopped 1h30min to 1h45min after the start of the test, for the three airflow rates studied.

Figure 27 shows, more specifically, the concentrations measured during the acetone ground spill tests, with ventilation through the top of the room at a low airflow rate (A), high rate (B) and very high rate (C). The far field concentrations decline when the room ventilation rate increases, with concentrations reaching 170 mg/m³ at the low rate (A), 125 mg/m³ at the high rate (B) and 80 mg/m³ at the very high rate (C). For the near field concentrations, a sharp variation in concentrations can also be noted as a function of changes in the ventilation rate. Concentrations swing between 150 and 300 mg/m³ at the low rate (A), between 70 and 125 mg/m³ at the high rate (B) and between 50 and 60 mg/m³ at the very high rate (C). It should be noted that at the very high rate, the far field concentrations are higher than the near field concentrations. Swings in the near field stopped 1h30min to 1h45min after the start of the test, for the three airflow rates studied.

Figure 28 illustrates, more specifically, the concentrations measured during the tests that involved putting acetone on a rag and manually cleaning an aluminum part on a table, with ventilation through the top of the room at a low airflow rate (A), high rate (B) and very high rate (C). The far field concentrations decline when the room ventilation rate increases, with concentrations reaching 200 mg/m³ at the low rate (A), 100 mg/m³ at the high rate (B) and 80 mg/m³ at the very high rate (C). For the near field concentrations, high concentration peaks can be seen in the early moments of cleaning, with the peaks seeming to be of the same intensity, regardless of the ventilation rate used. It should be noted that at the low rate and outside of the cleaning-related peaks, far field concentrations are higher than near field concentrations.

Figure 29 illustrates, more specifically, the concentrations measured during the tests that involved spraying acetone followed by manual cleaning of an aluminum part on a table, with ventilation through the top of the room at a low airflow rate (A) or a very high rate (C). The results are very similar to those of Figure 28, where no spraying was involved. The intensity of the peaks here seems to be slightly more constant, however, than those in Figure 28. The far field concentrations decline when the room ventilation rate increases, with concentrations reaching 200 mg/m³ at the low rate (A) and 80 mg/m³ at the very high rate (C). For the near field concentrations, high concentration peaks can be seen in the early moments of spraying and cleaning, with the peaks seeming to be of the same intensity, regardless of the ventilation rate used. It should be noted that at the low rate and outside of the spraying-related peaks, the far field concentrations are higher than the near field concentrations.
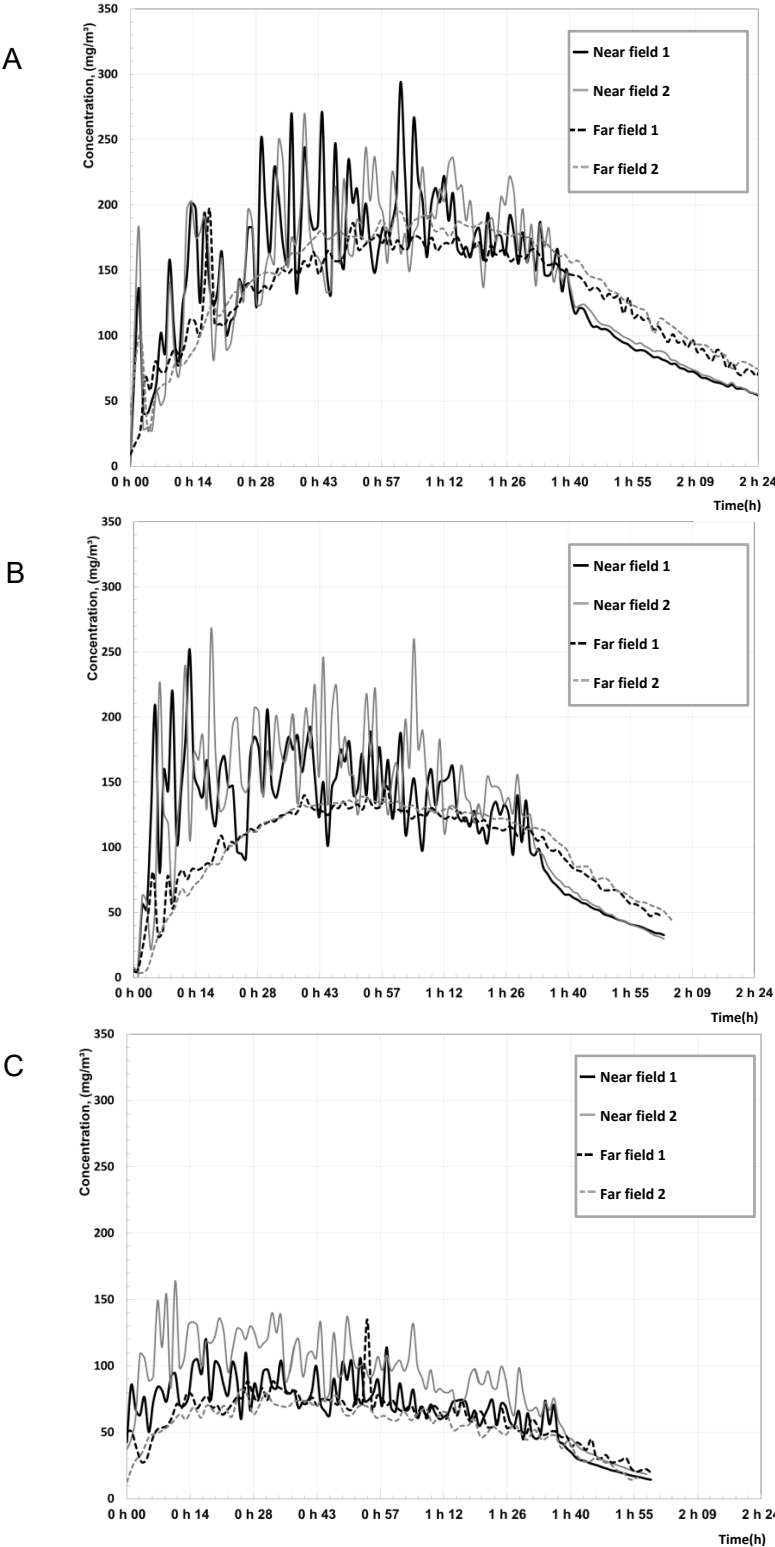
Figure 26.   Examples of profiles of concentrations measured during evaporation tests at low (A), high (B) and very high (C) ventilation rates.
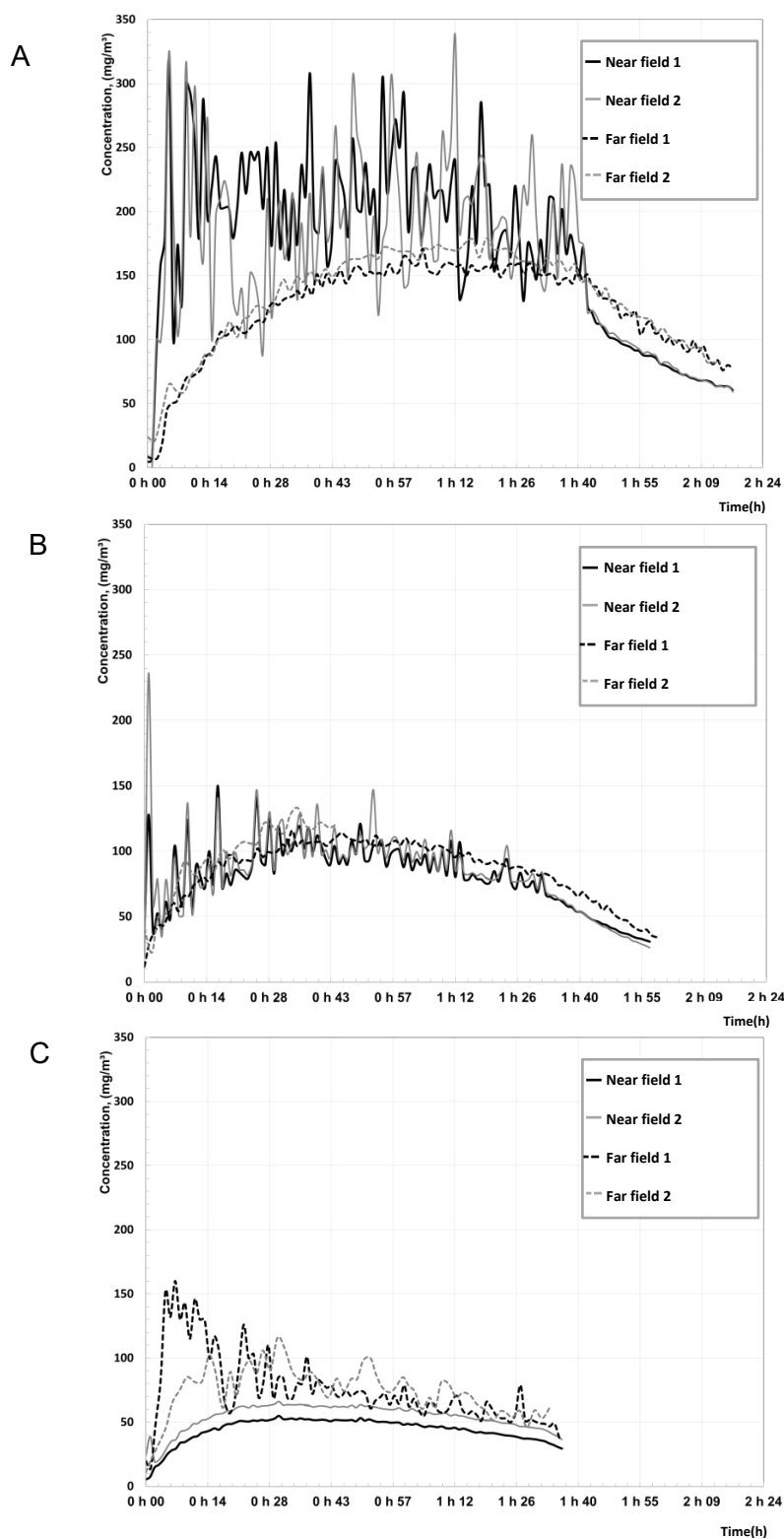
Figure 27.   Examples of profiles of concentrations measured during spill tests at low (A), high (B) and very high (C) ventilation rates.
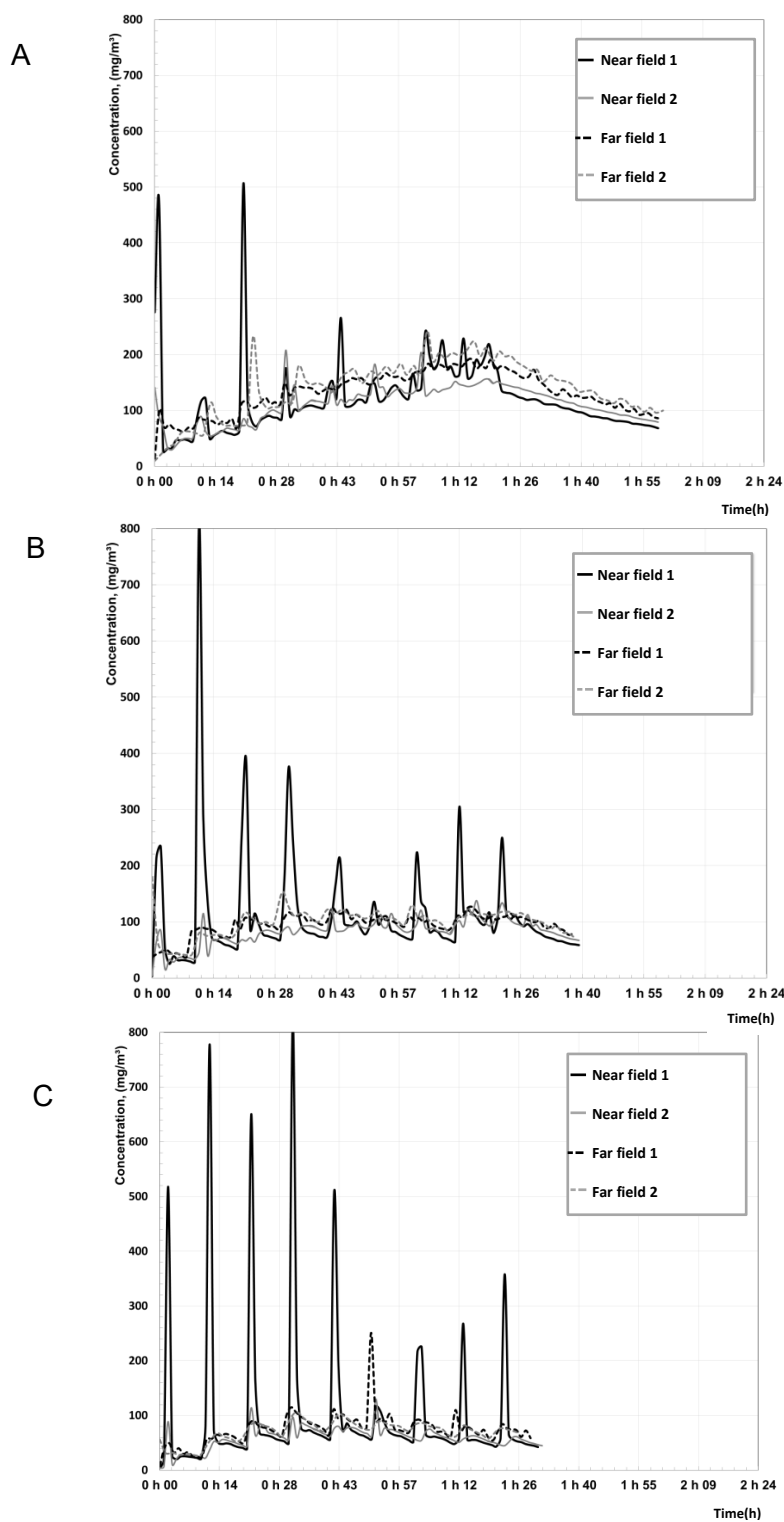
Figure 28.   Examples of profiles of concentrations measured during tests involving rag application followed by manual cleaning at low (A), high (B) and very high (C) ventilation rates.

A

C
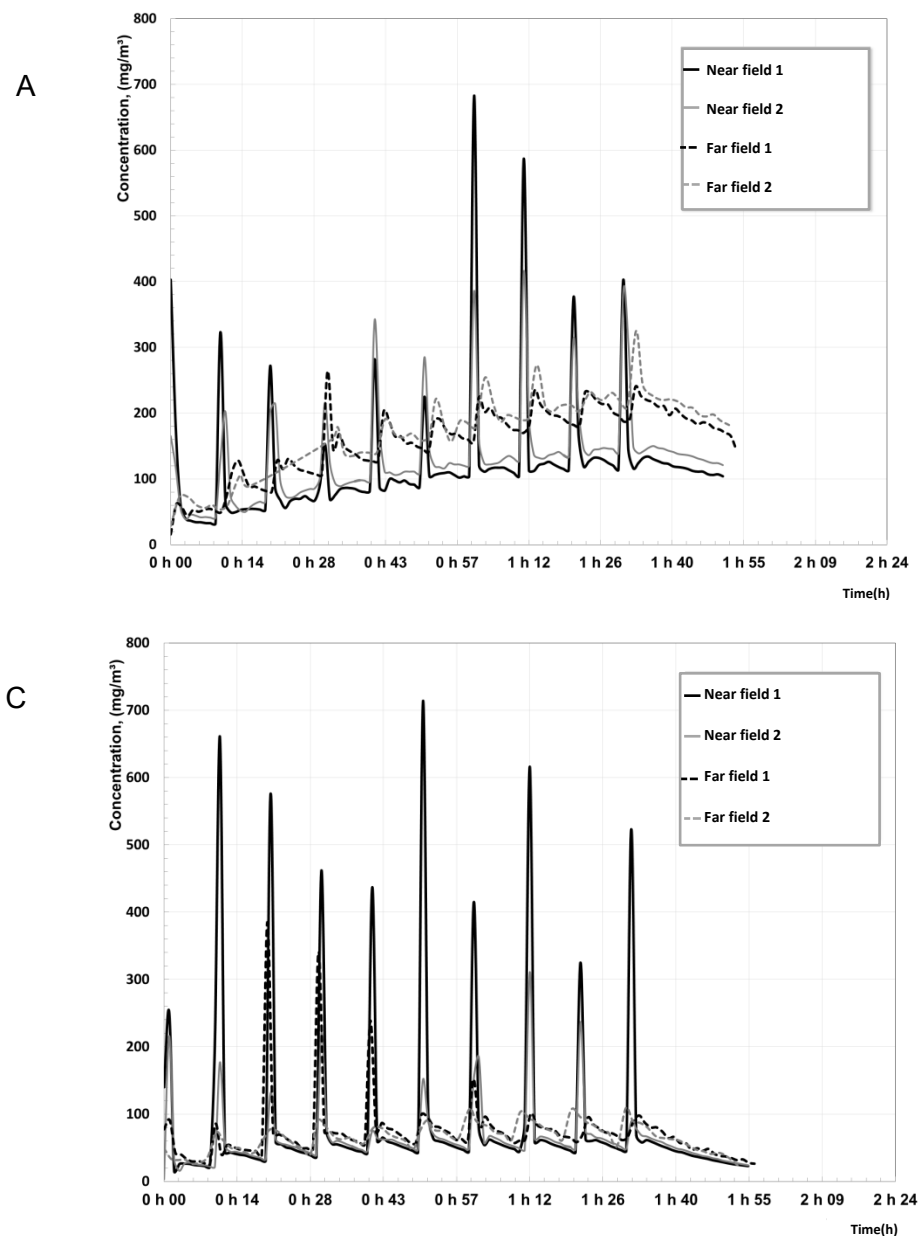
Figure 29.   Examples of profiles of concentrations measured during tests involving acetone spraying followed by manual cleaning at low (A) and very high (C) ventilation rates.

Figure 30 illustrates the results of various tests performed under the same ventilation airflow conditions (low rate), but with ventilation either through the floor (left-hand column) or the ceiling (right-hand column). Figure 30A thus shows the two situations for the evaporation tests, Figure 30B the two situations for the spill tests, Figure 30C for the tests involving application of acetone with a rag followed by manual cleaning, and Figure 30D the two situations for the tests involving acetone spraying followed by manual cleaning.

The concentration profiles are fairly similar, but it can be seen that the concentrations for ventilation through the ceiling are generally lower, and the concentration peaks lower, than in the tests performed under the same conditions, but with the ventilation through the floor.

More substantial differences can also be seen between measurements taken within the same field: near or far. For instance, in Figure 30B with ventilation through the floor, the two concentration curves in the near field are easy to tell apart.

Tables 4 and 5 give the mean concentrations (C_{98}) measured during evaporation of acetone in the near field and the far field, respectively. As observed for figures 26 to 30, the effect of an increase in the ventilation rate on the concentrations, as well as the differences between the concentrations in the two fields, is worth noting. For the evaporation or spill tests, the concentrations in the near field are significantly higher than those in the far field ($p < 0.01$), whereas that is not the case for the tests involving application with a rag or spraying followed by manual cleaning. Thus, the concentrations in the near field are 23% and 18% higher than those in the far field for the evaporation and spill processes, respectively. In contrast, the concentrations in the near field are 3% and 13% lower than those in the far field for the application with a rag and spray processes, respectively. It is also worth noting that for the spill scenario with a very high ventilation rate through the ceiling, the concentrations in the near field are lower than those in the far field, i.e., 49 mg/m³ as opposed to 70 mg/m³.

Comparing the C_{98} measurements taken by each instrument in each field provides information about the symmetry of the concentrations and homogeneity of the fields. Mean differences of 10% [0.7 – 40%] in the far field and 21% [0.1 – 60%] in the near field were calculated between the two measurement points (GC1/GC2 and PID1/PID2 respectively). The data are a sign of good homogeneity in each field.

Analyses of variance (ANOVA) were performed to determine which parameters contribute significantly to explaining the variability of the concentrations (C_{98}) in the near and far fields (log-transformed values). The following parameters were evaluated: *scenario* (evaporation, spill, application with rag and manual cleaning, spray and manual cleaning), *airflow rate* (low, high and very high) and *air intake position* (floor or ceiling).

The parameters having significant effects on near field concentrations were *airflow rate*, *air intake position* and *scenario* ($p < 0.01$). The parameters having significant effects on far field concentrations were *airflow rate* and *air intake position* ($p < 0.01$). The parameter *scenario* was therefore not a variable that made a significant contribution to enhancing the model for concentrations in the far field ($p = 0.18$).
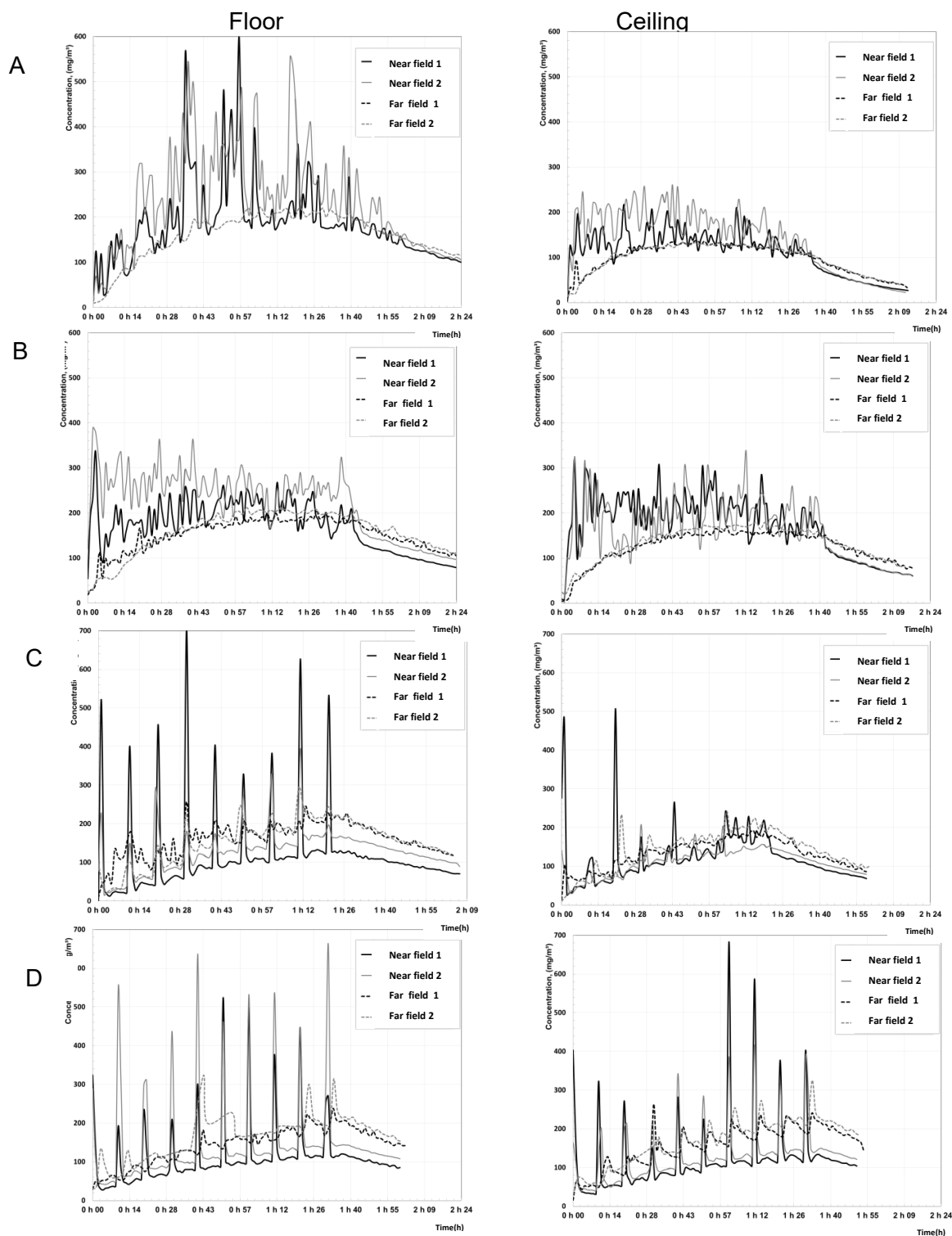
Figure 30.   Examples of profiles of concentrations measured during tests of evaporation (A), spill (B), cleaning (C) and spray with cleaning (D) with low rate ventilation through the floor (left) and the ceiling (right).

Table 4.   Mean concentrations of acetone (C_{98}, mg/m³) measured in the near field during human-scale tests.

	Evaporation					Spill					Rag application and manual cleaning					Spray and manual cleaning				
Air intake	Floor		Ceiling			Floor		Ceiling			Floor		Ceiling			Floor		Ceiling		
Ventilation rate	L	H	L	H	VH	L	H	L	H	VH	L	H	L	H	VH	L	H	L	H	VH
Mean concentration per test	261	97	197	156	100	262	181	175	91	55	131	110	114	84	59	154	105	137	-	66
	202	93	173	143	81	198	151	122	88	44	125	100	121	115	101	115	90	112	-	96
	234	111	216	177	101	228	182	189	79	57	125	146	114	96	56	119	87	92	-	72
	179	111	164	137	76	153	159	183	76	46	117	112	131	148	93	116	93	82	-	79
	249	103	165	153	103	259	142	188	93	52	106	141	113	87	56	129	85	131	-	55
	172	93	167	141	83	180	133	202	88	41	126	92	166	144	101	123	-	122	-	63
Mean	216	101	180	151	91	213	158	177	86	49	122	117	127	112	78	126	92	113		72
Process mean	148					137					111					101				
Near field mean	125																			

Airflow rate: low (L), high (H), very high (VH)

Table 5.   Mean concentrations of acetone (C_{98}, mg/m³) measured in the far field during human-scale tests.

	Evaporation					Spill					Rag application and manual cleaning					Spray and manual cleaning				
Air intake	Floor		Ceiling			Floor		Ceiling			Floor		Ceiling			Floor		Ceiling		
Ventilation rate	L	H	L	H	VH	L	H	L	H	VH	L	H	L	H	VH	L	H	L	H	VH
Mean concentration per test	165	104	163	99	66	160	114	150	72	75	154	127	142	101	70	159	121	159	-	68
	168	105	159	101	68	155	108	148	95	78	163	98	123	96	74	139	118	144	-	76
	175	-	150	109	60	157	136	144	97	71	159	118	145	112	69	133	119	114	-	61
	-	-	148	110	67	154	113	136	88	62	144	84	136	104	68	126	105	107	-	58
	-	-	152	108	64	164	127	139	96	74	147	116	152	116	71	158	111	173	-	60
	-	-	143	111	71	157	-	129	91	59	132	91	130	115	71	133	122	154	-	60
Mean	169	105	153	106	66	158	120	141	90	70	150	106	138	107	71	141	116	142		64
Process mean	120					116					114					116				
Far field mean	116																			

Airflow rate: low (L), high (H), very high (VH)

5.2.2 Estimating using the two-zone model

The modelling using the two-zone model was done based on experimental data and took an exponentially decreasing emissions model and a constant generation model into consideration.

Table 6 gives the air speeds measured at 50 cm from the source at two measuring points for the different scenarios. The speeds ranged from 0.01 to 0.08 m/s for the scenarios indicated in the table, i.e., evaporation, rag application and spray, whereas they ranged from 0.01 to 0.25 m/s for the spill (on the ground) scenario. These air speeds were used to calculate the β coefficients, according to equation 1.

The emission rates calculated with the balance for the evaporation and spill scenarios were 155 mg/min [122 – 178 mg/min] on average, while the α coefficients were 0.022 min^{-1} [0.20 – 0.25 min^{-1}] on average. For the application with a rag and spray scenarios, the emission rates were either (1) calculated for the constant emission rate model (by dividing the mass of solvent by the time used of T_{98}, i.e., the last application + 10 minutes), or (2) determined using the mean coefficient of 0.022 min^{-1} for the exponentially decreasing emissions model.

Table 6.   Air speeds measured at the boundary of the two fields according to the different scenarios evaluated

	Evaporation / application with rag* / spray*					Spill				
Air intake	Floor		Ceiling			Floor		Ceiling		
Ventilation rate	L	H	L	H	VH	L	H	L	H	VH
Speed (m/s)	0.01	0.02	0.01	0.04	0.06	0.01	0.01	0.01	0.06	0.30
	0.01	0.03	0.01	0.05	0.1	0.01	0.03	0.02	0.07	0.20
Mean speed (m/s)	0.01	0.025	0.01	0.045	0.08	0.01	0.02	0.015	0.065	0.25

*Estimate based on evaporation model;
Airflow rate: low (L), high (H), very high (VH)

The radius of the near field (half sphere) was adapted to obtain concentration estimates (C_{98}) (exponentially decreasing emissions model) as close as possible to the mean concentrations measured in the near field. Table 7 gives the parameter estimates of the radius of the hemisphere and the β coefficient obtained for each of the 57 tests (3 repetitions per situation consisting of one scenario, one air intake position and one ventilation rate).

The geometric means of the estimated β coefficients are respectively 2.3, 3.8, 5.4 and 5 m³/min for the evaporation, spill, application with a rag and spray scenarios. The geometric means of the estimated β coefficients are respectively 2.8 and 4.8 m³/min for the floor and ceiling ventilation scenarios. The geometric means of the estimated β coefficients are respectively 3.7, 3 and 6.5 m³/min for the low (L), high (H) and very high (VH) ventilation rate scenarios.

Table 7.   **Estimated parameters of near field radius and β coefficient, by air intake position and ventilation rate (3 repetitions per situation)**

	Radius (m)			β (m³/min)		
Scenario: Evaporation						
Floor–L	0.8	0.8	0.7	1.21	1.21	0.92
Floor–H	0.9	0.8	0.8	3.82	3.02	3.02
Ceiling–L	1.2	1	1.1	2.72	1.88	2.28
Ceiling–H	0.5	0.5	0.5	2.12	2.12	2.12
Ceiling–VH	0.4	0.5	0.4	2.42	3.77	2.42
Scenario: Spill						
Floor–L	0.8	0.8	0.8	1.21	1.21	1.21
Floor–H	0.9	0.7	0.7	3.05	1.85	1.85
Ceiling–L	0.8	0.9	1.2	1.81	2.29	4.07
Ceiling–H	0.7	0.8	0.7	6.01	7.84	6.01
Ceiling–VH	0.6	0.6	0.6	16.9	16.9	16.9
Scenario: Application with rag and manual cleaning						
Floor–L	2.2	2.2	1.8	9.12	9.12	6.12
Floor–H	0.8	0.7	0.9	3.02	2.31	3.82
Ceiling–L	1.6	2	2.3	4.83	7.53	9.96
Ceiling–H	0.8	0.8	1	3.02	3.02	4.71
Ceiling–VH	0.7	0.7	0.7	7.78	7.78	7.78
Scenario: Spray and manual cleaning						
Floor–L	1.8	2	1.5	6.12	7.53	4.23
Floor–H	0.8	0.8	0.8	2.31	2.31	2.31
Ceiling–L	1.5	2.9	2.5	4.23	15.84	11.79
Ceiling–VH	0.7	0.5	0.5	7.78	3.96	3.96

L: low airflow rate, H: high airflow rate, VH: very high airflow rate

When the ventilation rate is high (H) or very high (VH), the radii that can be used to estimate accurately enough the concentrations measured in the near field are in the range between 0.5 m and 1 m, regardless of the scenario. For the evaporation and spill scenarios, the β coefficients are higher when the airflow rate is high or very high, reaching 16.9 m³/min for the spill with very high ventilation through the ceiling. That situation is the one for which the concentrations in the near field are the lowest, for all of the 19 situations evaluated, and also the one with the highest measured air speeds, i.e., 0.25 m/s. For the rag application and spray scenarios, high β coefficients were estimated independently of the ventilation rate. To obtain a high β coefficient

for situations with low air speeds, a much larger radius must be used, consistent with equation 1. This radius ranges from 1.5 m to 2.9 m for the low airflow rate tests of the two scenarios.

Figure 31 shows the concentration profiles in the near field for a high (A) and a low (B) ventilation rate with, in each case, two estimates: one for exponentially decreasing emissions and the other for constant emissions. Figure 32 gives the concentrations in the far field. The experimental test conditions are specified in the two figures, with a near field diameter of 0.5 m for case A and 0.9 m for case B.

Generally speaking, the two generation models are consistent with observational data. For the exponentially decreasing emissions model, a good fit was noted in the early stages of the simulation, with concentrations under this model increasing faster. Conversely, for the constant generation emission model, a good fit was seen in the second half of the tests, especially when emissions ceased, with a significant decline in concentrations.

The concentrations (C_{98}) in Figure 31A are 153 mg/m³ and 141 mg/m³ for the two experimental measurements, 174 mg/m³ for the data estimated by the constant emissions model and 139 mg/m³ for the data estimated by the exponentially decreasing emissions model. The concentrations (C_{98}) in Figure 31B are 189 mg/m³ and 183 mg/m³ for the two experimental measurements, 203 mg/m³ for the constant emissions model and 174 mg/m³ for the exponentially decreasing emissions model.

The concentrations (C_{98}) in Figure 32A are 108 mg/m³ and 111 mg/m³ for the two experimental measurements, 74 mg/m³ for the constant emissions model and 65 mg/m³ for the exponentially decreasing emissions model. The concentrations (C_{98}) in Figure 32B are 144 mg/m³ and 135 mg/m³ for the experimental measurements, 119 mg/m³ for the constant emissions model and 111 mg/m³ for the exponentially decreasing emissions model.

Figure 33 provides concentration profiles of the near and far fields for a spill scenario with estimates produced using the exponentially decreasing emissions model. The concentrations in the near field are lower than those measured in the far field. The modelling yields estimates that are very close for the two fields. The β coefficient of this experiment is the highest of all the tests run, i.e., 16.9 m³/min. This factor was determined taking into consideration an airflow speed at the interzonal boundary of 0.25 m/s, with a near field (hemisphere) diameter of 0.6 m.
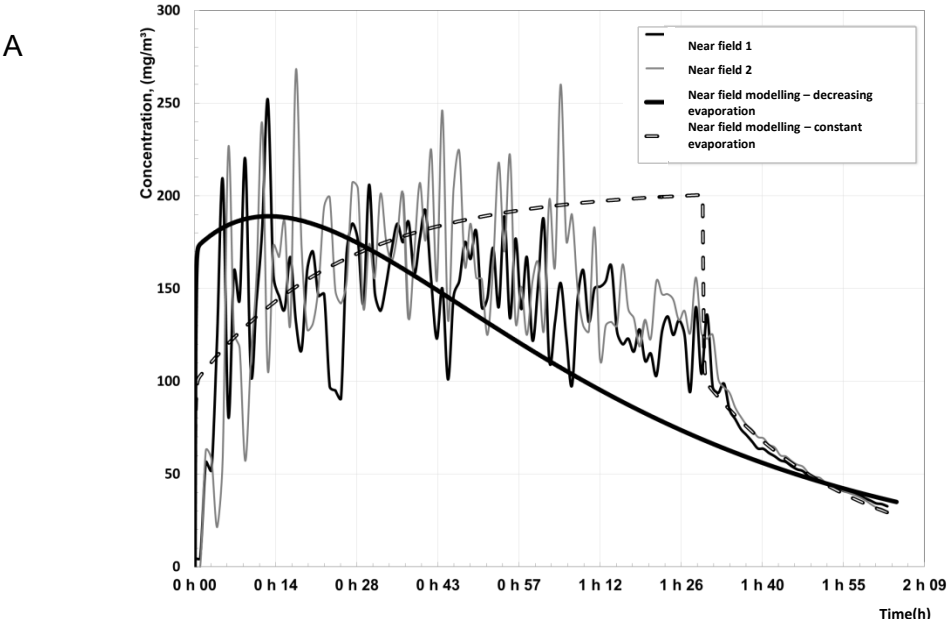
A

Test conditions: Evaporation scenario with high rate of ventilation through the ceiling
Near field radius = 0.5 m, interzonal air speed = 0.045 m/s, β = 2.12 m³/min

B
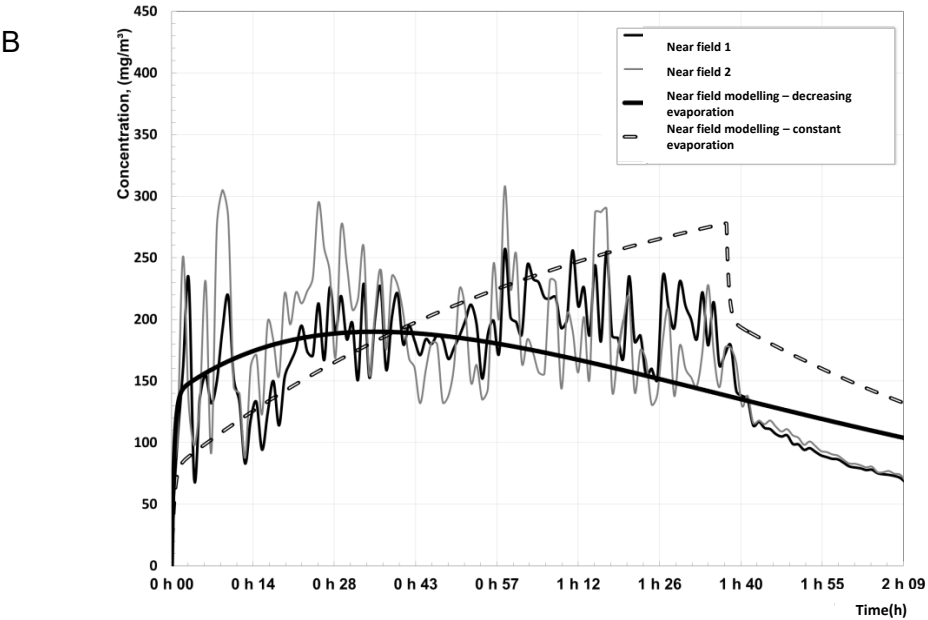
Test conditions: Spill scenario with low rate of ventilation through the ceiling
Near field radius = 0.9 m, interzonal air speed = 0.015 m/s, β = 2.29 m³/min

**Figure 31.   Profiles of near field concentrations measured and estimated by the two-
zone model, with exponentially decreasing emissions and constant emissions.**

A

Test conditions: Evaporation scenario with high rate of ventilation through the ceiling
Near field radius = 0.5 m, interzonal air speed = 0.045 m/s, β = 2.12 m³/min

B

Test conditions: Spill scenario with low rate of ventilation through the ceiling
Near field radius = 0.9 m, interzonal air speed = 0.015 m/s, β = 2.29 m³/min

Figure 32.   Profiles of far field concentrations measured and estimated by the two-zone model, with exponentially decreasing emissions and constant emissions.
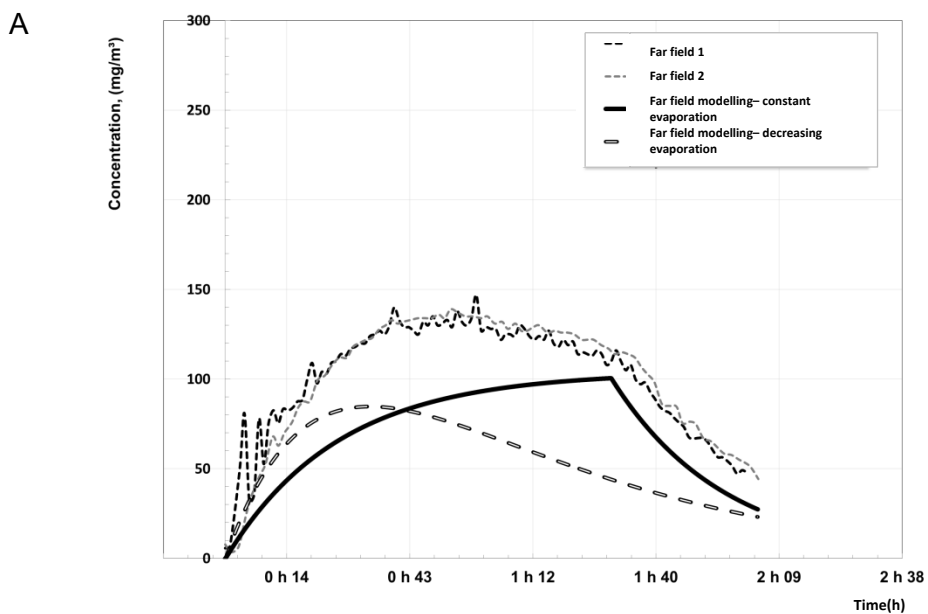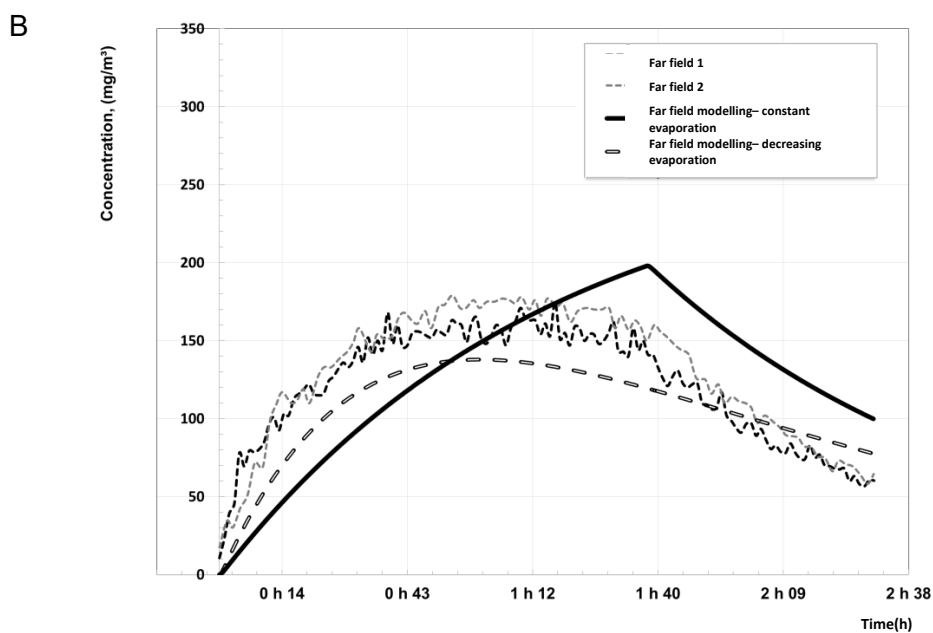
Test conditions: Spill scenario with very high rate of ventilation through the ceiling
Near field radius = 0.6 m, interzonal air speed = 0.25 m/s, β = 16.9 m³/min

**Figure 33.   Profiles of concentrations measured and estimated by the two-zone model,
with exponentially decreasing emissions.**

Figure 34 shows profiles of near and far field concentrations for the scenario of application with a rag followed by manual cleaning, with estimates produced using the exponentially decreasing emissions model. Modelling using the two-zone model does not consider application of 2 mL of acetone every 10 minutes. The mean concentrations (C_{98}) measured were 108 mg/m³ for the experimental measurements in the far field and 121 mg/m³ for the experimental measurements in the near field. The concentrations estimated by the model were 115 mg/m³ in the near field and 70 mg/m³ in the far field. Outside the concentration peaks, the concentrations measured in the near field were lower than those in the far field. This difference can also be seen toward the end of the generation, after 1h12min. Similar results were obtained for the concentrations at the low airflow rate (Figure 35) and for the spray scenario (Figure 36). In some cases, the mean concentrations in the near field were lower than those in the far field, despite the presence of concentration peaks (figures 35 and 36). The modelling does not allow estimation of a lower concentration in the near field than in the far field.

Test conditions: Scenario of application with rag followed by manual cleaning, with high rate of ventilation through the ceiling
Near field radius = 0.6 m, interzonal air speed = 0.05 m/s, β = 3.6 m³/min

Figure 34.   Profiles of concentrations measured and estimated by the two-zone model, with exponentially decreasing emissions.
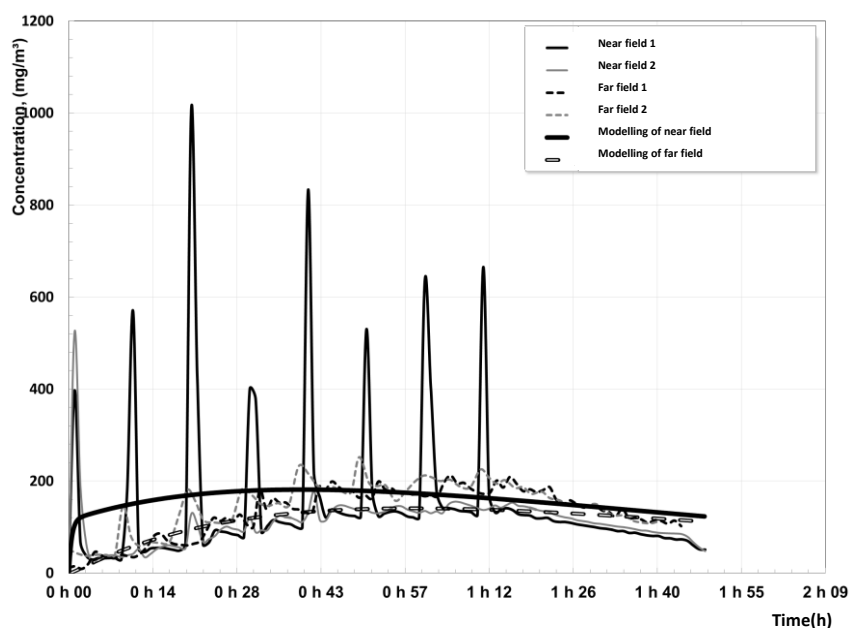
Test conditions: Scenario of application with rag followed by manual cleaning, with low rate of ventilation through the ceiling
Near field radius = 1.6 m, interzonal air speed = 0.01 m/s, β = 4.8 m³/min

Figure 35.   Profiles of concentrations measured and estimated by the two-zone model, with exponentially decreasing emissions.
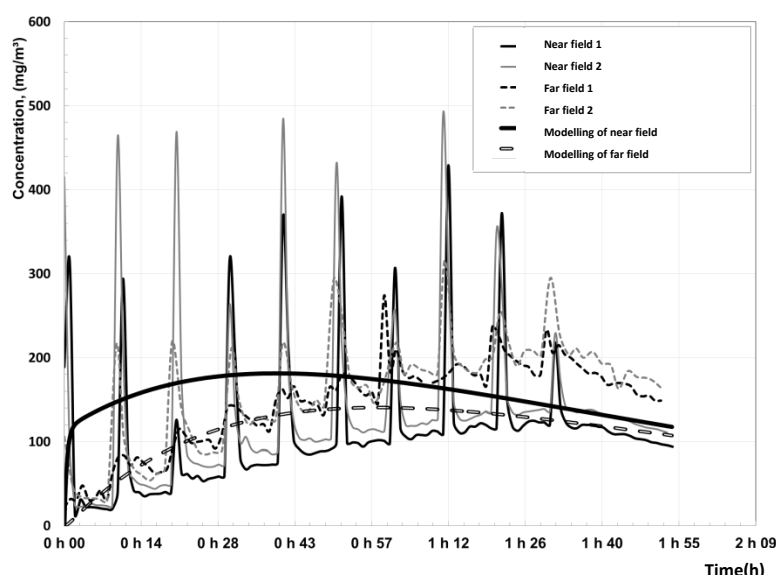
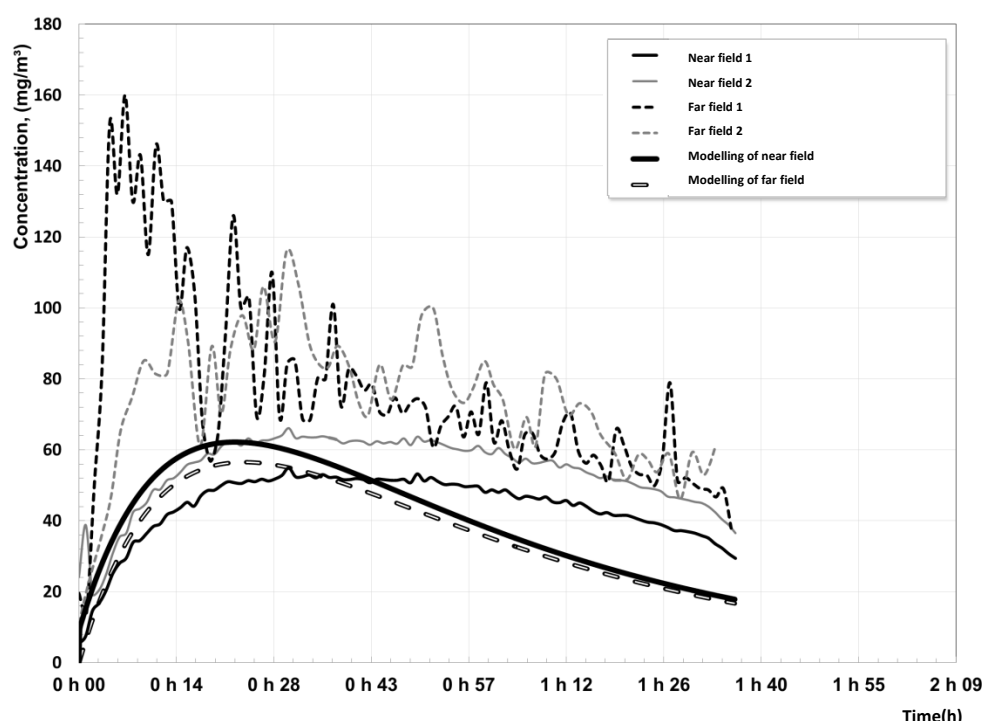Test conditions: Scenario of spraying followed by manual cleaning, with high rate of ventilation through the ceiling
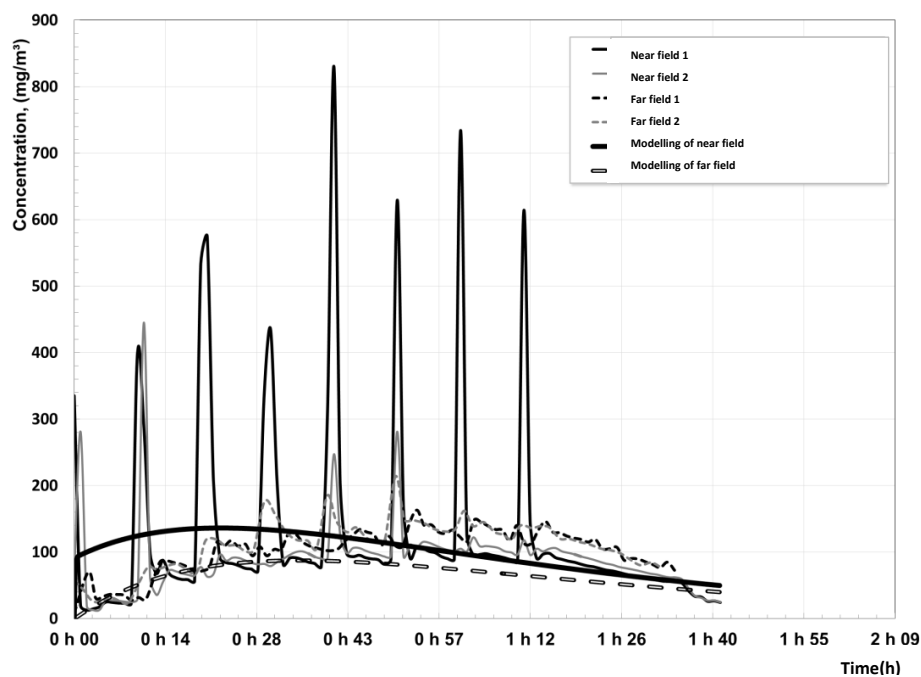Near field radius = 0.5 m, interzonal air speed = 0.08 m/s, β = 4 m³/min

**Figure 36.   Profiles of concentrations measured and estimated by the two-zone model,
with exponentially decreasing emissions.**

5.2.3 Computational fluid dynamics simulations

CFD simulations focused on four scenarios representative of the full range of tests conducted in the human-scale room. The first two scenarios correspond to the tests of acetone evaporation on a table with low and high rates of ventilation through the floor. Scenarios 3 and 4 correspond to the tests of evaporation on a table with low and high rates of ventilation through the ceiling.

Figure 37 sets out the concentration profiles modelled by CFD and those estimated by the single-zone model with exponentially decreasing emissions. While the profiles are comparable, the concentrations increase faster under the single-zone model. The concentration peaks are also reached sooner than with the CFD modelling. The mean concentrations over the simulation time interval are still very close, however. The biggest difference was seen for the scenario of the high rate of ventilation through the ceiling, where the mean concentration was 53.9 mg/m³ for the single-zone model, compared with 50.5 mg/m³ for the CFD model. For the two models and the two air intake positions (floor and ceiling), the concentrations with a high ventilation rate were approximately half those obtained with low ventilation.
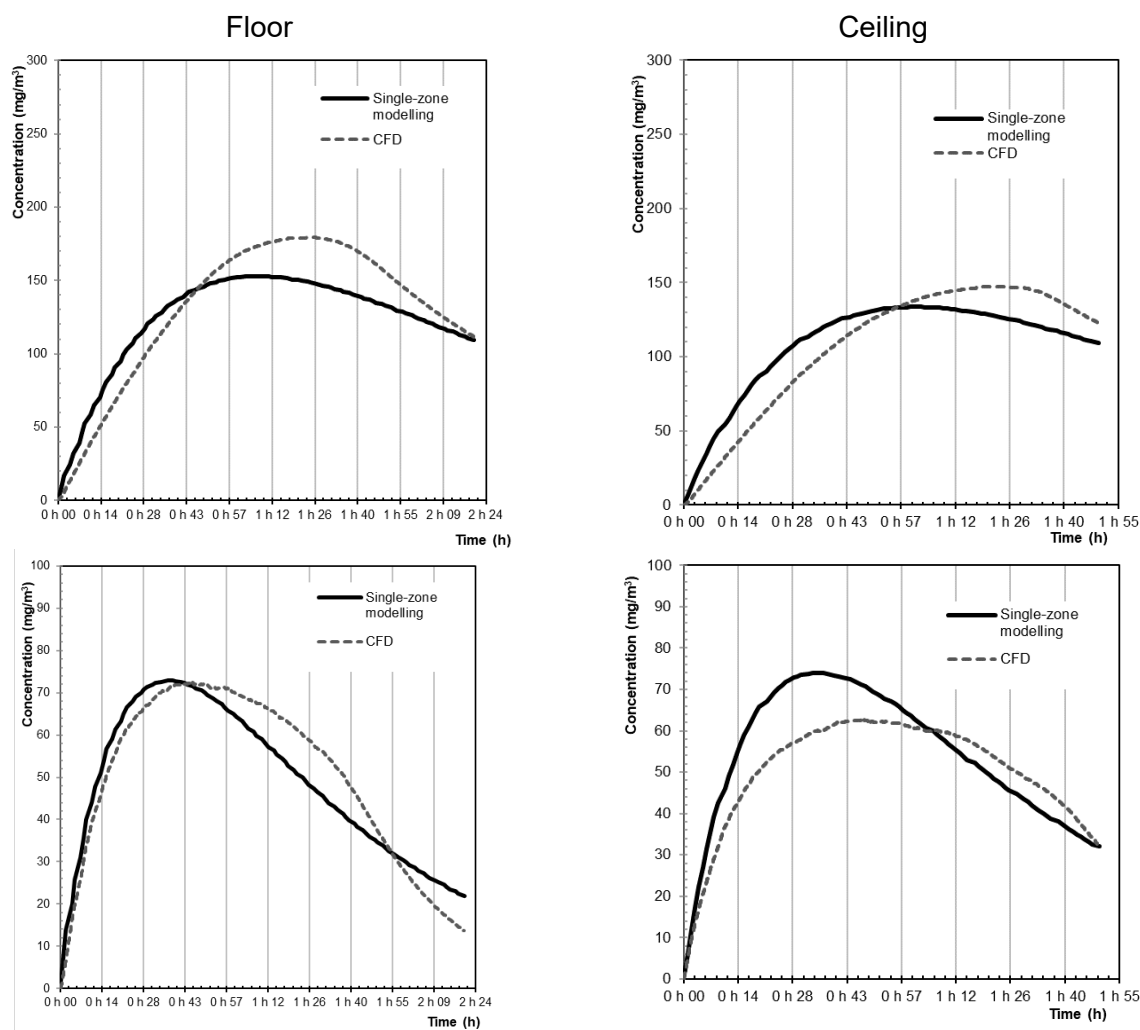
Figure 37.   Profiles of concentrations modelled by CFD and those estimated by the single-zone model, with exponentially decreasing emissions, low rate of ventilation (top) and high rate of ventilation (bottom).

Comparing the CFD model concentrations with the results of the two-zone model requires estimating the interzonal airflow rate (β). Table 7 in the preceding section gives the coefficient β estimates obtained for the all tests done in the human-scale room. These coefficients are based on the assumption that the near field is shaped like a half sphere. However, estimating concentrations in a half-spherical volume with the numerical code used in this study is a very complex task. As a result, the near field was defined as being a cube with 40 cm sides, and the β coefficients were determined based on the mean airflow speeds at the interzonal boundary obtained by CFD simulation.

Table 8 compares the airflow speeds measured at the boundary of the near and far fields, with the speeds obtained by CFD. The numerical results were determined by calculating the arithmetic mean of the speeds at 10 positions, all located at the boundary of the near and far fields. This distance is less than the one used for the experimental measurements (50 cm from the source).

However, the numerical and experimental results show that the airflow speed is relatively constant in the immediate environment of the source, regardless of the ventilation position and rate used. The speeds modelled as a function of time correspond to a normal distribution around a mean value; the standard deviation of the speed for each scenario is also given in Table 8.

Table 8.   Comparison between measured and simulated speeds at the interzonal boundary.

Air intake position	Floor		Ceiling	
Ventilation rate	L	H	L	H
Measured mean speeds (m/min)	0.6	1.5	0.6	2.7
CFD simulated speeds and standard deviation (m/min)	0.5 (0.1)	1.6 (0.2)	0.4 (0.1)	1.8 (0.3)

L: low; H: high

The near field concentrations obtained by CFD modelling were compared with the results of the two-zone model with exponentially decreasing emissions. The near field surface area (FSA) was set at 0.84 m^2. This value corresponds to the surface area of the near field (cube with 40 cm sides) from which a surface area of 0.12 m^2 was subtracted to account for the table where the evaporation occurs. Using equation 1 and the mean airflow speed at the interzonal boundary (S) determined numerically (Table 8), an interzonal airflow rate β was estimated for the modelled scenarios. Figure 38 shows the β coefficients obtained and the associated standard deviations for the cases of ventilation through the floor and through the ceiling. It can be seen that high airflow ventilation increases the β coefficients by a factor of almost 4 compared with low airflow ventilation. Taking into account the standard deviations associated with the interzonal airflow rates, the values are relatively independent of the air intake position.
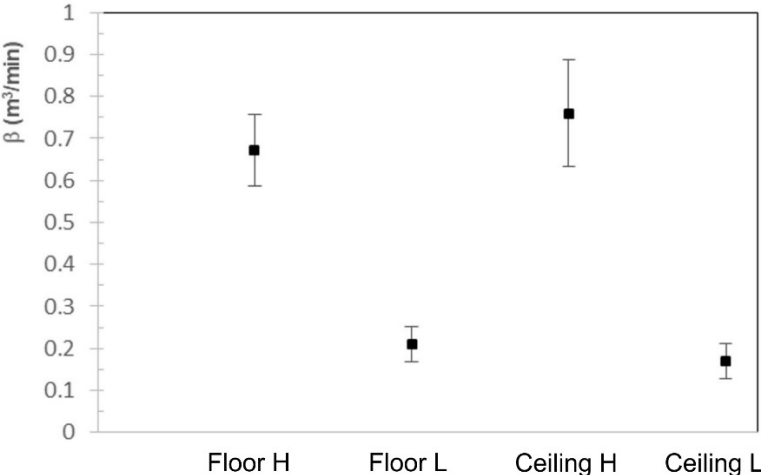

Figure 38.   Interzonal airflow rates estimated by CFD modelling for two air intake positions (floor and ceiling) and two ventilation rates (H: high and L: low).

Figure 39 compares the profiles of near field concentrations obtained using the two-zone model with the results of the CFD model. The results of the two-zone model are presented on three distinct curves. The concentration profiles estimated with the interzonal airflow rates β of Figure 38 are represented by the continuous black curves. The profiles represented by the continuous grey curves show the impact of the standard deviation of the β coefficients on the concentration profiles. These curves were obtained from the two-zone model with $\beta-\sigma$ (lower curve) and $\beta+\sigma$ (upper curve). In the first 30 minutes of simulation, the CFD concentration profiles were clearly lower than the results of the two-zone model. Thereafter, the results from the two models were similar, especially in the decreasing phase of the concentrations obtained by CFD modelling. Ventilation through the floor gives a mean concentration (C_{98}) of 228 mg/m^3 for the two-zone model, compared with 181 mg/m^3 for the CFD model. Ventilation through the ceiling shows similar differences, with C_{98} = 240 mg/m^3 and 172 mg/m^3 for the two-zone model and CFD model respectively.

The results in Figure 39 were obtained for a near field volume equivalent to a cube with 40 cm sides (0.064 m^3) around the emission source. In the two-zone model, the size of this volume directly influences the near field concentration, as the concentration depends on the β coefficient, which is directly proportional to the near field surface area (FSA). Unlike the two-zone model, which gives only two concentration values (near field and far field), the instances of CFD modelling show that concentrations reach the highest levels in the immediate environment of the source, but that it is not possible to establish a "boundary" between the near and far fields. Concentrations vary in both time and space; and the variations are greater in the case of a high ventilation rate.

Figure 40 shows the mean estimated concentrations in the near field for the case of a high rate of ventilation through the floor as a function of the size of the field. Concentrations are presented for 5 sizes in the near field, corresponding to a cube with sides of 14 cm, 26 cm, 40 cm, 52 cm and 64 cm, respectively (near fields 1, 2, 3, 4 and 5). The smaller the volume of the near field, the higher the concentrations. The difference is very substantial between fields 1 and 2, where the mean concentrations, estimated in the first hour, are 1,757 mg/m^3 and 466 mg/m^3, respectively. The mean concentrations in the first hour for near fields 3, 4 and 5 show less significant differences, with 180, 108 and 83 mg/m^3 respectively. It is also worth noting that the instant swings in concentration become smaller as the size of the near field increases.
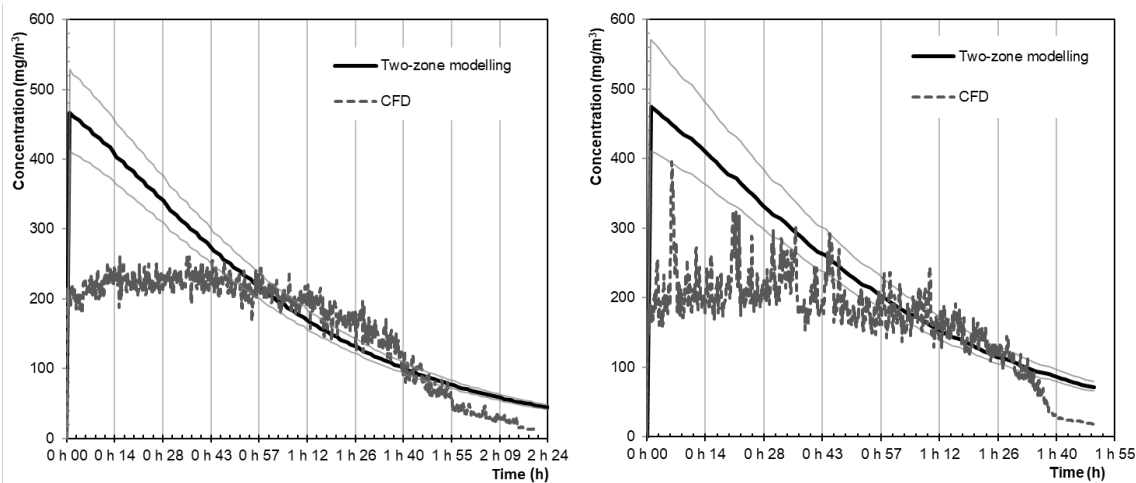
Figure 39.   Comparison between near field concentrations with high ventilation rate, with air intake through the floor (left) and through the ceiling (right).
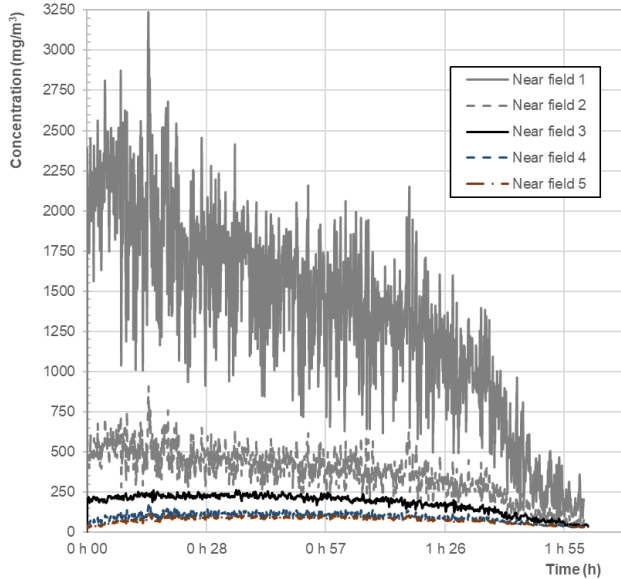

Figure 40.   Influence of size of near field on concentrations (high ventilation rate with air intake through the floor).

6. DISCUSSION

This research project explored various aspects of modelling for the purpose of estimating occupational exposure to solvent vapours and improving the prediction accuracy of certain models. In conducting a variety of small-scale and human-scale tests, the research focused on determining emission rates for pure solvents and mixtures, as well as on investigating the behaviour of solvent vapours released into the air and subjected to different experimental ventilation conditions.

6.1   Stage I – Small-scale laboratory testing

6.1.1 Experimental determination of exponentially decreasing emission rates α

The emission rates were determined following the approach developed by Keil and Nicas (2003). According to this approach, the exponentially decreasing emissions model accurately estimates solvent vapour concentrations for small spills. The α calculations performed during the study were in the same order of magnitude as those reported by Keil and Nicas, although they did differ. The values measured in this project were lower. For a spill of 3 mL of acetone in a watch glass, the mean α parameter in this study was 0.0681 min^{-1} , whereas for Keil and Nicas it was 0.16 min^{-1}. The environmental conditions under which the tests were conducted may explain some of the variation. Keil and Nicas reported temperatures between 21 and 25°C, whereas the tests in this study were done at temperatures more in the 20-to-22°C range. However, Keil and Nicas stated that the variations between the extreme temperature and pressure conditions of their study did not cause variations of greater than 3%. They reported a geometric mean airflow speed above the evaporation zone of 0.057 m/s. The air speeds during the tests without ventilation were lower in this study, i.e., under 0.01 m/s. When ventilation was used to determine α coefficients (see figures 13 and 14), the coefficients varied according to a linear relationship with air speed. Air speed was therefore a major explanatory variable of α values. A last point that could explain possible variations was that the geometry of the watch glass used may have influenced the spill surface area and therefore the α coefficient. Nevertheless, the tests done over the course of this study by comparing spills in a watch glass and spills in a Petri dish revealed significant variations only at spilled volumes of 1 mL. In a further demonstration of the influence of environmental conditions, the α coefficients reported in section 6.2.1 (human-scale testing) for acetone (20 mL) show that the coefficients measured using exactly the same method as for the small-scale tests were 0.022 min^{-1} [0.20 to 0.25 min^{-1}] on average, whereas they were 0.017 min^{-1} and 0.02 min^{-1} during the small-scale tests with air speeds of 0.01 m/s and 0.5 m/s, respectively. The temperature and relative humidity conditions were different between the two tests: 21°C and 20% relative humidity for the small-scale tests, as opposed to 24°C and 40% relative humidity for the human-scale tests.

The observed variations and the many parameters influencing emission in the case of small spills are indicative of the difficulty of accurately determining emission rates.

Figure 41 shows concentrations of estimated α parameters for a 10 mL spill for 69 solvents according to Keil and Nicas's equation, and according to equations 12 and 13 arrived at on the basis of experimental data. The third method used to calculate the α parameter was to consider a ventilation rate of 0.5 m/s by multiplying the result of equation 13 (without ventilation) by a factor of 2.55 (factor associated with ventilation, obtained from Figure 14 by dividing the value of α at

0.5 m/s by that at 0.05 m/s for a volume of 10 mL). A linearity in the estimates in comparison with those of Keil and Nicas was noted, regardless of the equation used. In addition, the estimates with ventilation are very close to those of Keil and Nicas (line 1:1).
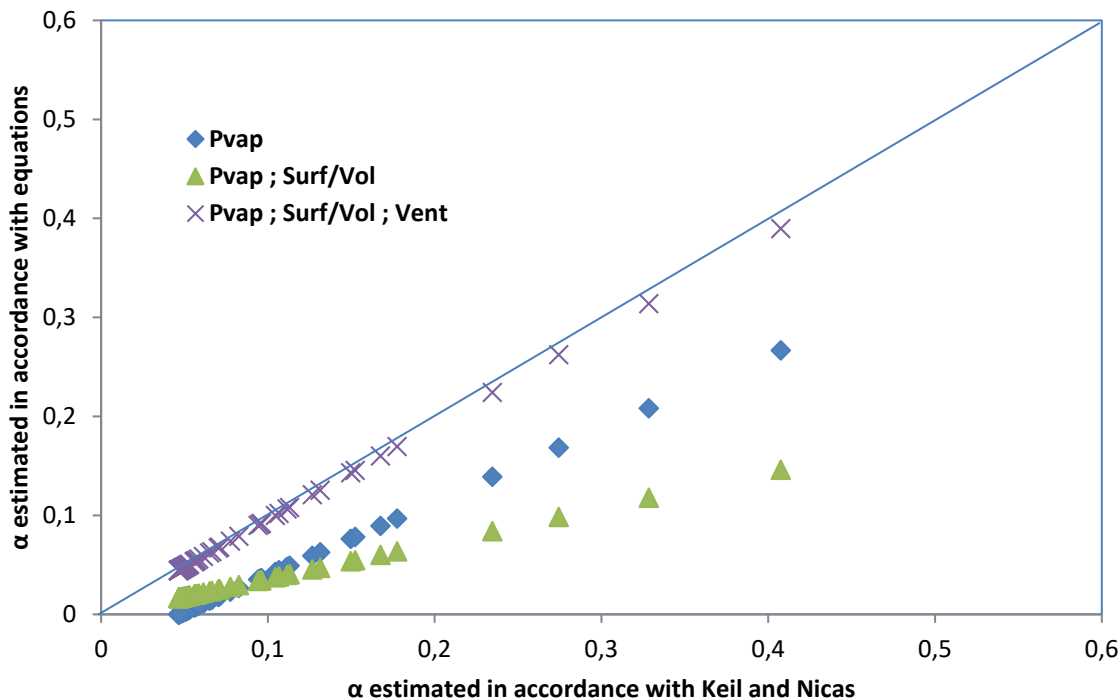
Figure 41.   Estimated coefficient *α* values for 69 solvents, according to two calculation methods.

A user seeking to estimate a coefficient *α* could therefore use the equations presented here, taking ventilation into account or not. There is a certain linearity between ventilation and the *α* values measured for 10 mL and 20 mL of acetone. Tests could be conducted with the same ventilation parameters for many different solvents at different volumes to compile a more comprehensive database and to allow the concept of air speed above the emission source to be introduced into a multiple linear regression model. The proposed model does, however, constitute an improvement in knowledge for estimating emission rates in the case of small spills.

6.1.2 Incorporation of concept of non-ideality into calculation of generation rate for solvent mixtures

The small-scale tests done in the lab enabled solvent vapour concentrations to be measured in a 0.083 m³ box and the measurements to be compared with estimates from modelling using the well-mixed box model with exponentially decreasing emission rates. Concentrations for pure solvents, aqueous solvents and organic solvent mixtures were determined.

Estimates that considered non-ideality, that is, corrected estimates, were substantially higher than non-corrected estimates. For instance, for 10% MEK-H$_2$O, a maximum corrected concentration of 1012 ppm was calculated, whereas the non-corrected C$_{max}$ was 415 ppm for a measured

concentration of 1209 ppm. That shows the importance of considering the activity coefficient γ when doing modelling calculations for non-ideal mixtures. If non-ideality is not considered, the concentration estimates will be inaccurate and that will result in underestimating concentration peaks and overestimating the times required to reach the maximum concentration.

No reference to evaluation by physico-chemical models for non-ideal mixtures was found in the literature. The data presented in this study are therefore original. They validate the utility of the UNIFAC model for estimating γ coefficients. Taking non-ideality into consideration when estimating α will therefore improve the accuracy of the models used to estimate occupational exposure.

6.2   Stage II – Human-scale testing in various work situations

Nineteen different human-scale situations were tested, each three times for four different scenarios (evaporation, spill, application with a rag and manual cleaning, spray and manual cleaning), for three airflow rates (low, high, very high) and two air intake positions (floor, ceiling). The concentrations were measured in the near field and the far field, at two different locations in each field.

In general, the analysis of variance showed that all of the variables had an effect on the near field concentrations, whereas only airflow rate and air intake position had an effect in the far field. Increasing the ventilation rates caused a significant drop in concentrations in both fields. In cases of very strong ventilation rates and cases of application with a rag or spray, the C_{98} concentrations in the near field were sometimes lower than those in the far field. It was also noted that when generation ceased, between 1h30min and 1h45min after the start of the tests (see figures 26, 27, 28 and 29), the concentrations in the near field dropped below those in the far field. Figure 33 illustrates a case of significant reversal characterized by lower concentrations in the near field than those measured in the far field. In that situation, ventilation was through the ceiling and the airflow speeds measured 50 cm from the source were 0.25 m/s, i.e., a speed far greater than those measured in the other tests. The hypothesis put forward is that the fresh air (uncontaminated by acetone fumes) is propelled directly down towards the ground and then goes past the spill zone in the near field. It is impossible at the moment with the two-zone model to take this phenomenon of uncontaminated fresh air arriving in the near field into account; it is therefore surprising to obtain concentrations in the near field that are lower than those in the far field, regardless of the parameters used in the model. Even if a perfectly mixed room were simulated, the concentrations in the near field would be at best equal to those in the far field. The research team was not able to find any studies in the literature that report this phenomenon of lower concentrations in the near field. The experimental data presented are therefore original, and studies could be undertaken to validate the possibility of incorporating this phenomenon into existing numerical models.

The phenomenon of the arrival of fresh air may also explain the constant difference of approximately 10 mg/m³ measured throughout the Figure 33 test, where the concentrations closest to the air intake were lower than those in the same field, but on the other side of the source. The two PID measurements provide us with information in particular about the symmetry and homogeneity of the near field, while the two GCs in the far field, being located at the far ends of the room, tell us about the homogeneity of the room's ventilation. The measured concentrations are, however, quite similar in each field, with mean differences of 10% [0.7 – 40%] in the far field and 21% [0.1 – 60%] in the near field between the two measuring points (PID1/PID2 and

GC1/GC2). One of the assumptions of the two-zone model is that the concentrations in the near field and the far field are homogeneous. This homogeneity assumption regarding the two zones was therefore partly validated in the experimental setup of this study. Earnest and Corsi also reported concentrations in the near field measured at different locations. They noted good homogeneity, with measured concentrations that varied by less than 10% for half of the time (Earnest and Corsi, 2013). However, not all authors report such homogeneity. Keil and Zhao obtained concentration measurement variations in the near field of up to 400% between two measuring points, and only 25% of their tests indicated concentrations in this field that varied by a factor of less than 2 (Keil and Zhao, 2017). Keil also reported a certain degree of symmetry in concentrations in the near field in connection with air movements in that zone. Keil demonstrated that when air movements in that zone are simulated, concentration symmetry increases (Keil, 2015). It is hard to compare different studies to one another, however, as the size of the rooms, the airflow rates and air speeds, and the assumptions underlying the geometry and size of the near field can all vary.

The purpose of the modelling was to assess the model's input parameters, especially the determination of parameter β and the radius of the near field hemisphere. These parameters were optimized to obtain an estimated concentration similar to the measured concentrations. When the two-zone model with exponentially decreasing emissions was used, the mean estimated coefficient β was 3.9 m³/min [0.92 – 16.9 m³/min]. A similar approach, aimed at optimizing the model's input parameters in order to obtain measured concentrations, was used by Keil and Zhao (2017). They reported optimized β coefficients of 4.8 m³/min [0.4 – 18.7 m³/min] over the course of 74 experiments in different rooms (Keil and Zhao, 2017).

While the β coefficients varied with the concentrations measured, the radii obtained through optimization of measured and estimated concentrations for the evaporation and spill scenarios were very homogeneous, with a geometric mean of 0.72 m (GSD of 1.3). When this radius was used for the near field geometry, the solvent vapour concentration at a distance of 30 cm from the source could be estimated accurately enough. In contrast, for the rag application and spray scenarios, the optimized radii were larger and varied more broadly, with respective mean radii (GM) of 1.1 m (GSD of 1.6) and 1.2 m (GSD of 1.9). The near field volumes were therefore larger in these scenarios. These results correspond to the data in the literature indicating that the broader the source and/or the more it is moving, and the more the task is spread out, the larger the volume of the near field will be (von Grote et al., 2003, 2006).

The profiles of the concentrations calculated by CFD simulation were compared with the results of the exponentially decreasing single-zone model. While the profiles are similar, differences can be seen with respect to change over time in concentrations and maximum values reached for a given ventilation scenario. In the CFD code, a dimensionless coefficient is used to represent the decline in the emission rate over time. That means that the emission rate is approximated by a series of straight lines of variable slope. In contrast, the one- and two-zone models implicitly account for the exponentially decreasing emission rate. As a result, a difference can be seen in the mass transfer of the contaminant in the air between the CFD model and the exponentially decreasing emission model.

Comparing the near field concentration profiles of the two-zone model with the results of the CFD model highlighted significant differences in the first 30 minutes of contaminant emission. The low airflow rate results have not been presented, but the differences between the two models are even more significant. The two-zone model is based on the assumption that contaminant transport

occurs solely by advection, that is, carried by the speed of the ambient air. This assumption is valid when air speeds at the near-field/far-field interface are high enough that advection is the dominant transport mechanism. Other mechanisms, such as molecular diffusion, caused by concentration gradients, and turbulent diffusion, caused by eddies and random flow fluctuations, also contribute to transport between the two zones. Nevertheless, what seems to affect the results the most is the volumetric mass density of the contaminant. With a relative vapour density to air of 2, acetone fumes tend to concentrate on the work bench and then drop toward the floor of the room. As a result, part of the contaminant is carried into the far field without advection coming into play. This transport mechanism is especially significant when the ventilation rate in the room is low. CFD simulations run without a ventilation rate showed that the contaminant is indeed transported into the far field without any air movement being required.

CFD modelling provided a way to document the concentration gradient around the source for the evaporation and spill scenarios (see Figure 40). A concentration gradient that tends to drop off quickly, with concentrations falling from 1,757 to 83 mg/m³, can be seen. While for the two-zone model estimates, the speeds were static and a function of experimental measurements, with CFD simulation, the interzonal speeds can be adapted to the size of the zone chosen. Modelling in a near field defined by a cube with 52 cm sides gives a mean concentration of 108 mg/m³; this concentration is very close to the experimental concentrations for this test (mean of 101 mg/m³). The test corresponds to a β of 1.2 m³/min. This coefficient is relatively low in comparison with the β values calculated earlier, i.e., coefficients of 3.82, 3.02 and 3.02 m³/min. That is due in part to the fact that the CFD simulation is the mean of all the near field concentrations, whereas the experimental measurements were taken at a distance of 30 cm from the source. The coefficients are therefore not directly comparable.

6.3   Scope and limitations

As mentioned in the introduction, the modelling of occupational exposure plays a major role in occupational hazard prevention. Modelling is a flexible, inexpensive alternative for estimating concentrations. Users must be mindful, however, that models are, by definition, representations of reality and that they are based on a variety of assumptions.

A number of assumptions were therefore formulated in this study, especially for the two-zone model. While the input parameters of the model were fairly well controlled for the spill and evaporation scenarios (interzonal airflow speed, emission rate, ventilation rate and air speed), two variables were estimated for the rag application and spray scenarios, i.e., interzonal airflow speed and emission rate. It is therefore difficult to assess each variable independently and to draw any conclusions about the optimization of parameter β with an estimated emission rate.

To assess the parameters of the two-zone model, a number of assumptions were made. A near field geometry corresponding to a hemisphere or a cube was chosen; the research team also agreed that the representative measurement for the breathing zone was located 30 cm above the source; it also estimated emission rates for the rag application and spray scenarios. The results presented here are therefore based on these assumptions, and all users of a model must state their own assumptions according to their needs. These assumptions may also explain differences in the results of many studies.

The results presented in this report show that modelling is still a valid method of estimating chemical concentrations in the workplace. Its use for estimating occupational exposure should be encouraged. Modelling is not, however, intended for verifying compliance with an exposure standard, and certainly not for establishing a worker exposure profile.

Modelling should, if possible, incorporate a way of accounting for the variability or uncertainty of certain input parameters so that information about the probability of the predicted concentrations is available to users of the model. It is worth noting that the 2018 release of IH Mod 2.0[1] features a probabilistic simulation module.

---

[1] https://ihmod.org/

7. CONCLUSION

The purpose of this project was to improve the accuracy of occupational hygiene models used to estimate workplace exposure to solvent vapours. It involved a variety of both small-scale and human-scale testing that focused specifically on determining emission rates for pure solvents and mixtures, as well as on investigating the behaviour of solvent vapours released into the air and subjected to different experimental ventilation conditions.

The emission rates were determined in accordance with the approach developed by Keil and Nicas (2003). The variations observed in coefficient α values were primarily due to the variables vapour pressure, surface area/volume ratio and air speed above the spill. A user seeking to estimate a coefficient α could therefore use the equations presented here, taking ventilation into account or not. The proposed model is an improvement in knowledge for estimating emission rates in the case of small spills.

The small-scale tests done in the lab provided vapour concentration measurements for pure solvents and mixtures, so that the measurements could be compared with the estimates from the well-mixed room model with exponentially decreasing emissions. Estimates that took non-ideality into account, that is, corrected estimates, were substantially higher than non-corrected estimates, and the times T_{max} of the concentration peaks could be used to estimate emission kinetics fairly accurately. That shows the importance of considering the activity coefficient γ when doing modelling calculations for non-ideal mixtures. If non-ideality is not considered, the concentration estimates will be inaccurate and that will result in underestimating concentration peaks and overestimating the times required to reach maximum concentrations. Taking non-ideality into consideration when estimating α therefore leads to an improvement in the accuracy of the models used to estimate occupational exposure to solvent mixtures.

Nineteen different human-scale situations were tested. In general, the analysis of variance showed that all of the variables had an effect on the near field concentrations, whereas only airflow rate and air intake position had an effect in the far field. Increasing the ventilation rate caused a significant drop in concentrations in both fields. In cases of very high ventilation rates and for the rag application and spray scenarios, the C_{98} concentrations in the near field were sometimes lower than those in the far field. The hypothesis put forward is that the fresh air (uncontaminated by acetone fumes) is propelled directly down towards the ground and then goes past the spill zone in the near field. The radii obtained through optimization of the measured and estimated concentrations for the evaporation and spill scenarios were very homogeneous, with a mean radius of 0.72 m (GSD of 1.3), and the corresponding mean estimated coefficient β was 3.9 m³/min [0.92 – 16.9 m³/min]. When this radius is used for the near field geometry, the solvent vapour concentration at a distance of 30 cm from the source can be estimated with sufficient accuracy. In contrast, for the rag application and spray scenarios, the optimized radii were larger and varied more broadly, with respective mean radii of 1.1 m (GSD of 1.6) and 1.2 m (GSD of 1.9). The analysis of the different variables, including some not considered in the two-zone model, is an original result of this study.

The CFD modelling provided a means of specifying the concentration gradient around the source for the evaporation and spill scenarios. The concentration gradient diminished rapidly, with concentrations dropping from 1,757 mg/m³ to 83 mg/m³ for a cube-shaped near field of 14 cm a side and 64 cm a side, respectively. The CFD modelling also highlighted contaminant

displacements due to vapour density relative to the air, without the need to involve advection. This transport mechanism is especially significant when the ventilation rate in the room is low. Analysis of the CFD modelling data improves our understanding of contaminant dispersion mechanisms.

This study underscores the importance of using different variables to estimate emission rates for small spills, taking the possibility of non-ideal mixtures into account and exploring different determinants of concentrations in the near and far fields. These findings improve our general understanding of solvent vapour dispersion and the models used in occupational hygiene to estimate worker exposure to such emissions.

BIBLIOGRAPHY

Arnold, S., Ramachandran, G., and Jayjock, M. (2009). Model selection. In C. Keil, C. Simmons and T. Anthony (Eds.), *Mathematical models for estimating occupational exposure to chemicals* (2nd ed., pp. 99–103). Fairfax, VA: American Industrial Hygiene Association.

Arnold, S. F., Shao, Y., and Ramachandran, G. (2017a). Evaluating well-mixed room and near-field-far-field model performance under highly controlled conditions. *Journal of Occupational and Environmental Hygiene, 14*(6), 427-437. doi: 10.1080/15459624.2017.1285492

Arnold, S. F., Shao, Y., and Ramachandran, G. (2017b). Evaluation of the well mixed room and near-field far-field models in occupational settings. *Journal of Occupational and Environmental Hygiene, 14*(9), 694-702. doi: 10.1080/15459624.2017.1321843

ASTM. (1997). *Standard guide for statistical evaluation of indoor air quality models.* Standard ASTM D5157-97. Conshohocken, PA: ASTM.

Bayatian, M., Ashrafi, K., Azari, M.R., Jafari, M.J., and Mehrabi, Y., (2018). Risk assessment of occupational exposure to benzene using numerical simulation in a complex geometry of a reforming unit of petroleum refinery. Environmental Science and Pollution Research, 25(12):11364-11375. doi: 10.1007/s11356-018-1318-6.

Bégin, D., Debia, M., and Gérin, M. (2008). *Recension des outils de comparaison des solvants* (Report No. R-567). Montreal, QC: IRSST.

Bennett, J. S., Feigley., C. E., Khan., J., and Hosni, M. H. (2000). Comparison of mathematical models for exposure assessment with computational fluid dynamic simulation. *Applied Industrial Hygiene, 15*(1), 131–144. doi: 10.1080/104732200301953

Bertrand, N., and Vincent, R. (2010a). Modélisation des expositions professionnelles aux agents chimiques: bilan et perspectives. *Hygiène et sécurité du travail, 220,* 21–33. Retrieved from www.inrs.fr/accueil/dms/inrs/CataloguePapier/ND/TI-ND-2333/nd2333.pdf

Bertrand, N., and Vincent, R. (2010b). Modélisation des expositions professionnelles aux agents chimiques: bilan et perspectives. *Hygiène et sécurité du travail, 220*(10)*,* 21–33.

Bruzzi, R. (2007). *New developments and applications in modelling occupational exposure to airborne contaminants*. (Doctoral thesis, Université de Lausanne, Lausanne, Switzerland).

Chauhan, N., Chauhan, R. P., Joshi, M., Agarwal, T. K., and Sapra, B. K. (2015). Measurements and CFD modeling of indoor thoron distribution. *Atmospheric Environment*, *105*, 7–13. doi: 10.1016/j.atmosenv.2015.01.029

Cherrie, J. W., Maccalman, L., Fransman, W., Tielemans, E., Tischer, M., and van Tongeren, M. (2011). Revisiting the effect of room size and general ventilation on the relationship between near- and far-field air concentrations. *Annals of Occupational Hygiene, 55*(9), 1006–1015. doi: 10.1093/annhyg/mer092

Choy, B., and Reible, D. (1996). UNIFAC Calculator [software]. Sydney, Australia: University of Sydney.

Debia, M., Bégin, D., and Gérin, M. (2009). Comparative evaluation of overexposure potential indices used in solvent substitution. *Annals of Occupational Hygiene, 53*(4), 391–401.

Demou, E., Hellweg, S., Wilson, M. P.*,* Hammond, S. K., and McKone, T. E. (2009). Evaluating indoor exposure modeling alternatives for LCA: A case study in the vehicle repair industry. *Environmental Science and Technology, 43*(15), 5804–5810.

Drolet, D., Goyer, N., Roberge, B., Lavoue, J., Coulombe, M., and Dufresne, A. (2010). *Stratégies de diagnostic de l'exposition des travailleurs aux substances chimiques* (Report No. R-665). Montreal, QC: IRSST.

Earnest, C. M., and Corsi, R. L. (2013). Inhalation exposure to cleaning products: Application of a two-zone model. *Journal of Occupational Environmental Hygiene, 10*(6), 328–335. doi: 10.1080/15459624.2013.782198

European Parliament and Council of the European Union. (30 December 2006). Regulation (EC) No 1907/2006 of the European Parliament and of the Council of 18 December 2006 concerning the Registration, Evaluation, Authorisation and Restriction of Chemicals (REACH), establishing a European Chemicals Agency, amending Directive 1999/45/EC and repealing Council Regulation (EEC) No 793/93 and Commission Regulation (EC) No. 1488/94 as well as Council Directive 76/769/EEC and Commission Directives 91/155/EEC, 93/67/EEC, 93/105/EC and 2000/21/EC. *Official Journal of the European Union L, 396,* 1-849.

Flynn, M. R. (2004). A stochastic differential equation for exposure yields a beta distribution. *Annals of Occupational Hygiene*, *48*(5), 491–497. doi: 10.1093/annhyg/meh032

Fransman, W., van Tongeren, M., Cherrie, J. W., Tischer, M., Schneider, T., Schinkel, J., and Tielemans, E. (2011). Advanced reach tool (ART): Development of the mechanistic model. *Annals of Occupational Hygiene*, *55*(9), 957-979. doi: 10.1093/annhyg/mer083

Gaffney, S., Moody, E., McKinley, M., Knutsen, J., Madl, A., and Paustenbach, D. (2008). Worker exposure to methanol vapors during cleaning of semiconductor wafers in a manufacturing setting. *Journal of Occupational and Environmental Hygiene*, *5*(5), 313–324. doi: 10.1080/15459620801988014

Gérin, M. (2002a). Solvants et prévention: nouvelles perspectives. In M. Gérin (Ed.), *Solvants industriels: Santé, sécurité, substitution* (pp. 1–12). Paris, France: Masson.

Gérin, M. (2002b). *Solvants industriels: Santé, sécurité, substitution*. Paris, France: Masson.

He, G., Yang, X. and Srebric, J. (2005). Removal of contaminants released from room surfaces by displacement and mixing ventilation: Modeling and validation. *Indoor Air, 15*(5), 367–380. doi: 10.1111/j.1600-0668.2005.00383.x

Hofstetter, E., Spencer, J. W., Hiteshew, K., Coutu, M., and Nealley, M. (2012). Evaluation of recommended REACH exposure modeling tools and near-field, far-field model in assessing occupational exposure to toluene from spray paint. *Annals of Occupational Hygiene*, *57*(2), 210–220. doi: 10.1093/annhyg/mes062

Hyun, S., and Kleinstreuer, C. (2001). Numerical simulation of mixed convection heat and mass transfer in a human inhalation test chamber. *International Journal of Heat and Mass Transfer, 44*(12), 2247–2260. doi: 10.1016/S0017-9310(00)00268-4

INRS. (2003). *Explosion et lieu de travail (ED 5001).* Paris, France: INRS.

INRS. (2013). *Tableau des maladies professionnelles: guide d'accès et commentaires*. Retrieved from http://www.inrs-mp.fr/mp/cgi-bin/mppage.pl

Jayjock, M., Logan, P., Mader, B., Owens, J., Eldrige, J, Costello, M., and Lieder, P. (2011). Modeled comparisons of health risks posed by fluorinated solvents in a workplace spill scenario. *Annals of Occupational Hygiene, 55*(2), 202–213. doi: 10.1093/annhyg/meq062

Jayjock, M. A., Armstrong, T., and Taylor, M. (2011). The Daubert standard as applied to exposure assessment modeling using the two-zone (NF/FF) model estimation of indoor air breathing zone concentration as an example. *Journal of Occupational and Environmental Hygiene, 8*(11), D114–D122. doi: 10.1080/15459624.2011.624387

Keil, C., and Murphy, R. (2006). An application of exposure modeling in exposure assessments for a university chemistry teaching laboratory. *Journal of Occupational and Environmental Hygiene, 3*(2), 99–106. doi: 10.1080/15459620500498109

Keil, C., and Nicas, M. (2003). Predicting room vapor concentrations due to spills of organic solvents. *AIHA Journal, 64*(4), 445–454. doi: 10.1080/15428110308984838

Keil, C., and Zhao, Y. (2017). Interzonal airflow rates for use in near-field far-field workplace concentration modeling. *Journal of Occupational and Environmental Hygiene, 14*(10), 793–800. doi: 10.1080/15459624.2017.1334903

Keil, C. B. (1998). The development and evaluation of an emission factor for a toluene parts-washing process. *American Industrial Hygiene Association Journal, 59*(1), 14–19. doi: 10.1080/15428119891010280

Keil, C. B. (2000). A tiered approach to deterministic models for indoor air exposures. *Applied Occupational and Environmental Hygiene, 15*(1), 145–151. doi: 10.1080/104732200301962

Keil, C. B. (2015). Experimental measurements of near-source exposure modeling parameters. *Journal of Occupational and Environmental Hygiene, 12*(10), 692–698. doi: 10.1080/15459624.2015.1029619

Keil, C. B., Simmons, C. E., and Anthony, T. (Eds.). (2009). *Mathematical models for estimating occupational exposure to chemicals* (2nd ed.). Fairfax, VA: American Industrial Hygiene Association.

Lau, J., and Chen, Q. (2007). Floor-supply displacement ventilation for workshops. *Building and Environment, 42*(4), 1718–1730. doi: 10.1016/j.buildenv.2006.01.016

Li, J., and Zhou, Y.-F., (2015). Occupational hazards control of hazardous substances in clean room of semiconductor manufacturing plant using CFD analysis. *Toxicology and Industrial Heath*, 31(2), 123-139. doi: 10.1177/0748233712469996

McGrattan, K., Hostikka, S., McDermott, R., Floyd, J., Weinschenk, C., and Overholt, K. (2017a). *Fire dynamics simulator technical reference guide. Vol. 1: Mathematical model* (6th ed.). Gaithersburg, MD: National Institute of Standards and Technology.

McGrattan, K., Hostikka, S., McDermott, R., et al. (2017b). *Fire dynamics simulator: User's guide* (6th ed.). Gaithersburg, MD: National Institute of Standards and Technology.

Morency, F. and Hallé, S. (2012). A simplified approach for modelling airborne nanoparticles transport and diffusion. *International Journal of Computational Methods and Experimental Measurements, 1*(1), 55–71.

Nicas, M. (1996). Estimating exposure intensity in an imperfectly mixed room. *American Industrial Hygiene Association Journal*, 57(6), 542–550. doi: 10.1080/15428119691014756

Nicas, M. (2003). Using mathematical models to estimate exposure to workplace air contaminants. *Chemical Health and Safety, 10*(1)*,* 14–21.

Nicas, M. (2009). The near field/far field (two-box) model with a constant contaminant emission rate. In C. Keil, C. Simmons and T. Anthony (Eds.), *Mathematical models for estimating occupational exposure to chemicals* (2nd ed., pp. 47–52). Fairfax, VA: American Industrial Hygiene Association.

Nicas, M. (2016). The near field/far field model with constant application of chemical mass and exponentially decreasing emission of the mass applied. *Journal of Occupational and Environmental Hygiene, 13*(7), 519–528. doi: 10.1080/15459624.2016.1148268

Nicas, M., and Neuhaus, J. (2008). Predicting benzene vapor concentrations with a near field/far field model. *Journal of Occupational and Environmental Hygiene, 5*(9), 599–608. doi: 10.1080/15459620802282375

Nicas, M., Plisko, M. J., and Spencer, J. W. (2006a). Estimating benzene exposure at a solvent parts washer. *Journal of Occupational and Environmental Hygiene, 3*(5), 284–291. doi: 10.1080/15459620600637390

Persoons, R., Maitre, A., and Bicout, D. J. (2011). Modelling the time profiles of organic solvent concentrations for occupational exposure assessment purposes. *Annals of Occupational Hygiene, 55*(4), 421–435. doi: 10.1093/annhyg/meq090

Persoons, R., Maitre, A., and Bicout, D. J. (2012). Modelling occupational inhalation exposure to concentration peaks of chemicals and associated health risk assessment. *Annals of Occupational Hygiene, 56*(8), 934–947. doi: 10.1093/annhyg/mes021

Plisko, J., and Spencer, J. W. (2008). Evaluation of a mathematical model for estimating solvent exposures in the workplace. *Journal of Chemical Health & Safety, 15(3),* 14–21.

Popendorf, W. (2006a). Vapor generation and behavior. In W. Popendorf (Ed.), *Industrial hygiene control of airborne chemical hazards* (pp. 109–140). Boca Raton, FL: Taylor & Francis Group.

Popendorf, W. (2006b). Vapor pressure in mixtures. In W. Popendorf (Ed.), *Industrial hygiene control of airborne chemical hazards* (pp. 141–171). Boca Raton, FL: Taylor & Francis Group.

Reinke, P., Jayjock, M., and Nicas, M. (2009). Well mixed rooms with changing conditions. In C. Keil, C. Simmons and T. Anthony (Eds.), *Mathematical models for estimating occupational exposure to chemicals* (2nd ed., pp. 33–45). Fairfax, VA: American Industrial Hygiene Association.

Reinke, P., and Keil, C. (2009). Well-mixed box model. In C. Keil, C. Simmons and T. Anthony (Eds.), *Mathematical models for estimating occupational exposure to chemicals* (2nd ed., pp. 23–31). Fairfax, VA: American Industrial Hygiene Association.

Reinke, P. H., and Brosseau, L. M. (1997). Development of a model to predict air contaminant concentrations following indoor spills of volatile liquids. *Annals of Occupational Hygiene, 41*(4), 415–435. doi: 10.1016/S0003-4878(96)00048-8

Robbins, C. A., Krause, M. W., Atallah, R. H., and Plisko, M. J. (2012). Comparison of exposure measurements to near field–far field modeled results for benzene and base solvents during a cleaning process using plain or 0.1% benzene spiked toluene and xylene. *Journal of Chemical Health and Safety*, *19*(6), 3–11.

Safe Work Australia (2012). *Guidance on the interpretation of workplace exposure standards for airborne contaminants*. Canberra, Australia: Safe Work Australia.

Spencer, J. W., and Plisko, M. J. (2007). A comparison study using a mathematical model and actual exposure monitoring for estimating solvent exposures during the disassembly of metal parts. *Journal of Occupational and Environmental Hygiene, 4*(4), 253–259. doi: 10.1080/15459620701205253

Tielemans, E., Warren, N., Fransman, W., and van Tongeren, M. (2011). Advanced REACH tool (ART): Overview of Version 1.0 and research needs. *Annals of Occupational Hygiene, 55*(9), 949–956. doi: 10.1093/annhyg/mer094

Triolet, J., and Sallé, B. (2009). *Évaluation de la vitesse d'évaporation et de la concentration d'un composé organique volatil dans l'atmosphère d'un local de travail* (Aide mémoire technique ED 6058). Paris, France: INRS.

Van Tongeren, M., Fransman, W., Spankie, S., Tischer, M., Brower, D., Schinkel, J., and Tielmans, E. (2011). Advanced REACH tool: Development and application of the substance emission potential modifying factor. *Annals of Occupational Hygiene, 55*(9), 980–988. doi: 10.1093/annhyg/mer093

Vézina, M., Cloutier, E., Stock, S., et al. (2011). *Enquête québécoise sur des conditions de travail, d'emploi, et de santé et de sécurité du travail (EQCOTESST)* (Report No. R-691). Montreal, QC: IRSST.

Von Grote, J., Hürlimann, C., Scheringer, M., and Hungerbühler, K. (2003). Reduction of occupational exposure to perchloroethylene and trichloroethylene in metal degreasing

over the last 30 years: Influences of technology innovation and legislation. *Journal of Exposure Science and Environmental Epidemiology*, *13*(5), 325. doi: 10.1038/sj.jea.7500288

Von Grote, J., Hürlimann, C., Scheringer, M., and Hungerbühler, K. (2006). Assessing occupational exposure to perchloroethylene in dry cleaning. *Journal of Occupational and Environmental Hygiene*, *3*(11), 606–619. doi: 10.1080/15459620600912173

Williams, P. R., and Mani, A. (2015). Benzene exposures and risk potential for vehicle mechanics from gasoline and petroleum-derived products. *Journal of Toxicology and Environmental Health, 18*(7–8), 371–399. doi: 10.1080/10937404.2015.1088810

Zhang, Y., Banerjee, S., Yang, R., Lungu, C., and Ramachandran, G. (2009). Bayesian modeling of exposure and airflow using two-zone models. *Annals of Occupational Hygiene*, *53*(4), 409–424. doi: 10.1093/annhyg/mep017